UNIVERSITY OF TRENTO - Italy
Department CIBIO

International PhD Program in *Biomolecular* Sciences

Department of Cellular, Computational and Integrative Biology – CIBIO

XXXIII Cycle

"Targeting the LIN28B/*let-7* axis by small molecules in Neuroblastoma"

Tutor:

Prof. Alessandro Quattrone

University of Trento, CIBIO

Ph.D. Thesis of

Simona Cocchi

University of Trento, CIBIO

Academic Year 2019/2020

Original authorship

Declaration:

I, Simona Cocchi, confirm that this is my own work and the use of all material from other sources have been properly and fully acknowledged.

TABLE OF CONTENTS

ABSTRACT

Neuroblastoma (NB) is a very heterogeneous tumour derived from undifferentiated cells of the neural crest. It is the most common extracranial solid tumour in children, characterised by a large variability of the clinical outcome. The clinically aggressive form of the disease, the high-risk neuroblastoma, affects about 50% of patients, which, unfortunately, despite the intensity of therapies, have a survival rate of less than 50%. Although the introduction of two new therapeutic solutions based on the use of 13-cis-retinoic acid and the immunotherapy with a chimeric monoclonal antibody against the GD2 ganglioside, 20% of patients affected by the high-risk disease are still entirely refractory to treatments, and 60% will relapse.

In this panorama, identifying new strategies specific for critical NB targets is endowed with great potential to improve the survival rate and long-term quality of life and reduce the elevated toxicity of current treatments.

LIN28B is an RNA binding protein extensively overexpressed in NB. Its exogenous expression in mouse sympatho-adrenergic lineage is able to reproduce the human disease, underlying the importance of LIN28B in NB pathogenesis. LIN28B prevents the maturation of *let-7* miRNA family members, an important group of tumour suppressors that induce differentiation and, at the same time, decrease cell proliferation.

We hypothesised that interfering with the LIN28B/*let-7* miRNA interaction could lead to an increase in *let-7* miRNA levels and, consequently, to a decrease in cell proliferation and an induction of cell differentiation, ultimately reducing NB aggressiveness.

First, we created NB cell lines with stable LIN28B down-regulation, and we observed an expected increase in *let-7* miRNA levels. We then verified if the rise in the *let-7* miRNAs could induce the cells' differentiation by analysing a panel of stemness and differentiation markers such as SOX2, SOX9 and β-III-tubulin, detecting a decrease in the stemness markers and an increase in the differentiation-related markers.

Following a high-throughput screening, performed and validated with two orthogonal biochemical techniques, the Alpha screen and the REMSA, we identified the epigallocatechin 3'-monogallate (EGCG) as the molecule with the best inhibitory activity on the LIN28B/*let-7* miRNA interaction. After the biochemical validation, we proceeded to assess EGCG activity *in vitro* on NB cell lines. EGCG resulted to be very unstable in cell culture conditions, therefore we decided to include the molecule in PLGA-PEG nanoparticles to preserve its stability in solution and improve

its activity. Upon encapsulation, we observed a substantial increase in EGCG effects, leading to a strong increment in mature *let-7* miRNAs and a consequent inhibition of cellular growth. Finally, we tested if the *let-7* miRNAs increment caused by EGCG treatment was sufficient to induce NB cells differentiation, as observed with stable LIN28B-downregulation. We detected an increase in differentiation marker levels suggesting that the treatment with EGCG nanoparticles is able to lead to the induction of neuronal differentiation processes in NB cells. Although these last results need to be confirmed with further experiments, they clearly show that the LIN28B/*let-7* miRNA axis represents a good therapeutic target and that EGCG and/or other molecules able to interfere with this interaction deserve further preclinical and clinical evaluation.

ABBREVIATIONS

ALPHA amplified luminescent proximity homogeneous assay

ALK anaplastic lymphoma receptor tyrosine kinase

ATA aurintricarboxylic acid

CDS cold shock domain

EGCG epigallocatechin 3'-monogallate

EMT epithelial-to-mesenchymal transition

GWAS genome-wide association studies

INSS International Neuroblastoma Staging System

INGR International Neuroblastoma Risk Group

INRGSS INRG Staging System

Let-7 lethal-7

mRNA messenger RNA

miRNA microRNA

NB neuroblastoma

NC neural crest

NCC neural crest cells

PHOX2B paired-like homeobox 2B gene

PLGA poly(lactic-*co*-glycolic acid)

PEG polyethylene glycol

RA 13-*cis*-retinoic acid

REMSA RNA mobility shift assay

SNP single nucleotide polymorphism

TFMG theaflavin monogallate

UTR 3' untranslated region

ZKD zinc knuckle domain

1. INTRODUCTION

1.1 NEUROBLASTOMA

Neuroblastoma (NB) is a tumour arising from undifferentiated cells of the neural crest's sympathetic nervous system. NB represents 10% of all childhood cancers and has a median age at diagnosis of 18 months, with 40% of patients diagnosed at infancy and 90% of patients less than 10 years old when diagnosed (London et al., 2005). The incidence of NB is about 10 cases per million in children under 15 years (Maris, 2010).

Typically, NB diagnosis follows the appearance of bone pain, anaemia, or hepatomegaly (Colon and Chung, 2011; Matthay et al., 2016).

The primary tumour can arise anywhere along with the sympathetic nervous system, generally in the adrenal medulla or paraspinal ganglia. In the majority of cases, NB develops in the abdomen (65%), otherwise in the neck (5%), chest (20%), or pelvis (5%) (Maris et al., 2007). This tumour is frequently metastatic at the level of bone marrow, lymph nodes, and rarely of the liver, lung, and central nervous system. Metastasis of NB leads to a 40% decrease in survival rate. Indeed, the symptoms can vary depending on the primary tumour site and the metastasis (Bagca and Avci, 2017).

The hallmark of NB is the considerable biological/pathological and outcome heterogeneity: in fact, it can range from spontaneous regression to rapid progression. These differences are determined by biological and clinical features, including age at diagnosis, disease stage and several numerical and structural chromosomal aberrations (Cheung and Dyer, 2013).

For years, NB has been classified according to several clinical and biological features, but the complexity and the variety of the disease required the development of a more specific classification system. In 1986 the International Neuroblastoma Staging System (INSS) was developed to create a universal staging system, aligning diagnosis and treatments criteria. The INSS classified the NB tumours based on clinical, radiographic and surgical evaluation of the patients and divided tumours into five stages: 1, 2, 3, 4 and 4s (Brodeur et al., 1988, 1993), which characteristics are summarised in **Table 1.1**

Table 1.1. International Neuroblastoma Staging System (INSS).

Stage	Definition
1	Localized tumor with complete gross excision, with or without microscopic residual disease; no metastasis to representative ipsilateral lymph nodes that were not attached to tumour.
2A	Localized tumor with incomplete gross excision; no metastasis to the lymph nodes.
2B	Localized tumor with or without complete gross excision, with metastasis to the ipsilateral lymph nodes but no tumour metastasis noted in any enlarged contralateral lymph nodes.
3	Unresectable unilateral tumor infiltrating across the midline, with or without regional lymph node metastasis; or localized unilateral tumor with contralateral regional lymph node metastasis, or midline tumor with bilateral infiltration (unresectable) or by lymph node involvement.
4	Any primary tumor with metastasis to distant lymph nodes, bone, bone marrow, liver, skin and/or other organs (except as defined for stage 4S).
4S	Localized primary tumor (as defined for stage 1, 2A or 2B), with metastasis limited to skin, liver, and/or bone marrow (limited to infants < 1 year of age).

Adapted from (Brodeur et al., 1993).

In 2004 the International Neuroblastoma Risk Group (INGR) integrated the old classification method with the INRG Staging System (INRGSS), in which the preoperative tumour imaging was essential for the classification (Monclair et al., 2009). Subsequently, another evolution of the classification system led to the identification of a list of clinical, pathologic, and genetic markers that allow to divide the tumours into three risk groups: low, intermediate, and high. Approximately 40% of patients are classified as high-risk, and only 50% of these patients will achieve long-term survival (Pinto et al., 2015). This classification system is based on the combination of seven different factors: the INRG staging system, age at the time of diagnosis, the grade of differentiation of the tumour, the histological category, MYCN status, chromosome 11q status and tumour cell ploidy (Pinto et al., 2015).

1.1.1 The genetics and epigenetics behind neuroblastoma

Although NB was initially classified as a familial tumour, we now know that most NB patients are affected by a sporadic form of the disease, while only 1-2% of the patients inherit the disease (Matthay et al., 2016).

The genetic bases of familial NB were initially explained with the 'two-hit model, in which a first germline mutation (first hit) is followed by a later acquired somatic mutation (second hit)

(Knudson and Strong, 1972). In the past two decades, the efforts to understand the genetic bases of familial NB led to the identification of two germline mutations as the two major genetic contributors: a loss-of-function mutation in the paired-like homeobox 2B gene (PHOX2B) (Trochet et al., 2004) and a gain-of-function mutation in the anaplastic lymphoma receptor tyrosine kinase (ALK) (Mossé et al., 2008).

In detail, the PHOX2B gene is considered a master regulator of neural crest cell lineage determination and/or maturation (Pattyn et al., 1999; Raabe et al., 2008). Indeed, the absence of PHOX2B in mice has been shown to lead to the aberrant development of both central and peripheral nervous systems, and in particular of the sympathetic ganglia (Pattyn et al., 1999), while mutations on PHOX2B lead to different diseases such as the congenital central hypoventilation syndrome (Amiel et al., 2003). In 2004 PHOX2B was identified as the first susceptibility gene in NB (Trochet et al., 2004).

Heritable gain-of-function mutations of ALK are the main predisposing factor for familial NB. ALK and its ligands are highly expressed during the development of the nervous system, where they control its functionality (Wellstein, 2012). ALK involvement in familial and sporadic NB was first shown in 2008, suggesting its role as an oncogenic driver of the disease (Mossé et al., 2008). Single-base missense mutations clustering in key regulatory regions of the ALK kinase domain have been shown to lead to the loss of the auto-inhibiting conformation of the kinase, leading to uncontrolled activation (Lee et al., 2010). Currently, R1275, F1174, and F1245 mutations account for around 85% of ALK mutations, and R1275Q mutation is the most common, being present in 45% of NB familial cases and a third of NB sporadic cases (Bresler et al., 2014). ALK mutations are correlated with MYCN amplification, and different studies have reported the cooperative activity of these two oncogenes in driving the development of NB (Zhu et al., 2012).

Besides the ALK and PHOX2B germline mutations associated with familial NB, different genetic alterations have been found in the context of this disease, including gene amplifications, polymorphisms, and chromosomal alterations.

MYCN has been identified as one of the main drivers of NB development. MYCN is a master regulator of transcription, which activates genes involved in proliferation, pluripotency, self-renewal and angiogenesis, features all associated with cancer hallmarks, and represses genes that lead to differentiation (Huang and Weiss, 2013). The status of MYCN, i.e. amplified or non-amplified, remains the most crucial aspect to determine the level of risk of the disease (Huang

and Weiss, 2013). *MYCN* amplification occurs in approximately 22% of NB cases and correlates with high-risk disease and poor outcome (Brodeur, 2003).

The development of single nucleotide polymorphism (SNP) array technology (Wang et al., 1998) significantly improved the study and understanding of this disease. This technique led to several genome-wide association studies (GWAS), which highlighted new mutations linked to NB, important to understand and classify the disease in low- or high-risk.

A GWAS performed by Diskin and colleagues allowed identifying two new risk genes: HACE1 and LIN28B. In particular, the study showed that low HACE1 and high LIN28B expression levels in NB were associated with worse overall survival, suggesting an important role of these two genes in disease progression (Diskin et al., 2012). Moreover, in the same year, Molenaar et al. demonstrated that LIN28B forced expression in the sympathoadrenal cells of nude mice induced the development of a tumour mass recapitulating neuroblastomas features (Molenaar et al., 2012a), highlighting the oncogenic role of LIN28B in NB.

Another study also identified loss-of-function mutations in ATRX, a gene that encodes an SWI/SNF chromatin-remodeling ATP-dependent helicase. These mutations were correlated with age at diagnosis and poor prognosis (Cheung et al., 2012). Interestingly, ATRX mutations appear mutually exclusive to MYCN amplification. Moreover, ATRX is associated with telomerase-independent telomere maintenance, a mechanism known as alternative lengthening of telomeres (ALT) suppressed by wild-type ATRX in ALT-negative tumours (Bower et al., 2012; Clynes et al., 2015). **Figure 1.1** summarises the most important genetic variations in familial and sporadic NB cases reported during the time.

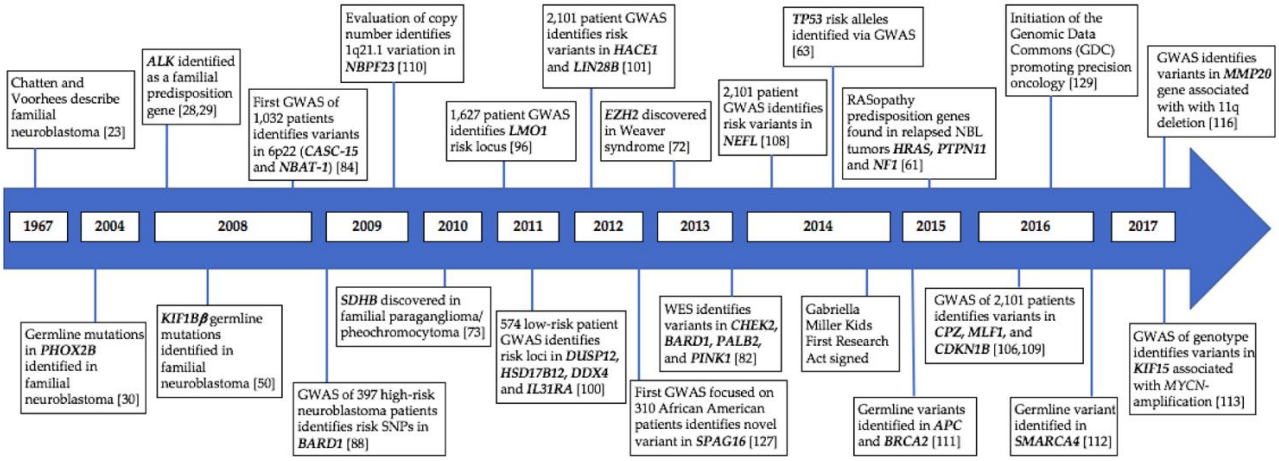

Figure 1.1. A timeline of genetic variation in familial and sporadic NB cases was reported (Barr and Applebaum, 2018).

Besides the importance of genetic mutations in both familial and sporadic forms of NB, several studies have highlighted the fundamental role of epigenetic in NB development and prognosis of the patients.

Epigenetic modifications are reversible changes that influence gene expression by regulating the chromatin accessibility, chromatin remodelling, DNA methylation and acetylation, histone modification and non-coding RNAs (Bird, 2007). The role of epigenetic modifications in NB has been analysed. In one of the first studies, a microarray-based DNA methylation profile was performed on primary neuroblastic tumours. Epigenetic changes characteristic for NB tumours were identified, such as the loss of DNA methylation on genes known to be involved in NB and hypermethylation on specific targets involved in cell development and proliferation (Decock et al., 2012; Mayol et al., 2012).

Nevertheless, the methylations do not involve only DNA but also structures that regulate epigenetics, such as the histone proteins. Other studies reported aberrant DNA methylation and histone methylation, and demethylation was associated with it. For example, lysine methyltransferase 5A (KMT5A), and H4K20me1 methyltransferase, seem to promote the survival of NB cells by suppressing p53 mediated apoptosis (Veschi et al., 2017). Overexpression of DOT1–like histone lysine methyltransferase has been correlated to the expression of high levels of MYCN and the E2F transcription factor, known triggers of NB associated with poor prognosis. Furthermore, lysine demethylase 4B (KDM4B) is another important actor in the epigenetic regulation of MYCN signalling via histone demethylation (Yang et al., 2015). On the other hand, methylation has an important impact on the epigenetic like the acetylation, a mechanism that was reported to be associated with cancer, including NB; for example, histone deacetylase 5 (HDAC5) mediated transcriptional suppression of CD9 in NB has been associated with poor diagnosis (Fabian et al., 2016).

1.1.2 Dysregulation of neural crest differentiation and neuroblastoma

NB is an extremely heterogeneous tumour deriving from undifferentiated cells of the neural crest. Neural crest (NC) cells are a transient population of multipotent cells that arise from the dorsal region of the closing neural tube beneath the embryonic ectoderm germ layer.

During embryogenesis, the NC cells undergo epithelial-to-mesenchymal transition (EMT), which enable these cells to delaminate, migrate and differentiate into a wide variety of cell types contributing to the development of specific anatomical structures within the organism. Given the

variety of lineages generated, the neural crest has been described as the fourth germ layer (Hall, 2000).

In detail, the migration of these cells involves two major pathways, the dorsolateral and the ventral. In the dorsolateral pathway, the cells become melanocytes, able to colonise the skin and hair follicles (Erickson et al., 1992; Mayer, 1973). In the ventral pathway, trunk neural crest cells (NCC) become sensory and sympathetic neurons, adrenomedullary cells, and Schwann cells (Le Douarin and Teillet, 1974; WESTON, 1963)).

The EMT process and part of the directionality of NC cell migration are influenced by multiple environmental signals, activation of transcriptional programs, and epigenetic events (Carmona-Fontaine et al., 2008; Theveneau and Mayor, 2012).

Dysregulation of factors involved in different neural crest maturation stages could affect cell specification, migration, and differentiation. These alterations lead to hyperplastic lesions, which ultimately results in NB development (Johnsen et al., 2019). The main actors involved in the perturbation of neural crest maturation and thought to be important for NB development are among the others: MYCN, LIN28B, ALK, PHOX2B, RHO, SWI/SNF, BMP, FGF, and wnt signalling pathways (**Figure 1.2**).

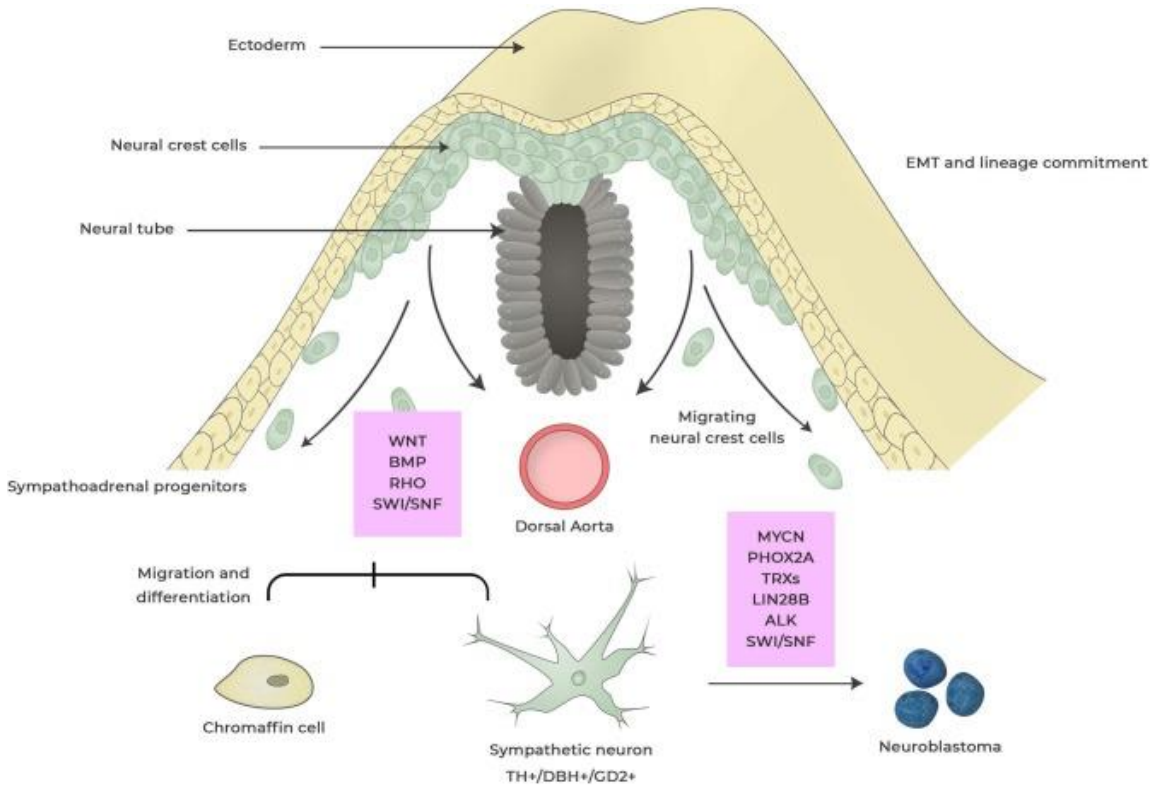

Figure 1.2. NB insurgence during neural crest development (Johnsen et al., 2019).

MYCN is expressed in high levels in the early post-migratory neural crest and has a critical role in regulating the ventral migration and expansion of cells within the neural crest during the normal sympathoadrenal development (Zimmerman et al., 1986). In physiological conditions, sympathoadrenal precursor cells maturate into neural or chromaffin cells. The insurgence of NB is often linked to the fact that aberrant sympathoadrenal precursor cells cannot respond adequately to signals that determine the neuronal or chromaffin cell fate (Marshall et al., 2014; Zimmerman et al., 1986). Several studies have shown that the increased and sustained expression of MYCN in NC cells is sufficient for NB development, clearly demonstrating that MYCN is a major oncogenic driver in neuroblastoma (Althoff et al., 2015; Olsen et al., 2017; Rasmuson et al., 2012; Weiss et al., 1997; Zhu et al., 2012).

During embryogenesis, LIN28B is important for maintaining an undifferentiated state (Marshall et al., 2014; Rybak et al., 2008). Indeed, LIN28B regulates the expression of *let-7* miRNAs, which regulates proliferation during the neural crest lineage commitment and maintenance of stemness in embryonic development (Rybak et al., 2008). LIN28B overexpression during NC maturation inhibits sympathoadrenal cell differentiation and accelerates NCC migration, leading to NB onset in two vertebrate models, Xenopus leavis and Danio rerio (Corallo et al., 2020).

ALK plays a crucial role in the proliferation of sympathetic neurons and enlargement of the sympathetic ganglion (Motegi et al., 2004). Therefore, aberrant ALK activation leads to cellular transformation within the neural crest (Johnsen et al., 2019). Moreover, ALK mutations, together with PHOX2B mutations, are germline mutations found in neuroblastoma.

Other factors play a crucial role in the insurgence of NB during NC differentiation. A coordinated set of signals derived from the Wingless (Wnt), bone morphogenetic protein (BMP), and fibroblast growth factor (FGF) pathways is necessary for the NC cells to acquire the mobility needed to migrate (Goldstein et al., 2005). The Wnt pathway is a signalling cascade involved in cell polarity and the initiation of migration of NC cells (Sebbagh and Borg, 2014). In NB patients, different factors of this signal cascade, such as Rho and ROCK2, have been found mutated (Dyberg et al., 2017; Molenaar et al., 2012b).

Interestingly, the mutations in Rho GTPases and related genes reported in NB have also been associated with other cancers like melanoma. Rho, Rac and Cdc42 are involved in the Eph/ephrin internalisation and signalling, which regulates cell migration, cytoskeleton remodelling, axon guidance, and stimulates angiogenesis tissue separation (Wislet et al., 2018; Xu and Wilkinson, 2013). High levels of Eph/ephrin are linked to low-risk NB (Tang et al., 2000).

BMP signalling also plays a crucial role in development. Indeed, during embryogenesis, the differentiation of sympathetic neurons in the neural crest is induced by the BMP family. BMPs induce differentiation by regulating a set of transcription factors such as Phox2b, Phox2a, Sox4, Sox11, Gata2/3, Hand2 and Ascl1 (Howard et al., 2000; Rohrer, 2011; Tsarovina et al., 2004). Interestingly, these factors have often been linked to NB. For example, *PHOX2B* is a master gene involved in the development of the entire peripheral autonomic nervous system (Pattyn et al., 1999). Mutations in *PHOX2B* block the entire transcriptional network involved in the differentiation of sympathetic neurons and promote the proliferation of neural precursors cell, with important biological consequences linked to the pre-neoplastic development (Dubreuil et al., 2000; Pattyn et al., 1999).
Finally, mutations in the *α-thalassaemia/mental retardation syndrome X-linked* (*ATRX*) have been identified in NB patients not older than 18 months with poor prognosis (Cheung et al., 2012). ATRX encodes for SWI/SNF chromatin-remodelling ATP-dependent helicases, responsible for the reorganisation of the nucleosome during transcription, replication, and DNA repair, required for DNA accessibility (Tang et al., 2010). This highlights the critical function of ATRX in cellular transformation. Furthermore, the SWI/SNF chromatin remodelling complex was reported as mutated in 20% of human cancer (St Pierre and Kadoch, 2017) and played an essential role in NB development in neural crest cells (Johnsen et al., 2019).

Taken together, the described evidence suggests that mutations on the different actors involved in the NC migration and maturation could have a catastrophic impact and determine the insurgence of NB. Moreover, the variety of the different lineages into which NC cells can differentiate could partially explain the heterogeneity characterising NB tumours.

1.2 CLINICAL LEVEL

1.2.1 Diagnosis

NB is characterised by a high heterogeneity of symptoms, position, and age of tumour insurgence, making the disease diagnosis difficult. In the last years, thanks to imaging techniques, measurement of metabolites, identification of cell surface targets and genetic analysis, the knowledge of the disease has increased, and new discoveries have allowed a better identification

and classification of NB patients (Johnsen et al., 2019). The complexity of the disease required the simultaneous evaluation of biological and genetic markers to obtain an accurate diagnosis. **Table 1.2** summarises some of the preliminary biological markers applied to diagnose NB in patients.

Table 1.2. preliminary biological markers used for NB diagnosis.

Marker applied in NB diagnosis	Note	References
A significant increase of catecholamine metabolites in urinary samples	observed in 90-95% of NB patients	Graham-Pole et al., 1983; LaBrosse et al., 1980
Disialoganglioside (GD2)	GD2 is a protein that plays an essential role during embryonic development in neural and mesenchymal stem cells. It was detected with immunohistochemical analysis. In the last 20 years, anti-GD2 antibodies have been used to treat high-risk NB in combination with GM-CSF and IL-2	Ladenstein et al., 2013; Mody et al., 2017
Neurotrophin receptors (TrkA, TrkB and TrkC)	TrK are tyrosine kinases required for proper development and maintenance of the peripheral nervous system. High expression of TrkA is a marker for low-grade NB inclined to spontaneous regression or differentiation. An increased expression of TrkB is associated with high-risk disease and poor prognosis. In high-risk NB patients, TrkB is activated by its ligand brain-derived neurotrophic factor that leads to autocrine and paracrine tumour cell survival.	Acheson et al., 1995; Haddad et al., 2017; Kogner et al., 1993; Matsumoto et al., 1995; Nakagawara et al., 1994

The genomic analysis is an essential instrument to deeply investigate the status of the patients. For example, NB low-risk patient-derived cells showed a hyperdiploid in their chromosomal makeup, while NB high-risk patient-derived cells showed a segmental chromosomal aberration (Ambros et al., 2009; Carén et al., 2010; Irwin and Park, 2015; Matthay et al., 2016; Morgenstern et al., 2014). Moreover, it is known that the most frequent chromosomal aberrations in high-risk

NB are the amplification of the *MYCN* gene and the rearrangements in the proximal area of the telomerase reverse transcriptase (*TERT*) that ultimately results in chromosomal changes, DNA methylation and enhanced TERT expression(Hungate et al., 2017; Maris, 2010; Peifer et al., 2015; Valentijn et al., 2015).

1.2.2 Therapies

At present, several therapeutic approaches are applied to treat NB depending on different criteria, such as the NB risk classification, the localisation of the tumour, and its size (https://www.cancer.net/cancer-types/neuroblastoma-childhood/types-treatment).
For children with very-low-risk and low-risk NB, the treatment approach aims to deliver the minimum therapy while maintaining excellent patient survival. Children with intermediate-risk NB are usually treated with two to eight cycles of chemotherapy. When possible, the residual primary tumour is then resected by surgery.
The current treatment regimen for high-risk NB is, instead, more complex and is the results of years of NB treatments in which new therapies have been added to old ones. In particular, the addition of radiation therapy, immunotherapy, autologous stem cell transplant, and differentiating agent 13-cis-retinoic acid has managed to increase patient survival from less than 15% to 50% (Smith and Foster, 2018). Unfortunately, although aggressive, the treatments have a long-term effect on less than 50% of high-risk NB patients (Applebaum et al., 2017).In detail, the therapeutic approach is divided into three main phases: induction, consolidation, and maintenance (**Figure 1.3**).

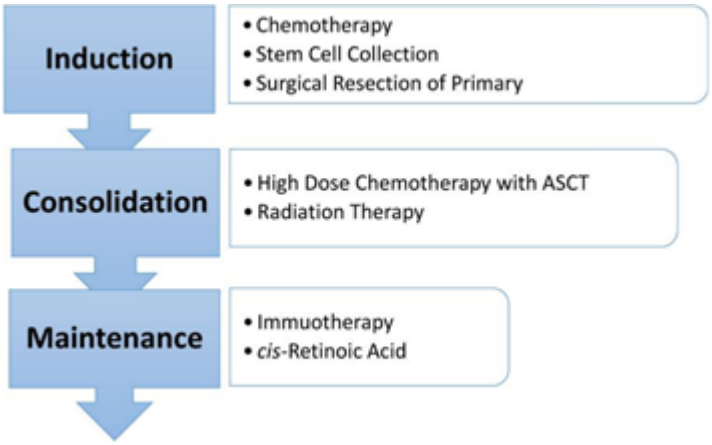

Figure 1.3. Schematic representation of NB high-risk patients treatments (Smith and Foster, 2018).

In the induction phase, NB patients receive 5-8 cycles of chemotherapy with platinum-based compounds, alkylating and topoisomerase agents, with a median of fourteen days of treatments per cycle (Garaventa et al., 2018; Kushner et al., 2004; Peinemann et al., 2015a). It has been demonstrated that chemotherapy before surgery increases tumour resection success by 45% (Adkins et al., 2004; Fischer et al., 2017).

The consolidation phase is based on chemotherapy, followed by autologous transplant (ASCT) of previously collected stem cells, to restore the bone marrow function. The chemotherapeutic agents used in this phase are different between the USA and Europe. In fact, in the USA, carboplatin, etoposide, and melphalan are used, while in Europe, busulfan/melphalan, endowed with reduced hepatic and renal toxicity, are the primary choice (Gaze et al., 2013; Ladenstein et al., 2017). In some cases, when a specific molecular target is identified, small molecules able to specifically hit that target are added to the therapy. For example, Crizotinib is used to inhibit the ALK and MET kinase activity (Malik et al., 2014; Mossé et al., 2013), Lorlatinib and Ceritinib are inhibitors respectively of ALK/ROS1 and ALK (Friboulet et al., 2014; Infarinato et al., 2016; Khozin et al., 2015; Shaw et al., 2014), TRK receptors family are inhibited by Entrectinib or Larotrectinib (Ardini et al., 2016; Iyer et al., 2016), or RAS MAPK/ERK pathways are targeted by drugs such as Binimetinib, Trametinib and Dabrafenib (Menzies and Long, 2014; Tanaka et al., 2016; Wright and McCormack, 2013).
Furthermore, the consolidation phase comprises radiation therapy, often characterised by high toxicity. The introduction of proton radiation therapy represents a great alternative that promises to reduce toxicity (Hattangadi et al., 2012; Peinemann et al., 2015b).

The last phase, the maintenance phase, is implemented for all the patients with residual NB tumour cells, resisting the intensive treatment regimen. In these cases, the strategy aims to prevent NB re-insurgence and is based on immunotherapy with an anti-ganglioside 2 (GD2) chimeric monoclonal antibody (Matthay et al., 2016; Yu et al., 2010). The best clinical outcome is obtained with the combination of the anti-GD2 antibody and 13-*cis*-retinoic acid and cytokines GM-CSF and IL-2 (Cheung et al., 2012; Zhou et al., 2015). The 13-*cis*-retinoic acid (RA) is one of the most potent differentiation inducers of NB cells, which acts by interfering with transcription, leading to cell proliferation arrest (Reynolds et al., 2003; Sidell et al., 1983). The use of RA in NB treatments represents a new approach that aims at reducing tumour size thanks to the differentiation of tumour cells.

1.3 *LET-7* MIRNA AND LIN28

1.3.1 *Let-7* miRNAs

MicroRNAs (miRNAs) are small non-coding single-stranded RNAs of about 22 nucleotides. They regulate gene expression post-transcriptionally through interaction with the 3' untranslated region (UTR) of target messenger RNAs (mRNAs) (Nilsen, 2007). The binding in the 3'-UTR can lead to either degradation or translation inhibition of the target mRNA. Interestingly, a single mRNA can be regulated by several miRNAs (Stallings, 2009).

The *Lethal-7* microRNA (*let-7* miRNA) has been one of the first miRNA discovered. It was firstly identified in *Caenorhabditis elegans*, where it is a key regulator of tissues developmental timing, therefore regulating the nematode development (Grosshans et al., 2005; Reinhart et al., 2000). Afterwards, *let-7* miRNAs were also identified in other species, and this conservation suggested a crucial role in the regulation of gene expression (Pasquinelli et al., 2000a). However, no *let-7* miRNA has been found in plants (Lee et al., 2016).

A BLAST (basic local alignment search tool) analysis performed comparing *let-7 miRNA* sequences of various species, among which *Caenorhabditis Elegans* (nematode), *Drosophila melanogaster* (fly), *Mus musculus* (mouse) and *Homo sapiens* (human), elucidated the presence of a highly conserved sequence of "UGAGGUAGUAGGUUGUAUAGUU" (Pasquinelli et al., 2000b, 2003). This sequence contains the so-called "seed sequence", essential for recognising the mRNA and, therefore, regulating its maturation. This finding suggested that *let-7* miRNA regulation is conserved across the animal species (Brennecke et al., 2005).

However, although the sequence is partially conserved, higher animals (e.g., mammals) have a set of *let-7* miRNA family members, while nematodes and flies have only one member. In detail, humans have 12 genomic loci, some of which clustered together, that encode nine mature *let-7* miRNAs: *let-7*a, *let-7*b, *let-7*c, *let-7*d, *let-7*e, *let-7*f, *let-7*g, *let-7*i and miR-98 (Roush and Slack, 2008; Ruby et al., 2006).

In mammals, *let-7* miRNAs are expressed during embryogenesis, and brain development and their levels remain elevated in adult tissues (Schulman et al., 2005; Sempere et al., 2004; Thomson et al., 2004). The specific role of *let-7* miRNAs in development still needs to be well-characterised. Nevertheless, it is known that the *let-7* miRNA family has two critical functions: it is a regulator of the terminal differentiation, and it is a tumour suppressor (Lee et al., 2016; Schulman et al., 2005).

1.3.2 *Let-7* miRNA biogenesis and maturation

Let-7 miRNA family maturation and expression are intensely regulated, demonstrating the importance to finely modulate its activity in cells. As depicted in **Figure 1.4**, the maturation of *let-7* miRNAs is a multistep process realised by a pool of different enzymes. Initially, *let-7* miRNAs are transcribed by RNA polymerase II in a long transcript called primary *let-7* (pri-*let-7*) (Cullen, 2004). Subsequently, a group of enzymes called complex of the microprocessor, the RNase-III Drosha and the double-stranded RNA-binding protein Pasha (DGCR8) process the pri-*let-7* in the nucleus leading to a hairpin structure of about 70 nucleotides called pre-*let-7* (Lee et al., 2003). This transcript is exported into the cytoplasm by exportin-5 and, here, is processed by a second RNase III called Dicer, leading to the mature *let-7* miRNAs with a length of about 22 nucleotides (Boyerinas et al., 2010; Hutvágner et al., 2001). The mature *let-7* miRNAs are incorporated into the RNA-induced silencing complex (RISC) that binds the target mRNA and inhibits its translation (Lai, 2002).

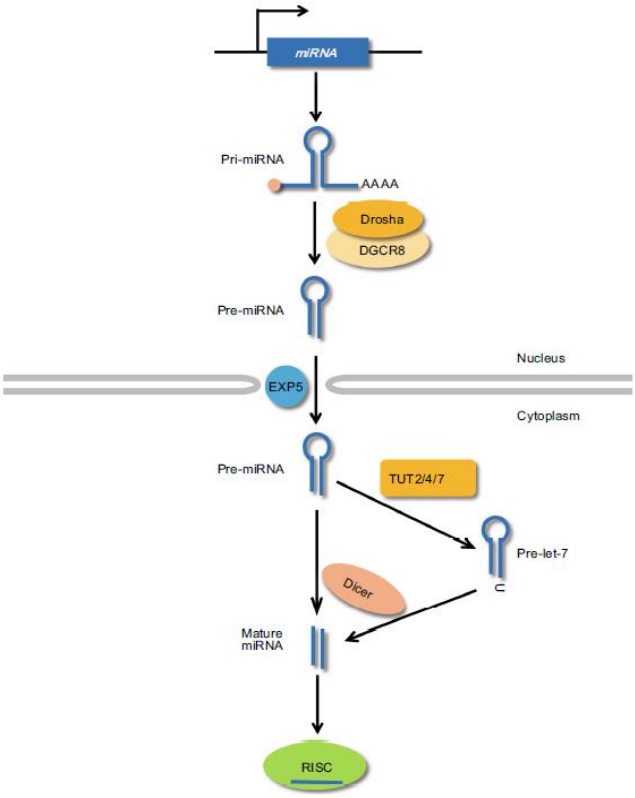

Figure 1.4. *let-7* miRNA biogenesis. The primary miRNA transcript is synthesised by RNA polymerase III and processed by Drosha and DGCR8 in the nucleus. This pre-miRNA is then exported in the cytoplasm, where Dicer further processes the precursor leading to mature *let-7* miRNA. The miRNA is then included into RISC complex and can bind its target mRNA. (adapted from Lee et al., 2016).

The mature *let-7* miRNA regulates several transcription factors, and most of them control the expression of *let-7* itself, creating auto-regulatory circuits. Among the others, the pluripotency promoting factors LIN28, OCT4, SOX2, NANOG, TCL3, or HMGA2, IMP proteins and MYC, are directly involved in these regulatory circuits (Boyerinas et al., 2008).

1.3.3 *Let-7* miRNA in cancer: targets and function

The role of *let-7* miRNAs in cancer has been extensively investigated over the years.
Let-7 miRNAs down-regulation has been associated with a poor prognosis in many cancer types, such as lung cancer (Takamizawa et al., 2004), head and neck squamous cell carcinoma (Childs et al., 2009), ovarian cancer (Shell et al., 2007), acute lymphoblastic leukaemia (Mi et al., 2007), hepatocellular cancer (Johnson et al., 2007), retinoblastoma (Nam et al., 2008), breast cancer (Yan et al., 2008) and prostate cancer (Ozen et al., 2008). Although most of the studies have reported a *let-7* miRNA downregulation in cancer, there are also tumours in which some *let-7* miRNA family members are found at higher levels, as in the case of *let-7*b and *let-7*i in high-grade lymphoma (Lawrie et al., 2009).
The role of *let-7* miRNAs as tumour suppressors has been elucidated in different studies. In particular, it has been demonstrated that these miRNAs play an important role in inhibiting tumour growth by regulating the activity of important oncogenes involved in proliferation and tumorigenesis.
Let-7 miRNAs have different targets, among which RAS, HMGA2 and MYC can be considered as the most characterised.
RAS was the first target of *let-7* miRNAs identified in mammals by a computational screening performed in *C. elegans* (Johnson et al., 2005). Moreover, the correlation between RAS and *let-7* miRNAs levels was observed in non-small cell lung cancer (NSCLC), where the ectopic overexpression of *let-7*g in a mouse model was shown to inhibit the tumour growth by RAS suppression (Kumar et al., 2008).
Another direct target of *let-7* miRNA family members is the High-mobility group AT-hook 2 (HMGA2), an embryonic oncofetal gene highly expressed in stem cells (Lee and Dutta, 2007; Mayr et al., 2007; Nishino et al., 2008; Shell et al., 2007). Interestingly, the expression of HMGA2 in stem cells correlates with low levels of *let-7* miRNAs, indicating that this circuit is directly involved in the maintenance of the undifferentiated state (Boyerinas et al., 2008). HMGA2 is generally overexpressed in different tumours, such as uterine leiomyomas, intracranial tumours, lung and

ovarian cancer. In all these tumours, the loss of *let-7* miRNAs and the consequent expression of HMGA2 is associated with high aggressiveness of the tumour (Peng et al., 2008; Qian et al., 2009). MYC proteins are one of the main *let-7* miRNAs family targets. MYC proteins (MYCN, C-MYC and MYCL) regulate different cell fate processes, which are often activated in various tumour types (Albihn et al., 2010). The alteration of MYC expression has been characterised in different cancers, such as colon, breast, and cervix (von Eyss et al., 2015; Kugimiya et al., 2015; Zhu et al., 2014). The mutations found in the *myc* gene leads to the increased expression of the protein, which consequently causes the altered expression of its targets involved in cell cycle regulation and apoptosis (Ruggero, 2009). In Burkitt lymphoma, *let-7*a miRNA has been shown to directly bind the 3'UTR of MYC mRNA and inhibit its expression (Sampson et al., 2007). A similar downregulation has also been detected in colon cancer (Akao et al., 2006; Sampson et al., 2007).
The discussed oncogenes are only some examples of the complex network modulated by *let-7* miRNA. Also, *let-7* regulates several critical components of the cell cycle, as revealed in lung cancer and hepatocellular carcinoma cell lines studies (cyclin A2, *CDC34 E2F5, CDK8 PLAGL2,* among others). Moreover, *let-7* miRNA inhibits different DNA replication components (e.g. *ORC1L; RRM1*) and transcription factors such as PLAGL2 and SOX9 (reviewed in Barh et al., 2010).

1.3.4 The RNA binding proteins LIN28A and LIN28B

LIN28 was described for the first time in 1984, when Ambros and colleagues studied its role in *C. elegans*, showing that LIN28 is a heterochronic gene that regulates developmental timing (Ambros and Horvitz, 1984). LIN28 protein has been found expressed in different tissues of the larva, including muscle and neurons, and its expression was demonstrated to be down-regulated in these tissues after the first larval stage in part by *lin-4* miRNA mediation. To achieve healthy development, it is crucial that the expression of LIN28 is timely regulated (Moss et al., 1997; Seggerson et al., 2002). When the 3' UTR of LIN28 is mutated, *lin-4* miRNA cannot bind its complementary sequence, and therefore the down-regulation fails. If LIN28 levels are maintained high, various events of the second larval stage are skipped, and the later stages occur prematurely, leading to an incorrect development (Moss et al., 1997).
Vertebrates have two LIN28 paralogs: LIN28A and LIN28B, encoding respectively for 209 and 250 amino acid proteins, which present a high degree of homology in their structure and functions. Both LIN28A and LIN28B share a similar structure characterised by a C-terminal cold shock domain (CSD) and two N-terminal tandem cysteine histidine cysteine (CCHC) zinc knuckle

domains (ZKD), linked by a flexible region (Guo et al., 2006; Nam et al., 2011; Wang et al., 2017). The *let-7* miRNA family members are the most studied LIN28A and B interactors. Studies of LIN28 A and B crystal structures have demonstrated that these proteins bind to precursor forms of *let-7* (pri- and pre-*let-7*) using both the CSD, which binds to the terminal loops (GNGAY motifs) of the *let-7* miRNA precursor and contributes to most of the LIN28-*let-7* binding affinity, and the ZKD, which interacts with a highly conserved GGAG sequence motif (Nam et al., 2011)(**Figure 1.5**).

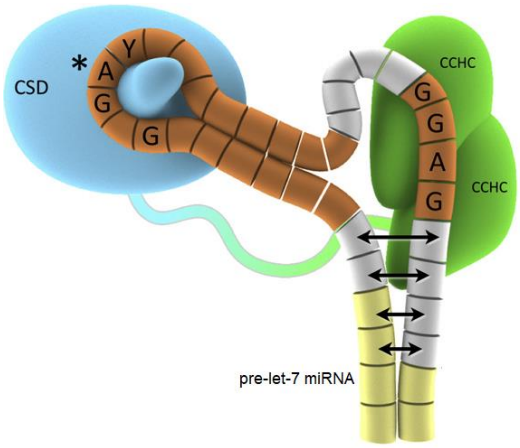

Figure 1.5. Schematic representation of LIN28A/B structure and interaction with pre-*let-7* miRNAs. LIN28 A/B structure: cold shock domain (CSD, blue), tandem cysteine histidine cysteine (CCHC) in the zinc knuckle domains (ZKD, green), flexible linker (blue and green). pre-*let-7* miRNA structure: sequence of interaction with LIN28 A/B (brown), terminal loop (yellow). Adapted from (Nam et al., 2011).

Upon binding, LIN28A and B prevent *let-7* miRNA maturation and lead to decreased levels of mature *let-7* miRNAs, influencing organismal differentiation and development. Despite the high degree of sequence identity, LIN28A and LIN28B bind the precursor of *let-7* miRNA at different stages of its maturation due to the distinct subcellular localisation of the proteins (Piskounova et al., 2011).

A schematic representation of LIN28A and LIN28B roles in *let-7* miRNAs regulation is shown in **Figure 1.6.**

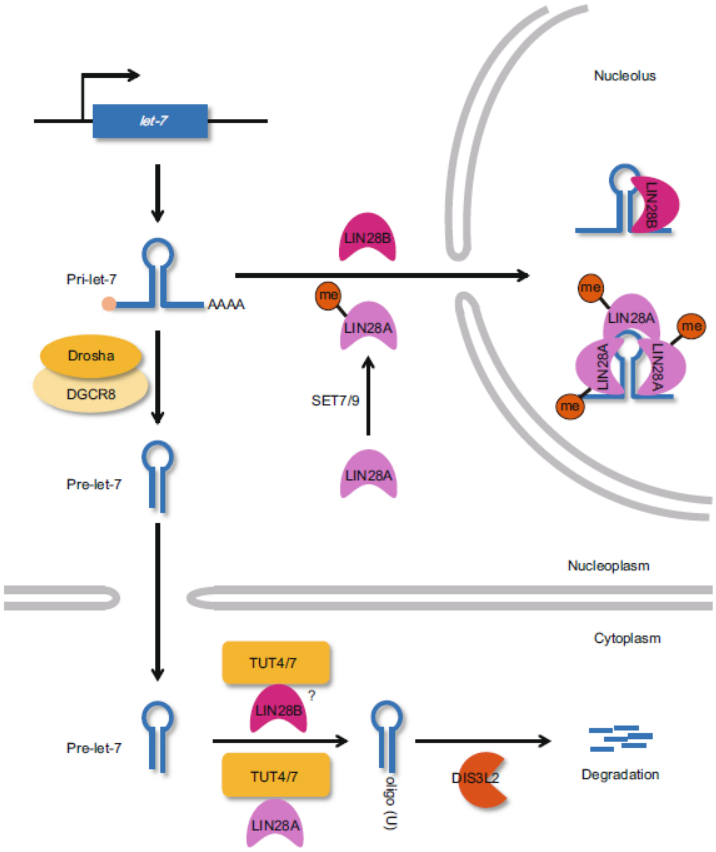

Figure 1.6. LIN28A and LIN28B regulate *let-7* miRNA biogenesis at different stages of miRNA maturation. LIN28A and LIN28B inhibit the maturation of *let-7* miRNA in different ways, both TUTase dependent and TUTase independent. Figure credit Lee et al., 2016.

LIN28A is predominantly cytoplasmic: it first binds the terminal loop of pre-*let-7* miRNA and recruits the terminal uridylyltransferase 4 (TUT4) that polyuridylates the miRNA and interferes with Dicer cleavage, leading to miRNA degradation (Hagan et al., 2009; Thornton et al., 2012). However, LIN28A can interfere with the processing of *let-7* miRNA also in the nucleus via Drosha mediation.

The precise mechanism by which LIN28B interferes with the biogenesis of *let-7* miRNA is still not clear since there is discordant evidence regarding its subcellular localisation. During the past years, different models of action have been proposed. A first model suggested that LIN28B binds pri-*let-7* in the nucleus, blocking the microprocessor activity (Newman et al., 2008). On the other hand, a second model suggested that LIN28B binds pre-*let-7* in the cytoplasm and inhibits the activity of Dicer (Rybak et al., 2008). Another work showed that LIN28B could induce the poly uridylation of pre-*let-7* directly via an unidentified TUTase, leading to miRNA degradation (Heo

et al., 2008). In 2011, Piskounova and colleagues demonstrated that LIN28B has a nucleolar localisation sequence, and therefore the inhibitory activity is exerted by sequestering pri-*let-7* miRNA in the nucleus (Piskounova et al., 2011). However, Suzuki and colleagues demonstrated that LIN28B directly interacts with the 3′-5′ endonuclease DIS3L2 in cancer cell lines that express the protein (Suzuki et al., 2015). Therefore, it seems that also LIN28B has an affinity for TUTase and takes part, similarly to LIN28A, in the cytoplasmatic down-regulation of *let-7* miRNA (Suzuki et al., 2015). In conclusion, the precise mechanism of LIN28B-mediated *let-7* repression and if this activity is TUTase dependent remains to be clarified.

Besides the long-isoform of 250 amino acids coding for both the CSD and the ZKD, LIN28B also has a short-isoform of 180 amino acids, lacking the CSD. This isoform conserves the ability to bind the precursor of *let-7* miRNA but is unable to inhibit the activity of the microprocessor and Dicer, so the protein cannot prevent the maturation of the miRNA (Mizuno et al., 2018a).
Interestingly, LIN28 A and B can also act in a *let-7*-independent way, altering gene regulation post-transcriptionally by directly targeting their mRNAs and influencing their translation. Indeed, LIN28A has been shown to bind the coding region and the 3'UTR of mRNAs involved in cell cycle regulation, as histone H2a, Cyclin A, Cyclin B and CDK4, leading to an increase of their expression, and consequently to the induction of cells proliferation (Xu et al., 2009).

1.3.5 LIN28B in cancer

In normal conditions, LIN28B is highly expressed in the early stage of development and in undifferentiated cells and tissues, and its expression decreases as the development proceeds or upon differentiation. LIN28B is normally absent in most differentiated cells in adults. In healthy tissues, LIN28B can be found expressed only in the testis, placenta and foetal liver (Guo et al., 2006). Many human cancers show reactivation of LIN28A or LIN28B, whose expression is usually mutually exclusive (Balzeau et al., 2017; Piskounova et al., 2011). LIN28A and LIN28B are recognised oncogenic drivers, which are abnormally expressed in ~15% of human cancer cell lines (Viswanathan et al., 2009).
LIN28B is reactivated and plays a role in different cancers such as ovarian cancer (Helland et al., 2011), prostate cancer (Tummala et al., 2013), Wilms tumour (Urbach et al., 2014), colon cancer (Pang et al., 2014), multiple myeloma (Manier et al., 2017), medulloblastoma (Hovestadt et al., 2014; Northcott et al., 2009) and neuroblastoma (Diskin et al., 2012). In these tumours, the high

expression of LIN28B and the consequent decrease of *let-7* miRNAs correlate with poor prognosis. LIN28B has also been shown to play an important role in cancer stem cell formation and tumour metastasis (Zhou et al., 2013). Finally, LIN28B expression has been correlated to chemotherapy resistance in several cancers (Balzeau et al., 2017).

The expression of LIN28B in human cancer can be induced by different processes, such as genomic amplification and aberrant hypomethylation. The analysis of SNP array data from 3330 primary tumours showed that amplifications of the locus 6q21 containing LIN28B are rare and, therefore, are not the principal mechanism of protein reactivation. The analysis of the methylation status of the CpG sites of LIN28B, instead, showed aberrant hypomethylation in cells expressing high levels of the protein, suggesting that this alteration can be responsible for the transcriptional activation of LIN28B in the tumours (Viswanathan et al., 2009). Another event that might cause LIN28B aberrant expression is the alteration of its regulators, such as mutations of miR-125b, which is one of the LIN28B direct inhibitors (Liang et al., 2010; Molenaar et al., 2012a).

1.3.6 LIN28B/*let-7* axis in neuroblastoma

The first genome-wide association study for familial NB unveiled SNPs in the *Lin28B* gene correlated with higher susceptibility to tumour development, more aggressive disease and a lower patient survival rate. Indeed, high levels of LIN28B in NB have been associated with the aggressive form of the disease and have been linked to poor prognosis (Diskin et al., 2012). Moreover, in 2012 Molenaar and colleagues demonstrated that LIN28B is an oncogenic driver in NB. Its forced expression in sympathoadrenal cells of nude mice was sufficient to induce the development of a tumour mass with the typical gene expression profile of NB: Dbh, Th, PhoX2b and MYCN (Molenaar et al., 2012a).

Since the physiological activity of LIN28B during the sympathetic nervous system development remains to be clarified, it is not completely clear why and in which manner the overexpression of LIN28B leads to NB (Hennchen et al., 2015). However, what is known is that LIN28B has a significant impact on the NB insurgence because it can coordinate the expression level of some oncogenes, such as RAN and AURKA, through the *let-7* miRNA family (Schnepp et al., 2015). Moreover, due to *let-7* miRNA mediation, the overexpression of LIN28B increases MYCN expression, one of the principal risk factors for developing NB (Molenaar et al., 2012; Powers et al., 2016). This highlights how the LIN28B-*let-7*-MYCN signalling axis plays a key role in NB insurgence.

LIN28B also has a role in NB development not dependent on the LIN28B/*let-7* signalling axis. For example, in a zebrafish model, it was observed that LIN28B overexpression leads to NB cell survival and migration by directly interacting with the transcription factor ZNF143, which is involved in the regulation of chromatin looping and gene expression (Tao et al., 2020). Different genes correlated to NB metastasis formation, such as *GSK3B*, *L1CAM*, and *ETV1,* are also regulated by this LIN28B circuit (Chikano et al., 2015; Gonzalez Malagon et al., 2018; Hur and Zhou, 2010; Raveh et al., 2009). Moreover, a further demonstration of LIN28B crucial role in NB is given by the fact that increased LIN28B expression induces neural crest cell migration, supporting NB onset (Corallo et al., 2020).

Based on these premises, the LIN28B/*let-7* axis can be considered an interesting molecular target in NB, whose inhibition could lead to cell proliferation arrest and cell differentiation induction. This potentially innovative therapeutic strategy deserves further exploration.

2. PROJECT AIM

Neuroblastoma (NB) is a tumour arising from neural crest cells during the sympathetic nervous system development. The median age at diagnosis is 18 months, and 90% of the children that develop the disease have less than 10 years. The tumour's main characteristic is its biological heterogeneity which reflects a large variability in the clinical outcome, ranging from spontaneous regression to rapid progression.

Unfortunately, 50% of patients are affected by the clinically aggressive form of NB. Despite the strength of the current therapies mainly focused on eliminating the cancer cells and characterised by high toxicity, 20% of these children are entirely refractory to the treatment, and 60% will relapse. There is an urgent need to find new strategies to improve the survival rate and long-term life quality. Indeed, identifying new therapeutic approaches specific for selected targets holds great promise for improving the survival rate and reducing chemotherapies' side effects.

In the last years, the characterisation of new targets in NB has been one of the main focus due to the importance of increasing the knowledge on the disease and creating target specific treatments.

In this panorama, the LIN28B/*let-7* miRNAs axis assumes a critical interest. Indeed, LIN28B is an oncogenic driver in NB, and its overexpression is associated with a poor prognosis. When LIN28B is overexpressed, the principal consequence is the inhibition of *let-7* miRNA maturation and expression. *Let-7* miRNAs are tumour suppressors that directly regulate genes involved in different essential functions such as cell proliferation, differentiation, and migration. The activity of LIN28B and, thus, the decrease of *let-7* miRNAs level promotes the maintenance of undifferentiated cellular state, increasing tumour growth and aggressiveness.

Therefore, therapeutic strategies able to interfere with the LIN28B/*let-7* axis are endowed with the potential of affecting fundamental features of a tumour, such as proliferation and stemness maintenance, promoting cell differentiation, and ultimately leading to tumour mass regression.

Basing on this hypothesis, this project aimed at:

- creating a cellular model to evaluate the biological consequences of LIN28B inhibition, with a particular focus on the induction of differentiation;
- identifying a small molecule able to interfere with the LIN28B/*let-7* miRNA interaction, leading to the increase of miRNA maturation, using both high- and low-throughput screening approaches;
- evaluating and characterising the biological effects induced by the molecule on NB cell lines using different *in vitro* assays.

Given the urgent medical need for novel therapeutic approaches in NB treatment, the final ambitious goal of this project was to identify and preliminary characterise a new candidate molecule for further preclinical and clinical studies.

3. RESULTS

3.1 LIN28B DOWNREGULATION

With the aim to better understand the effects of the LIN28B/*let-7* axis modulation in NB we created LIN28B down-regulated models in NB cell lines. We used two NB cell lines with different MYCN amplification status to study the impact of LIN28B/*let-7* axis modulation in the presence/absence of another prognostic aberration typical of high-risk NB. In detail, we selected the NB69 and CHP134 cell lines, which express different LIN28B levels and are, respectively, MYCN-non amplified and MYCN-amplified. The stable downregulation was obtained with lentiviral particles loaded with a shRNA sequence targeting human LIN28B (shLIN28B). A scrambled shRNA was used as control. We evaluated LIN28B mRNA expression level via RT-qPCR, detecting a statistically significant reduction of about 53% in CHP134 and 40% in NB69 compared to the control (**Figure 3.1A**). We also verified the effective modulation of LIN28B protein by immunoblotting (**Fig 3.1B**, *left*). The quantification of three biological replicates showed a statistically significant LIN28B reduction of 54% and 66% for CHP134 and NB69, respectively, compared to the control (**Fig 3.1B**, *right*). As extensively discussed in the introduction, LIN28B expression causes the inhibition of *let-7* miRNAs maturation leading to a decrease in their expression levels and consequently to the induction of cell differentiation and the decrease in tumour proliferation (Hennchen et al., 2015; Roush and Slack, 2008). To address if the downregulation of LIN28B indeed affects this process, we evaluated the levels of four *let-7* miRNA family members (*let-7d, let-7f, let-7g, let-7i*) by RT-qPCR in shLIN28B CHP134 and shLIN28B NB69 cells. The results showed a statistically significant increase in almost all the *let-7* miRNA family members in both cell lines (**Figure 3.1C**).

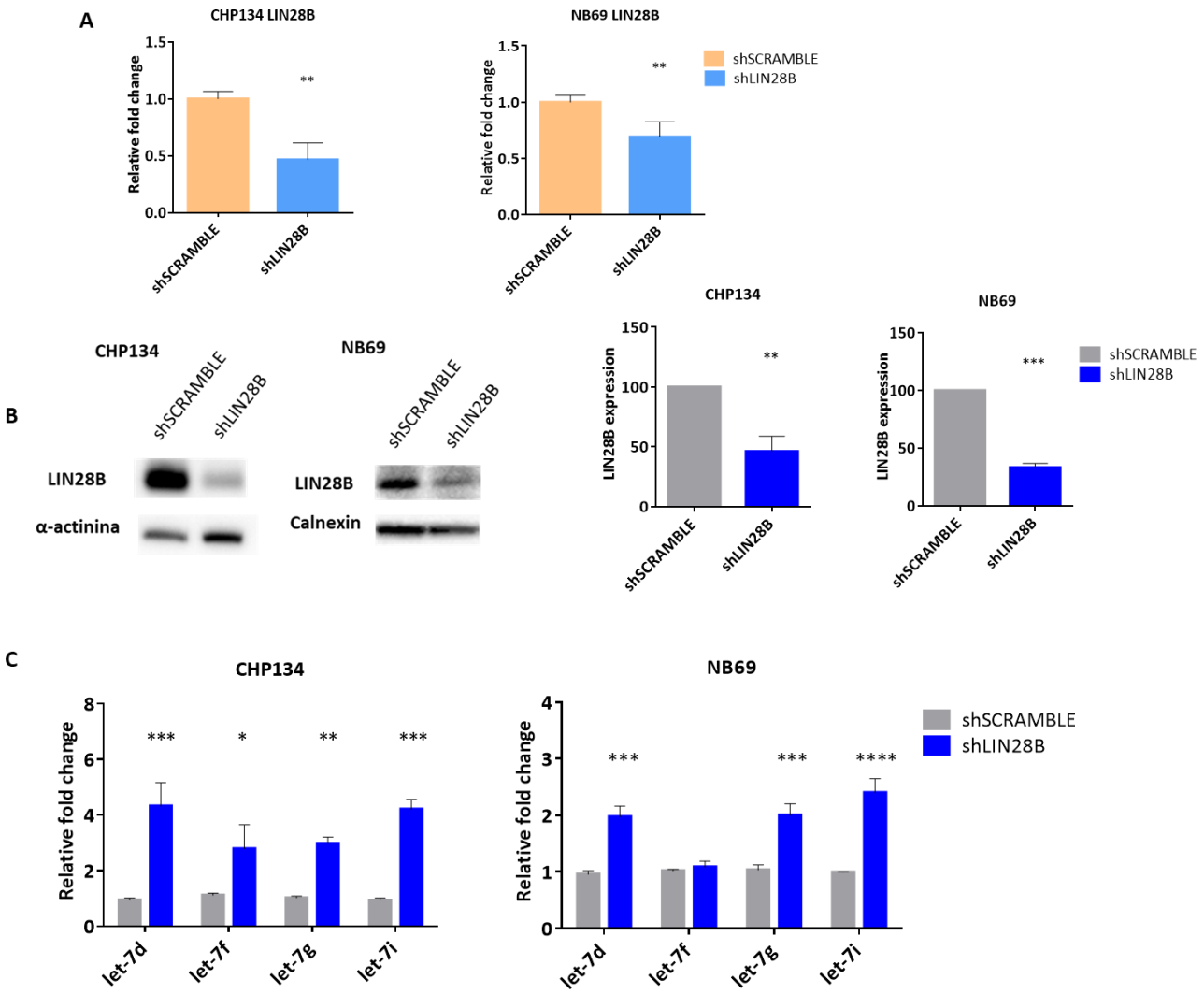

Figure 3.1. LIN28B down-regulation leads to an increase of *let-7 miRNA*s levels.

(A) LIN28B protein expression levels in shLIN28B CHP134 and shLIN28B NB69 cells. shscramble was used as negative control. Representative results of n = 3 biological replicates (left). Quantification of three biological replicates by densitometry analysis. Mean ± SD (right). The statistical analysis was performed using GraphPad Prism, t-test analysis (** P< 0.01; *** P< 0.001). **(B)** LIN28B mRNA expression levels analysed by RT-qPCR in shLIN28B CHP134 and shLIN28B NB69 cell lines. shscramble was used as negative control (indicated as value of 100). The statistical analysis was obtained using GraphPad Prism 6, *t*-test analysis (** P< 0.01). **(C)** *let-7* miRNAs expression levels analysed by RT-qPCR in shLIN28B CHP134 and shLIN28B NB69 cell lines. Fold change relative to scramble control is shown. Mean ± SD. n = 2 biological replicates, n = 3 technical replicates each. U6 was used as housekeeping. The statistical analysis was performed using GraphPad Prism, 2 way-Anova (*P< 0.05; ** P< 0.01; *** P< 0.001; **** P< 0.0001), data distribution has been controlled for normality.

Since the expression of mature *let-7* miRNA family members induces the block of cell proliferation and promotes cell differentiation (Roush & Slack, 2008), we wondered if the general increase of mature *let-7* miRNAs observed in LIN28B down-regulated models was sufficient to induce differentiation in our cell lines. To assess the increase of differentiation, we evaluated the mRNA variation of several stemness-associated markers, such as SOX2 and SOX9. In detail, SOX2 is a stemness-associated marker correlated with inhibition of neural differentiation (Wakamatsu et al., 2004), while SOX9 is a transcriptional factor that drives the cell-specific lineage progenitors and is a direct target of *let-7* miRNAs (Barh et al., 2010; Mizuno et al., 2018b). The induction of differentiation is correlated with a decrease of these markers. Moreover, we analysed the variation of the growth associated protein 43 (GAP43), a sympathetic nervous system differentiation marker that plays a critical role in neuronal growth and stabilisation (Ortoft et al., 1993; Zhao et al., 2012). The expression of GAP43 increases during the differentiation. The results showed that the stable down-regulation of LIN28B and the consequent increase of *let-7* miRNAs led to a significant decrease of SOX2 and SOX9 in both CHP134 and NB69 cell lines. Furthermore, GAP43 mRNA increased, even if statistically significantly only in NB69 cells (**Figure 3.2**).

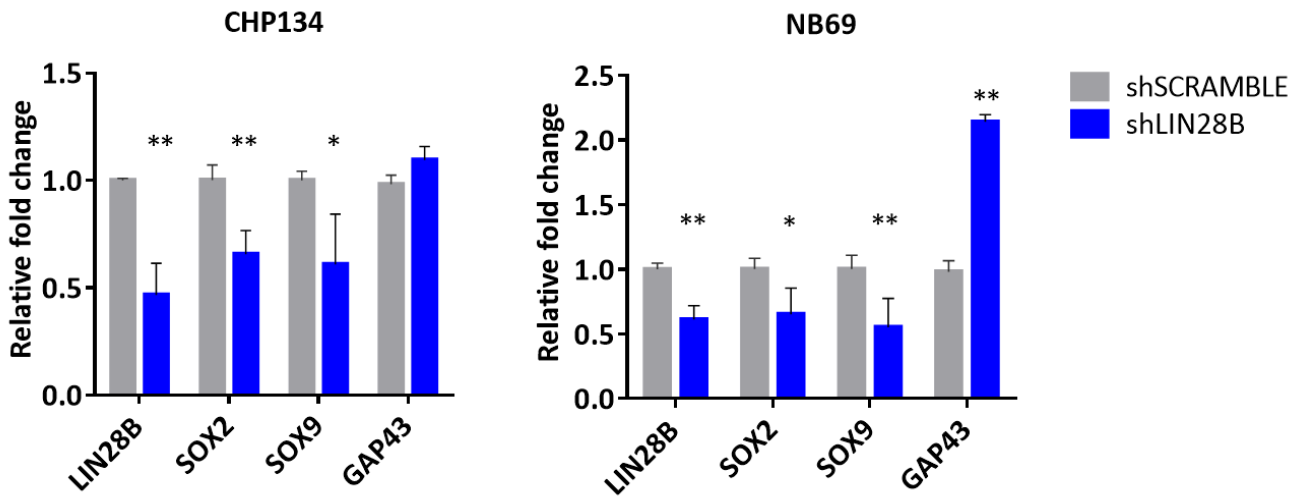

Figure 3.2. LIN28B stable down-regulation leads to a variation of SOX2, SOX9 and GAP43 mRNA levels.

SOX2, SOX9 and GAP43 mRNA expression levels analysed by RT-qPCR in shLIN28B CHP134 and shLIN28B NB69 cell lines. shscramble was used as negative control. SDHA was used as housekeeping. The statistical analysis was performed using GraphPad Prism, unpaired *t*-test

analysis (*P< 0.05; ** P< 0.01;). n = 3 biological replicates, n = 3 technical replicates each, data distribution has been controlled for normality.

3.2 LIN28B/*LET-7* MIRNA AS A DRUGGABLE TARGET

As discussed previously, the heterogeneity and complexity of NB has represented an important obstacle for the development of new therapies. The LIN28B/*let-7* miRNA axis is an interesting druggable target in NB, due to the LIN28B overexpression and the consequent *let-7* miRNA decrease in high-risk disease. Moreover, the activity of *let-7* miRNAs directly correlates with cell proliferation and differentiation, therefore the inhibition of LIN28B activity and the restoration of *let-7* miRNA levels could lead to a reduction of tumour aggressiveness.

In the light of these evidences, we decided to perform a drug screening with the aim to find molecules able to interfere with the interaction between the protein and the miRNA. The screening was performed using two commercial small molecule libraries (MicroSource Discovery Library, TimTec NDL-3000 Library) comprising a total of 5000 molecules, which included FDA approved drugs, natural molecules or drug-like compounds characterised by chemical diversity.

The screening was conducted exploiting the amplified luminescent proximity homogeneous assay (Alpha) technology (Ullman et al., 1994), a technique suitable for a high-throughput format. In this type of assay, a streptavidin-coated donor bead and an acceptor bead coated with an anti-c-MYC antibody are linked together by the specific interaction between the biotinylated precursor *let-7* miRNA and the c-MYC-tagged LIN28B. Following a laser excitation of 680 nm, the ambient oxygen is converted into singlet oxygen by the donor beads' photosensitisers. The molecular oxygen produced reaches the acceptor beads, which produces the emission of light with a wavelength of 570nm. This process only occurs if the donor and the acceptor beads are brought together by the specific protein-RNA interaction. On the contrary, if the protein-RNA interaction cannot take place because of an interfering molecule, a decrease or the absence of emitted fluorescence by the donor beads is observed. **Figure 3.3A** shows a schematic drawing of the Alpha assay technique.

To perform the screening and the following biochemical validation phase, we produced a recombinant LIN28B protein (rLIN28B) by transiently transfecting HEK293T cells. The purification protocol was optimised to increase the amount and stability of the protein obtained. In detail, the rLIN28B protein produced, presented a six-Histidine-tag (His6X tag) used during the purification process and a c-MYC tag essential to perform the Alpha assay. As a substrate for the interaction with the rLIN28B we used a 5'-biotinylated ssRNA corresponding to the precursor

of *let-7*g miRNA (Bi-pre-*let-7*g miRNA), whose interaction with LIN28B has been extensively characterised (Shaik Syed Ali et al., 2012). As positive control, in the place of the Bi-pre-*let-7*g miRNA, we used a Bi-pre-*let-7*g-mut miRNA which, due the lack of an adenine in the conserved motif essential for the interaction, is not able to bind to LIN28B protein, simulating the absence of interaction between LIN28B and the precursor of *let-7*g miRNA.

The Alpha protocol was carried out in collaboration with Dr. Vito d'Agostino according to the PerkinElmer AlphaScreen Guide. The compounds screened were used at a concentration of 75 nM. The specificity and reproducibility of the screening were confirmed by a Z factor of 0.64 and a signal to background ratio of 13.8.

41 compounds (0.82% of the total compounds tested) were selected as hits (**Figure 3.3B**) and were subjected to further validation by the RNA Electrophoretic Mobility Shift Assay (REMSA) (Rio, 2014).

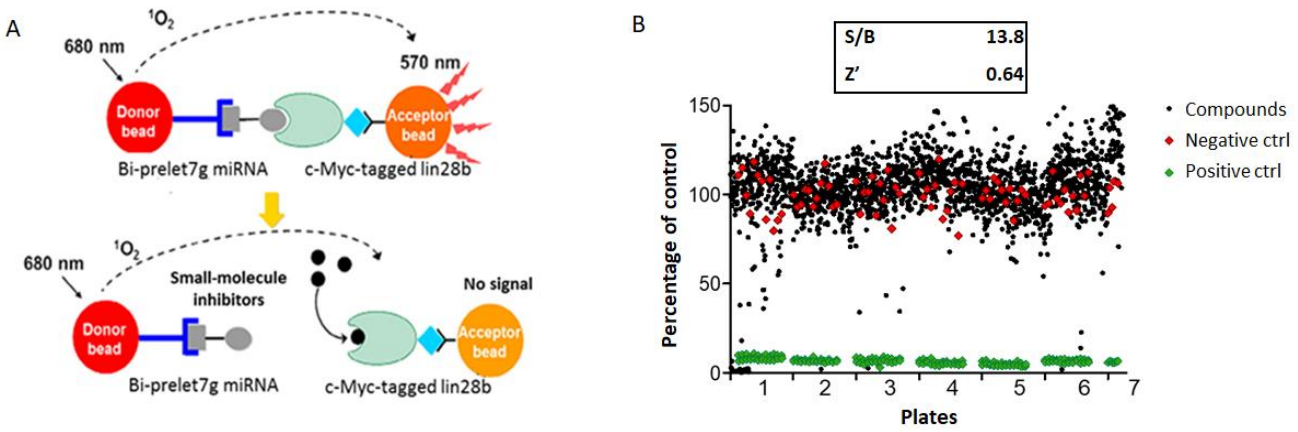

Figure 3.3. Alpha assay principle and screening.

(A) Schematic drawing of the alpha assay technique. The alpha assay exploits a donor bead linked to a biotinylated-pre-*let-7* miRNA and an acceptor bead linked to a c-Myc tagged recombinant LIN28B protein. After excitation at 680 nm, if the donor and the acceptor are close due to the interaction between the miRNA and the protein, an emission of light at 570 nm is observed; on the contrary, as when a molecule is able to interfere with the LIN28B/*let-7* binding, a decrease or the absence of the signal is registered (adapted from PerkinElmer AlphaScreen Guide). **(B)** Dot plot summarising the screening results reported as percentage of the average of negative controls. A Bi-pre-*let-7*g miRNA was used as a substrate for the interaction with the rLIN28B. No addition of drug was used as negative control (highlighted in red), whereas a Bi-pre-*let-7*g-mut miRNA used instead of the Bi-pre-*let-7*g miRNA was used as positive control (highlighted in green).

The REMSA assay allows to visualise the direct interaction between the two ligands inside a gel. In detail, in a first moment a fluorescent-labelled RNA, the protein and the molecule of interest are incubated together for a specific time at room temperature. Subsequently, the three elements are separated by electrophoresis on a gel. If the molecule of interest interacts either with the protein or with the RNA, thus interfering with their binding, the protein-RNA complex does not form, and the free mRNA probe is detected in the lower part of the gel. On the contrary, if the molecule of interest does not interact with any of the ligands, the protein-RNA complex does form and is detected as a band in the upper part of the gel. A schematic drawing of the REMSA technique is depicted in **Figure 3.4A**.

To perform the REMSA assay we used a Cyanine 3-labelled pre-*let-7*g miRNA (Cy3-pre-let7g miRNA) and the purified rLIN28B protein presenting the 6XHis and the c-MYC tags. As positive control, we used the free Cyanine 3-labelled per-*let-7*g miRNA without adding the purified rLIN28B protein. The drugs tested were used at a concentration of 10 µM. **Figure 3.4B** shows a representative image of the REMSA assay performed for the validation of the molecules selected after the Alpha screening.

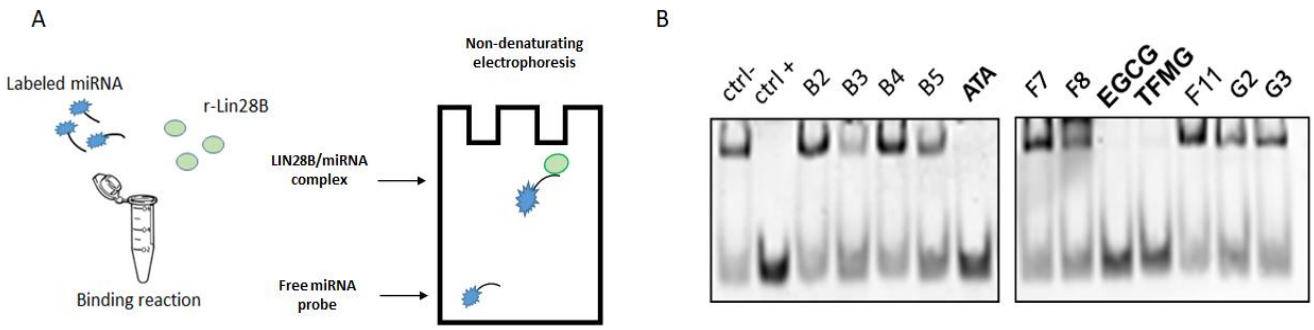

Figure 3.4. REMSA principle and validation.

(A) Schematic representation of REMSA assay. The rLIN28B protein, a Cy3-labeled miRNA and the tested molecule are incubated together. The complex is then separated by electrophoresis. If the LIN28/*let-7* interaction does not occur, as in the case of a molecule able to interfere with the LIN28/*let-7* interaction or as in the case of the free Cy3-labeled miRNA, a band in the lower part of the gel is detected. Instead, when the LIN28/*let-7* interaction occurs, a band in the upper part of the gel is detected. **(B)** Representative REMSA results for the validation of the hits selected by the Alpha assay screening. rLIN28B plus Cy3-labeled miRNA are used as negative control, whereas the free Cy3-labeled miRNA is used as positive control.

Based on the results of the REMSA assay validation, we finally selected 3 hits as candidate inhibitors: epigallocatechin 3'-monogallate (EGCG), theaflavin monogallate (TFMG), and aurintricarboxylic acid (ATA), whose chemical structures are depicted in **Figure 3.5**. Interestingly, the first two hits share the same epigallocatechin sub-scaffold and are characterised by a high degree of structural similarity. The third hit has already been reported as LIN28B inhibitor as a result of a drug screening conducted in parallel by another group using different approaches (Lightfoot et al., 2016).

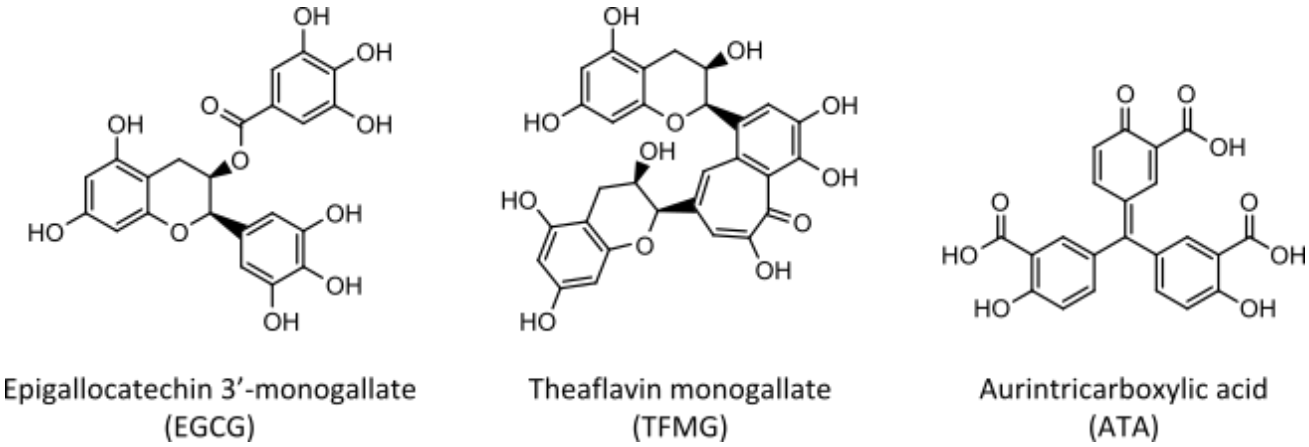

Figure 3.5. EGCG, TFMG and ATA chemical structures.

In collaboration with Mattia Sturlese from the Molecular Modelling Section of the University of Padua, we investigated the binding of the hit compounds to the LIN28B protein by performing a structure-based molecular modelling study. Starting from three different experimentally solved structures, we created by homology modelling a reliable 3D-model of LIN28B, which contains both the cold shock domain (CSD) and the zinc knuckle domain (ZKD) of the protein. According to the docking calculation, it resulted that EGCG, TFMG, and ATA have a good steric complementarity with the pre-*let-7* miRNA binding site of LIN28B. All the hits place an aromatic group of their structure in the pocket formed by Cys151, His152, Tyr130, Met160 and Lys149, establishing hydrophobic contacts, electrostatic interactions, and hydrogen bonds with this pocket. The docking prediction suggested that EGCG is able to form a hydrogen bond between its gallic acid group and the backbone of Cys151. Gallic acid is also involved in π–π stacking with Tyr130 and the methylene moieties belonging to Lys149. In addition, EGCG is involved in a further hydrogen bond between a catechin hydroxyl group and Lys123 (**Figure 3.6**). This binding

model is also supported by the docking results for TFMG, in which the common substructure retains the same pattern of interaction observed for EGCG, driven again by the catechin parts of the molecule. The less effective binding of TFMG compared to the structurally related EGCG could be ascribed to its greater exposition to the solvent due to the additional substituent, not involved in molecular interactions.

Also for the ATA compound the docking results suggested the ligand may be accommodated in the ZKD binding site within the same pocket of CAT derivatives. The main interactions are mediated by two salicylic moieties: one establishes a hydrogen bond between the backbone of His152 and the Cys151 with the carboxyl group and the hydroxyl group respectively; the second salicylic unit may establish a salt bridges between the carboxyl group and the positively charged side-chain of Lys123.

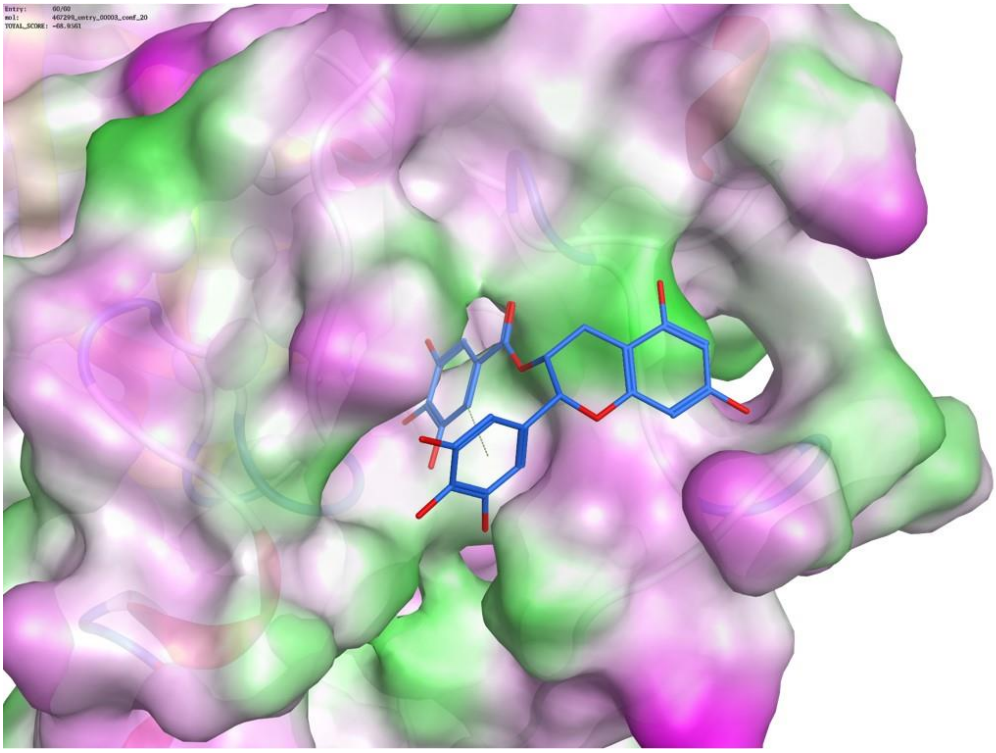

Figure 3.6. Docking calculation 3D view of EGCG in its binding site inside LIN28B protein.

Subsequently, in collaboration with the Bio-organic Chemistry Laboratory led by Prof. Ines Mancini, we designed and synthesised some analogues of the active molecules identified during the screening. In detail, we produced analogues of the (+)catechin (CAT) scaffold shared by EGCG and TFMG (highlighted in purple **Figure 3.7A**), and analogues of the aurintricarboxylic acid (ATA). The chemical modifications introduced on the CAT and ATA scaffolds were selected based

on the predicted energy values of their complexes with the protein (E > -7.0 kcal/mol) and based on their higher number of interactions (hydrogen bonds, π-π interaction or electrostatic interactions). In particular, our main goal was to decrease the molecule's hydrophilicity by converting the hydroxyl groups into acetyl or ether derivatives and by inserting hydrophobic moieties.

Figure 3.7B shows the chemical structure of the synthesised CAT analogues. The chemical modifications introduced on the (+)catechin scaffold are highlighted in purple.

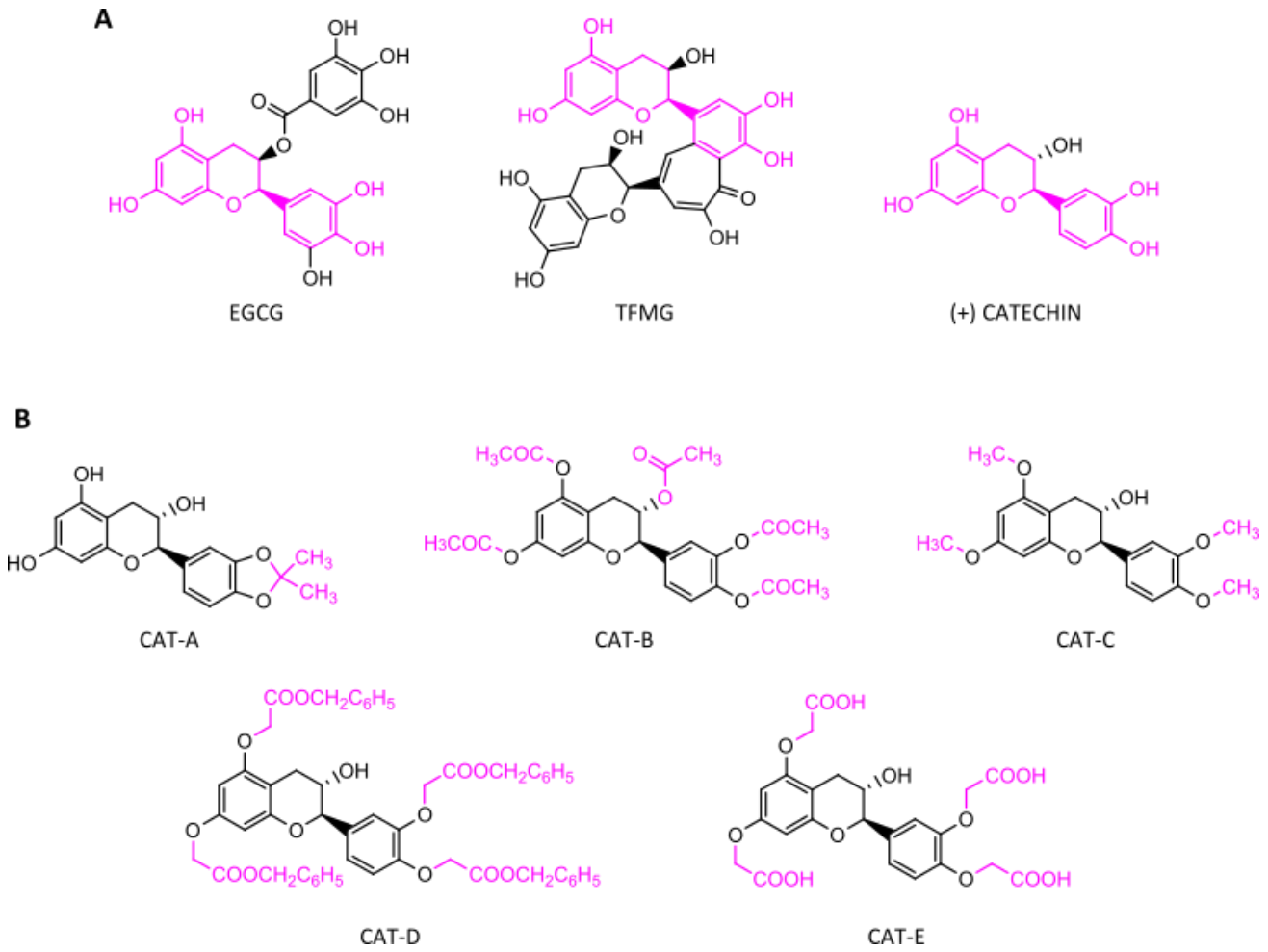

Figure 3.7. The designed and synthesised CAT analogues.

(A) The (+)catechin (CAT) scaffold shared by EGCG and TFMG is highlighted in purple. **(B)** The chemical structure of the synthesised CAT analogues. The chemical modifications introduced on the (+)catechin scaffold are highlighted in purple.

We also designed several ATA analogues presenting acetyl or methyl ether moieties (**Figure 3.8A**), the foreseen modifications are highlighted in purple, but unfortunately it has not been

possible to synthesise them. Indeed, when we started to work synthetically with ATA, we discovered that the commercial compound sold as aurintricarboxylic acid is actually a mixture composed of the ATA monomer (from 7 to 14%) and several ATA oligomers and polymers. This is known from the middle of the 1970s and is due to the synthetic process used to produce it (González et al., 1979).

Therefore, we focused our synthetic efforts on producing ATA derivatives in the form of monomers. In detail, we synthesised ATA-A, ATA-B, which indeed is the ATA monomer, and ATA-C, whose chemical structures are depicted in **Figure 3.8B**.

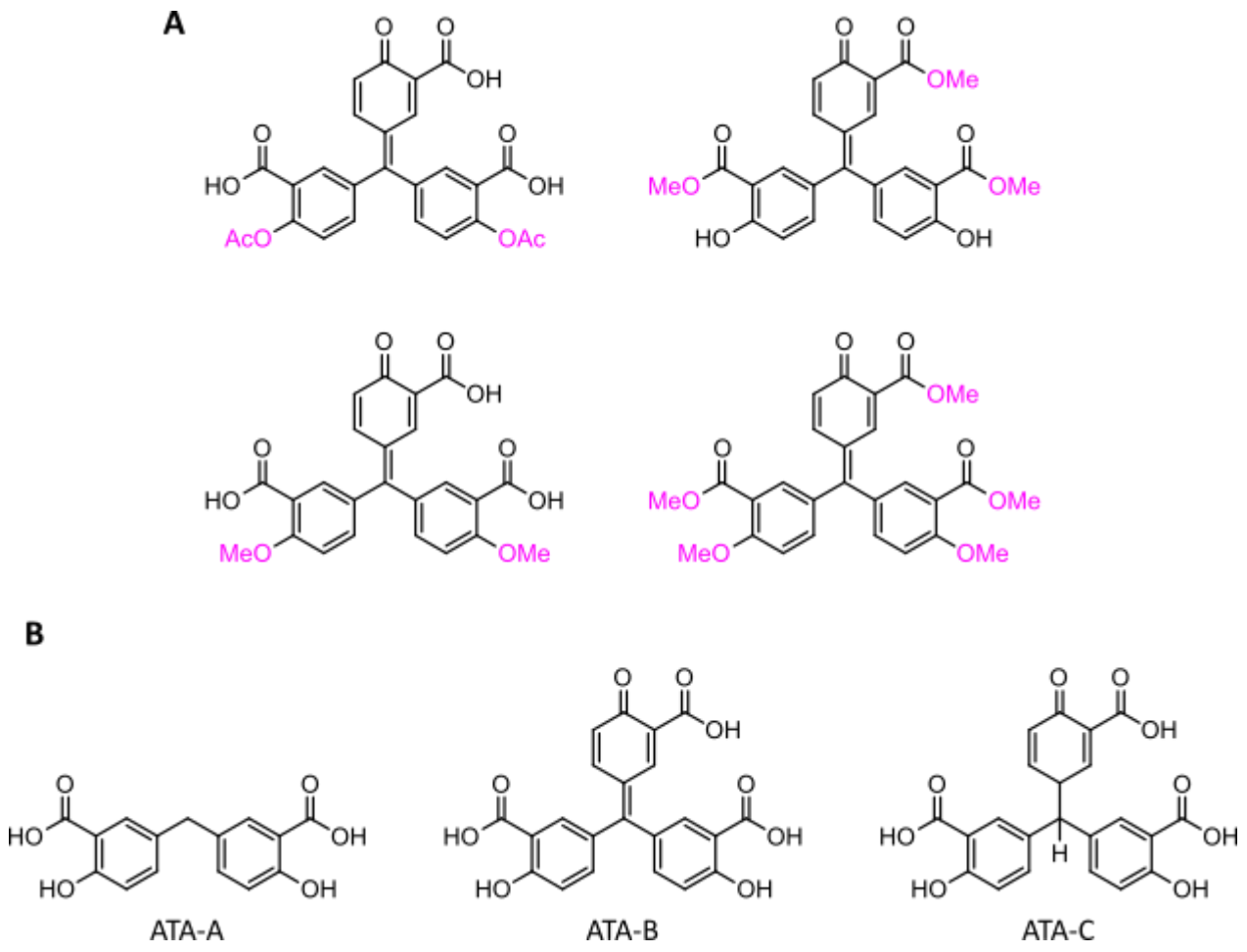

Figure 3.8. The designed and synthesised ATA analogues.

(A) The designed ATA analogues. The foreseen chemical modifications are highlighted in purple.

(B) The chemical structure of the synthesised ATA analogues.

We then evaluated all the synthetic products using the Alpha and REMSA assays and compared them to EGCG and the commercial ATA identified in the screening.

Table 3.1 summarises the level of inhibition of the rLIN28B/pre-*let-7*g complex formation calculated in both the assays and expressed as percentage of control. The results highlighted that the synthesised analogues are not more potent than the reference compound. In detail, all the CAT analogues resulted to be less active than EGCG and CAT-E was totally unable to inhibit the rLIN28B/pre-*let-7*g complex formation, and was, therefore, classified as not functional (nf). Regarding the ATA analogues, ATA-B and ATA-C resulted to be more or less as active as the commercial ATA, while ATA-A, which lacks the 3-carboxy-*p*-benzoquinone like moiety, resulted to be not functional. In general, the ATA series proved to be less active than the CAT series. Moreover, the EGCG showed the best inhibitory activity in both the biochemical assays used, and therefore we decided to select it as lead compound.

Table 3.1. Level of inhibition of the rLIN28B/pre-*let-7*g complex formation by EGCG, TFMG, ATA and the synthesised analogues by Alpha and REMSA assays.

	REMSA	ALPHA
EGCG	69%	50%
TFMG	65%	52%
CAT-A	15%	46%
CAT-B	10%	42%
CAT-C	17%	29%
CAT-D	30%	10%
ATA	28%	51%
ATA-A	nf	nf
ATA-B	nf	20%
ATA-C	26%	53%

nf: not functional

To better characterise EGCG activity and potency, we performed a dose-response experiment by REMSA assay. In detail, we incubated the rLIN28B/Cy3-pre-*let-7*g complex with increasing concentrations of EGCG (1 μM, 5 μM, 10 μM, 25 μM and 50 μM). As shown in **Figure 3.9** EGCG was able to inhibit the complex formation in a dose-dependent manner till a complete inhibition at the highest concentrations tested.

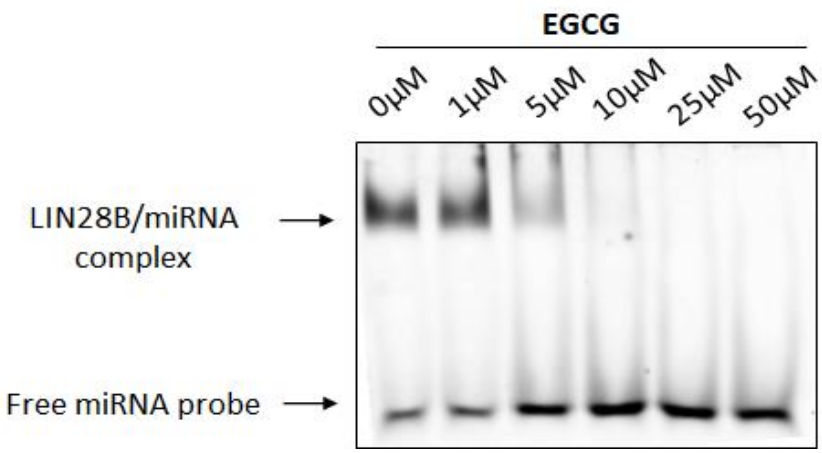

Figure 3.9. REMSA assay with increasing concentrations of EGCG.
REMSA assay was performed using the rLIN28B protein and the Cyanine 3-labelled pre-*let-7*g miRNA probe. Increasing concentrations of EGCG (0 μM, 1 μM, 5 μM, 10 μM, 25 μM and 50 μM) were tested. n= 1 technical replicate.

3.3 EGCG, BIOLOGICAL VALIDATION

After the biochemical validation, we evaluated the biological effects of EGCG on several NB cell lines carrying a different MYCN status. In particular, we used the SK-N-AS, NB69 and SK-N-FI cell lines, which are MYCN non amplified, and the Kelly and CHP134 cell lines, which are MYCN amplified (Sidarovich et al., 2014). Immunoblotting analysis showed that the cell lines tested express variable LIN28B levels, with the Kelly line expressing the highest levels of LIN28B and the SK-N-AS line having little or no LIN28B (**Figure 3.10A**). We started by testing the cytotoxicity of EGCG using the CellTiter-Glo® Luminescent Cell Viability Assay, a homogeneous method based on the quantitation of the ATP present, which is an indicator of metabolically active cells and therefore can be used for determining the number of viable cells in culture. We treated the cells with increasing concentrations of EGCG (ranging from 1 μM to 300 μM) for 48h and constructed dose-response curves to evaluate the sensitivity of the cells to the treatment (**Figure 3.10B**). In detail, we considered the growth inhibition 50 values (GI_{50}) derived from the curves. The GI_{50} value is defined as the compound concentration causing the 50% inhibition of the cellular growth, and is, therefore, a parameter to evaluate a compound cytotoxicity. In fact, since our main aim was to elucidate the biological effects induced by EGCG, with a particular interest in its

differentiation-inducing potential, we wanted to identify and avoid concentrations of the molecule that lead to critical cytotoxicity.

Figure 3.10C shows that each cell line has a specific sensitivity to EGCG. Indeed SK-NAS, NB69 and SK-N-FI showed GI_{50} values of respectively 82 μM± 7.6, 19.4 μM± 6.8, and 69 μM ± 7.3,while KELLY and CHP134 show GI_{50} values of respectively 21.3 μM± 5.2 and 48 μM ± 4.2. The data suggest no correlation between the cell sensitivity and LIN28B/MYCN status.

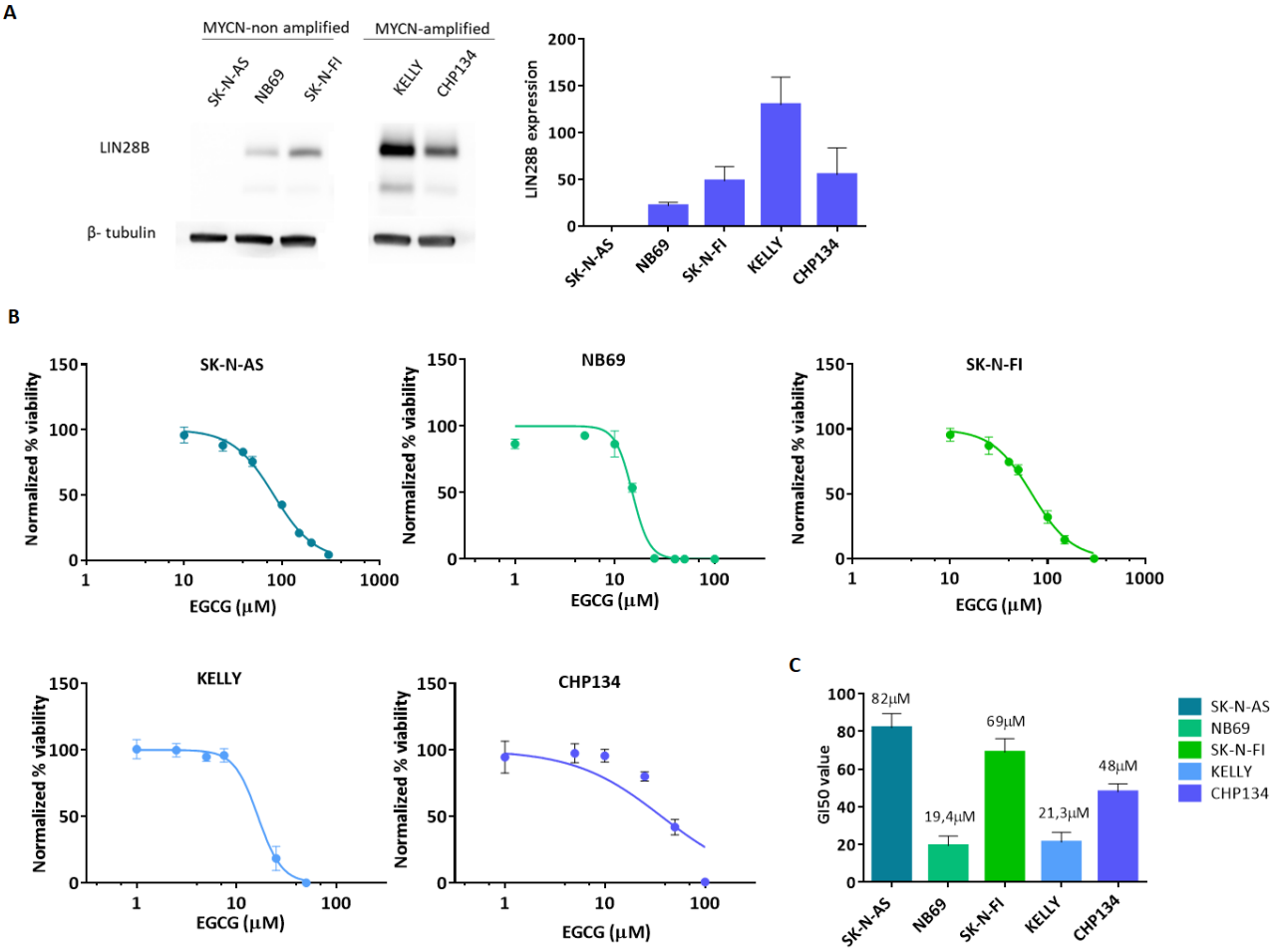

Figure 3.10. LIN28B expression levels in different NB cells and EGCG dose-response curves. **(A)** Representative immunoblotting showing the levels of LIN28B in NB cell lines SK-N-AS, NB69, SK-N-FI, KELLY and CHP134. β-tubulin was used as loading control. The graph on the right represents the quantification of two biological replicates obtained with densitometry analysis performed with Image Lab 3 Biorad Software. **(B)** Dose-response curves of NB69, SK-N-FI, KELLY and CHP134 cell lines. Cell growth was evaluated using the CellTiter-Glo® Luminescent Cell Viability Assay. The viability was calculated, normalising the treatments on the not treated cells. Representative dose-response curves are shown. **(C)** GI_{50} values calculated for each cell line analysed. The GI_{50} values were calculated from n = 3 biological replicates, n = 3 technical replicates each. Means ± SD.

Based on the cytotoxicity data, we selected two different EGCG concentrations to evaluate the effects of the molecules on *let-7* miRNA levels. We started by testing EGCG on the NB69 cell line, and we measured the variation of three *let-7* miRNA family members (*let-7d, let-7f, let-7g*) by RT-qPCR after 48h of treatment. In detail, we used 10 μM of EGCG, a concentration that is below the GI_{50} value for this cell line and 25 μM, which is around the GI_{50} value. Disappointingly, we detected no significant variation of *let-7* miRNA levels (**Figure 3.11**).

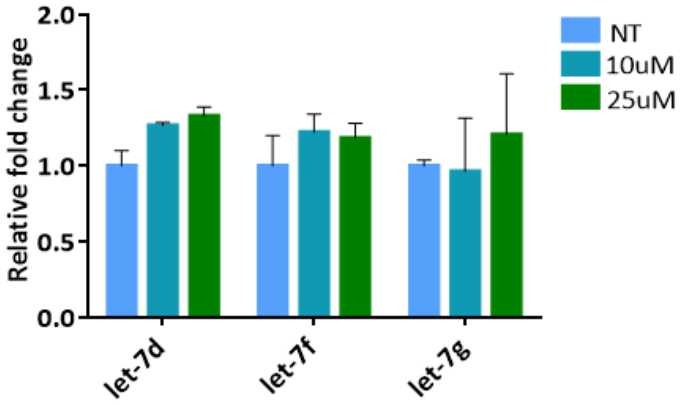

Figure 3.11. RT-qPCR performed on NB69 treated with EGCG.

RT-qPCR analysis of the expression of three *let-7* miRNA family members. The cells were treated for 48h with two different EGCG concentrations. The RT-qPCR shows the relative fold change, and the data are normalised on U6. n= 2 biological replicates, n=3 technical replicates each, mean ± SD.

Given the reported unfavourable stability of the molecule and the demonstration that EGCG oxidises in cell culture conditions (Cai et al., 2018), we hypothesised that the low effects of EGCG on *let-7* miRNAs levels could be due to its instability. Therefore, before proceeding with the quantification of *let-7* miRNAs levels upon EGCG treatment in other cell lines, we decided to test EGCG stability in solution by HPLC.

First, we constructed a calibration curve by injecting a series of EGCG solutions with different known concentrations (10 μM, 25 μM, 50 μM, 100 μM, 250 μM, 500 μM) in an Agilent 1200 High Performance Liquid Chromatography (HPLC) system equipped with an autosampler, a binary pump, a diode array detector. A Phenomenex Gemini 5 μm C18 110 Å column was used and the elution was performed in isocratic conditions with 80:20 water:acetonitrile and 0.01% TFA (pH 4-4.5). The flow rate and the detection were set at 1 $mL \cdot min^{-1}$, and at 280 nm, respectively. The calibration curve obtained by plotting the area of the peaks as a function of the concentration

presented a R^2 of 0.9978. This allowed us to determine that a signal corresponding to as low as 10 µM can be detected and that the signal recorded is proportional to the concentration of the injected solution (**Figure 3.12A**). The stability evaluation was performed using a solution with a concentration of 50 µM, by incubating EGCG in the same cell culture media used in the *in vitro* experiments (RPMI), and by evaluating the stability of the molecule by HPLC at different time points. The HPLC analysis clearly showed that EGCG, which has a retention time of t_R 5.9-6.0 min, is not stable in biological test condition, is reduced by more than 50% after 15 minutes and is completely degraded after 45 minutes (**Figure 3.12B** and **C**).

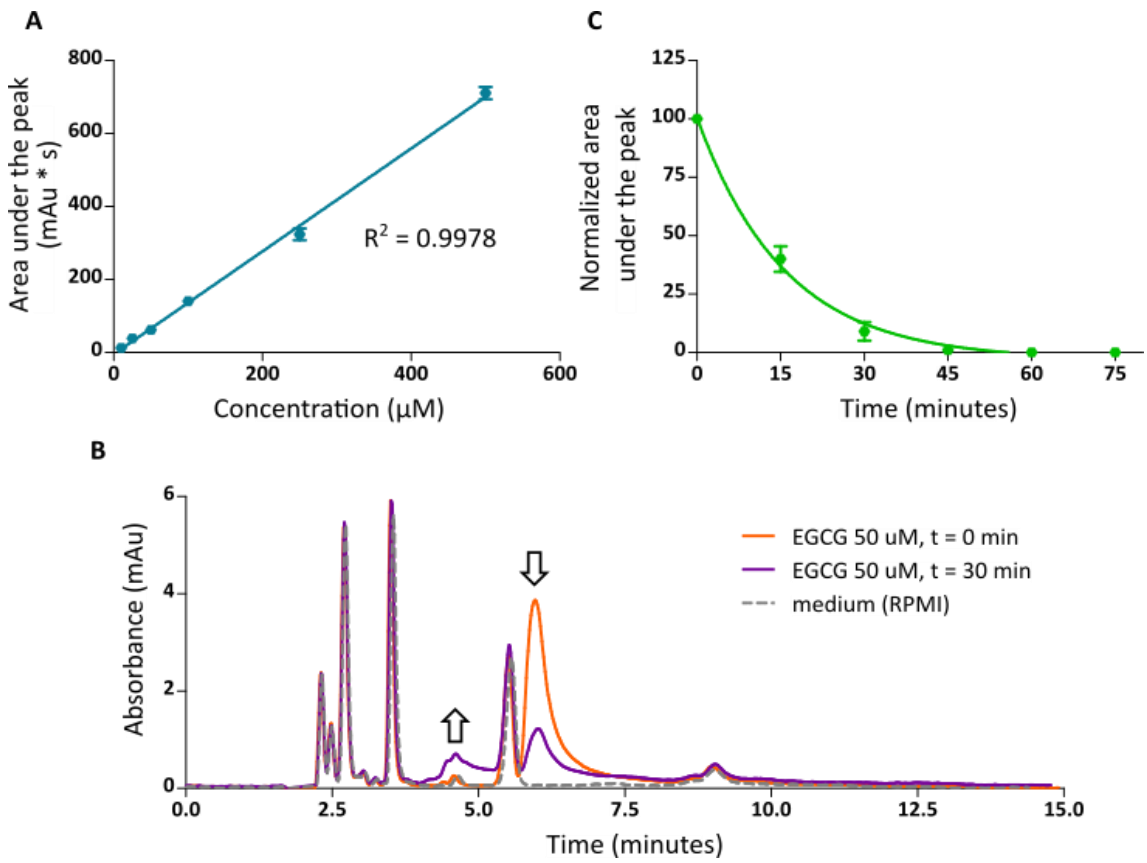

Figure 3.12. EGCG stability evaluation by HPLC analysis.

(**A**) EGCG calibration curve. A series of EGCG solutions with different known concentrations (10 µM, 25 µM, 50 µM, 100 µM, 250 µM, 500 µM) was injected in an Agilent 1200 High HPLC system. A Phenomenex Gemini 5 µm C18 110 Å column was used in isocratic conditions with 80:20 water:acetonitrile with 0.01% TFA (pH 4-4.5). The flow rate and the detection were set at 1 $mL \cdot min^{-1}$, and at 280 nm, respectively. n = 3 replicates, mean ± SD. R^2 0.9978. (**B**) Representative HPLC chromatogram of EGCG (50 µM) in RPMI at t = 0 and 30 minutes. The chromatogram of EGCG solution injected at t = 0 min is depicted in orange, whereas that of EGCG solution at t = 30

min is depicted in purple. Medium (RPMI) signals remain constant over time (gray). Arrows indicate EGCG instability in aqueous media and formation of degradation products. n = 3 replicates. (**C**) Percentage of EGCG over time (0, 15, 30, 45, 60 and 75 min). The area of EGCG peak was normalized on t = 0. n = 3 replicates, mean ± SD.

3.4 PLGA-PEG NANOPARTICLES

In an attempt to improve the stability and deliverability of EGCG in cells, we decided to include the molecule inside nano delivery systems.

There is a large variety of nano delivery systems that can be applied for this purpose, depending on the area of EGCG administration (Granja et al., 2017). For example, the nanoencapsulation of EGCG with lipids, carbohydrates and proteins can be used to improve the stability of the molecule in oral administration, leading to an increase of its concentration in blood (Cai et al., 2018), while gold, polymeric and lipid nanoparticles are used to improve the EGCG stabilization in intratumoral and intraperitoneal administration (Fang et al., 2005; Hsieh et al., 2011; Sanna et al., 2017).

In particular, poly(lactic-co-glycolic acid) polymer (PLGA polymer) nanoparticles are a well-studied nanocarrier system due to its high biocompatibility (Kumari et al., 2010).

In addition, the surface of this polymer can be easily functionalized with chemical groups which can direct the nanocarrier particles toward a specific target, making it possible to use them for targeted therapies (Elsabahy and Wooley, 2012). Lastly, these nanocarriers have an elevated encapsulation rate, allowing to incorporate a large amount of a drug (Elsabahy and Wooley, 2012; Makadia and Siegel, 2011). A combination of PLGA and polyethylene glycol (PEG) polymers has been used to improve the antiproliferative effect of EGCG in prostate cancer both *in vitro* and *in vivo.* Moreover, the functionalization with peptides specific for prostate cells improved the results, demonstrating that PLGA-PEG nanocarriers are also suitable for targeted therapy (Sanna et al., 2017).

Based on these encouraging premises, we decided to include EGCG into PLGA-PEG nanocarriers. A cartoon representing the structure of the EGCG containing PLGA-PEG nanocarriers is depicted in **Figure 3.13**. The EGCG containing PLGA-PEG nanocarriers were synthesized by Vanna Sanna (R&D Manager nanomater Srl) in collaboration with Prof. Mario Sechi (Chemistry Department, Sassari University).

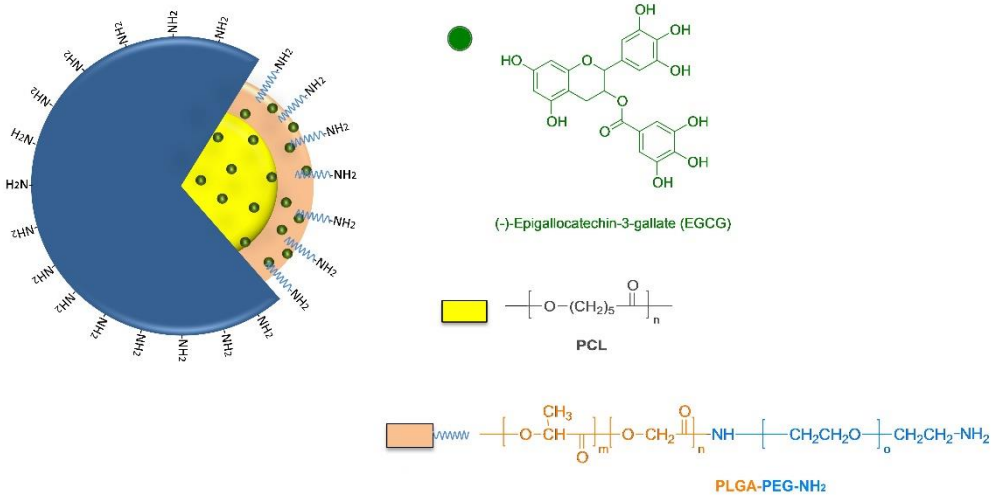

Figure 3.13. Schematic representation of the EGCG containing PLGA-PEG nanocarriers. Chemical structure of EGCG and PLGA-PEG polymers. The structure of the resulting nanoparticle is schematically represented. Adapted from Sanna et al., 2017.

To assess if the PLGA-PEG nanoparticles could penetrate into the cells, we treated the NB69 and CHP134 cell lines with PLGA-PEG nanoparticles containing the fluorophore Coumarin 6 (Cou6). In detail, we treated the cells for 48h with different concentrations of the nanoparticle containing solution (0 µg/µl, 0.0003 µg/µl, 0.003 µg/µl and 0.03 µg/µl), analysed the fluorescence intensity and quantified the number of cells carrying the fluorophore using the Operetta-High Content Imaging System. As shown in **Figure 3.14A** (*top*), the fluorophore contained in the nanoparticles can be found within the cells. Moreover, the fluorescence intensity and the number of Cou6 positive cells increase proportionally with the concentration of nanoparticles used (**Figure 3.14A,** *bottom*).

To better visualize the Cou6-containing nanoparticles (cou6-NP) inside the cells, we used a confocal microscope. The analysis of single confocal planes and their relative orthogonal projection demonstrated the presence of the nanoparticles content within the cell compartment (**Figure 3.14B**). We could not measure any fluorescent signal from the Cou6 in the nuclei of our cells (as pointed by the yellow arrow), indicating that the nanoparticles interact with our cells and their content is internalised and released into the cytoplasm. Furthermore, 100% of the analysed cells did have internalised the content of nanoparticles. This experiment clearly shows that the PLGA-PEG nanoparticle formulation is able to deliver drugs into our cells and it delivers them with a great efficiency.

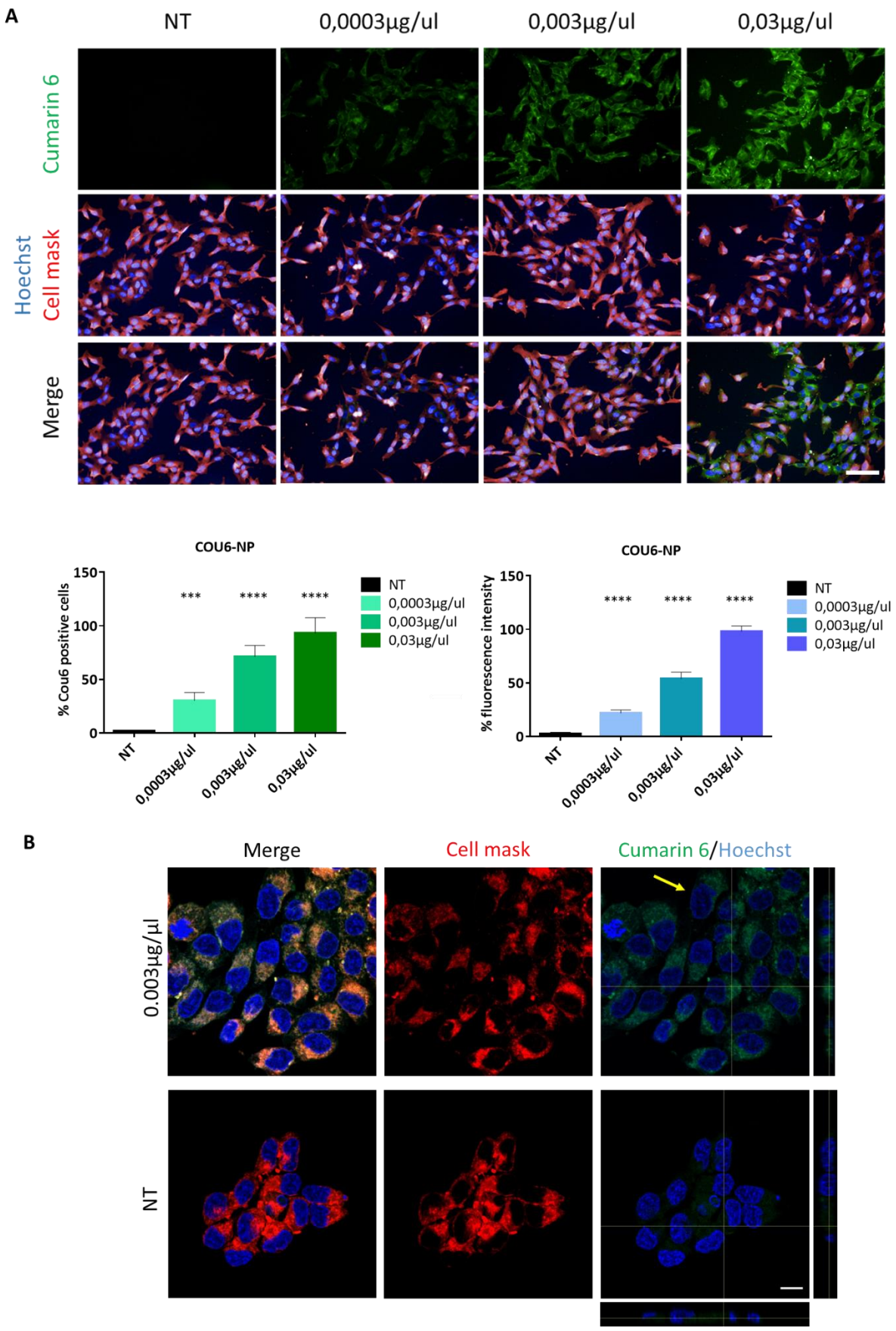
A
NT
0,0003µg/ul
0,003µg/ul
0,03µg/ul
Cumarin 6
Hoechst
Cell mask
Merge
COU6-NP
% Cou6 positive cells
150
100
50
0
***
****
****
NT
0,0003µg/ul
0,003µg/ul
0,03µg/ul
COU6-NP
% fluorescence intensity
150
100
50
0
****
****
****
NT
0,0003µg/ul
0,003µg/ul
0,03µg/ul
B
Merge
Cell mask
Cumarin 6/Hoechst
0.003µg/µl
NT

Figure 3.14. PLGA-PEG carrying Coumarin6 evaluation.

(A) Immunofluorescence analysis of NB69 treated with Cou6-containing nanoparticles carrying different dilutions of the fluorophore. Nuclei were stained with Hoechst 33342 (blue) and the cytoplasm with the CellMask™ Deep Red Stain (red). The yellow arrow points the nuclei of the cell. The fluorescence of Cou6 (green) was analysed using the Operetta-High Content Imaging System. The average number of Cou-6 positive cells and the average fluorescence intensity were quantified using the Harmony software. The data were normalised on the total number of cells in the wells. n = 6 technical replicates. The graph and the statistical analysis were obtained using GraphPad Prism 6, 2 way-ANOVA (*** P< 0.001; **** P< 0.0001) Scale bar 50 μm. Data distribution has been controlled for normality. **(B)** Analysis of CHP134 cells treated with 0,003 μg/ul of Cou6-NP using a confocal microscope. Nuclei were stained with Hoechst 33342 (blue) and cytoplasm was stained with the CellMask™ Deep Red Stain (red). Scale bar 10 μm.

3.5 TREATMENTS WITH EGCG INCLUDED IN PLGA-PEG NANOPARTICLES

We then evaluated the sensitivity of the previously described NB cell lines (NB69, KELLY and CHP134) to EGCG containing PLGA-PEG nanoparticles (EGCG-NP). To do so, we treated the cells with different concentrations of nanoparticles (1 μM, 2.5 μM, 5 μM, 7.5 μM, 10 μM, 15 μM). After 48h, we measured the effect induced by the treatment on cell growth using the CellTiter-Glo® Luminescent Cell Viability Assay. To exclude the possibility that the effect observed on cell proliferation was due to the PLGA-PEG carrier alone, we treated the cells with the same increasing concentrations of the empty-PLGA-PEG nanoparticles (empty-NP). The three cell lines showed variable sensitivity to EGCG-NP (**Figure 3.15A**), as previously observed in the treatments with non-encapsulated EGCG. Generally, the empty-NP showed no substantial toxicity, even at higher concentrations (**Figure 3.15A**). Considering the GI_{50} values derived from the dose-response curves, the nanoencapsulation led to a significant decrease of GI_{50} value in all the cell lines analysed, compared with the values obtained previously with non-encapsulated EGCG (**Figure 3.15B**).

This evidence suggests that the PLGA-PEG carrier stabilises the EGCG in solution and leads to higher concentrations of EGCG inside the cells.

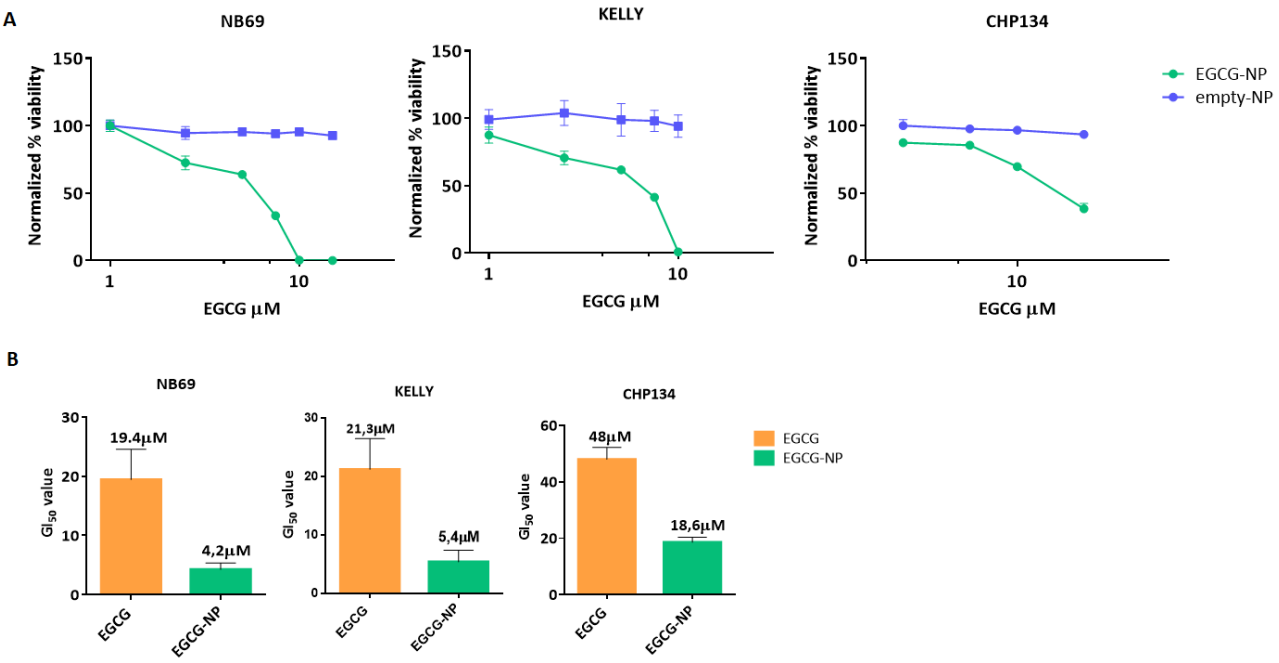

Figure 3.15. Dose-response curves on NB69, KELLY and CHP134 and GI_{50} values identification.

(A) Representative dose-response curves for EGCG-NP and empty-NP on three NB cell lines (NB69, KELLY, CHP134). The treatment was performed using different EGCG-NP and empty-NP concentrations, ranging from 1 µM to 15 µM. After 48h of treatment, the cell viability was calculated using the CellTiter-Glo Assay. The data are expressed as the percentage of viability normalized on not-treated cells. The graph shows one representative result of n = 3 biological replicates, n = 3 technical replicates each. **(B)** GI_{50} values calculated from the dose-response curves. The diagrams show the GI_{50} values for non-encapsulated EGCG and for EGCG-NP treatments. n = 3 biological replicates, n = 3 technical replicates each. Mean ± SD.

After evaluating the GI_{50} value of each cell line, we selected the concentration of EGCG-NP suitable to assess their effect on the levels of *let-7* miRNAs. In detail, we decided to use one dose of EGCG-NP below the GI_{50} value and one dose corresponding to the GI_{50} value. Since NB69 and KELLY presented a similar GI_{50}, they were treated using the same concentrations (2.5 µM and 5 µM). As shown in **Figure 3.16** (*top*), treating these lines with EGCG-NP led to a significant increase of *let-7* miRNAs levels, especially at the highest concentration tested. Moreover, the treatment performed on KELLY cells elucidated a dose-dependent effect of EGCG-NP treatment on the increase of *let-7* miRNAs levels. For the CHP134 cells, we selected only one concentration (10 µM) and the impact on *let-7* miRNAs levels was evident for all the family members analysed (**Figure 3.16**, *bottom*).

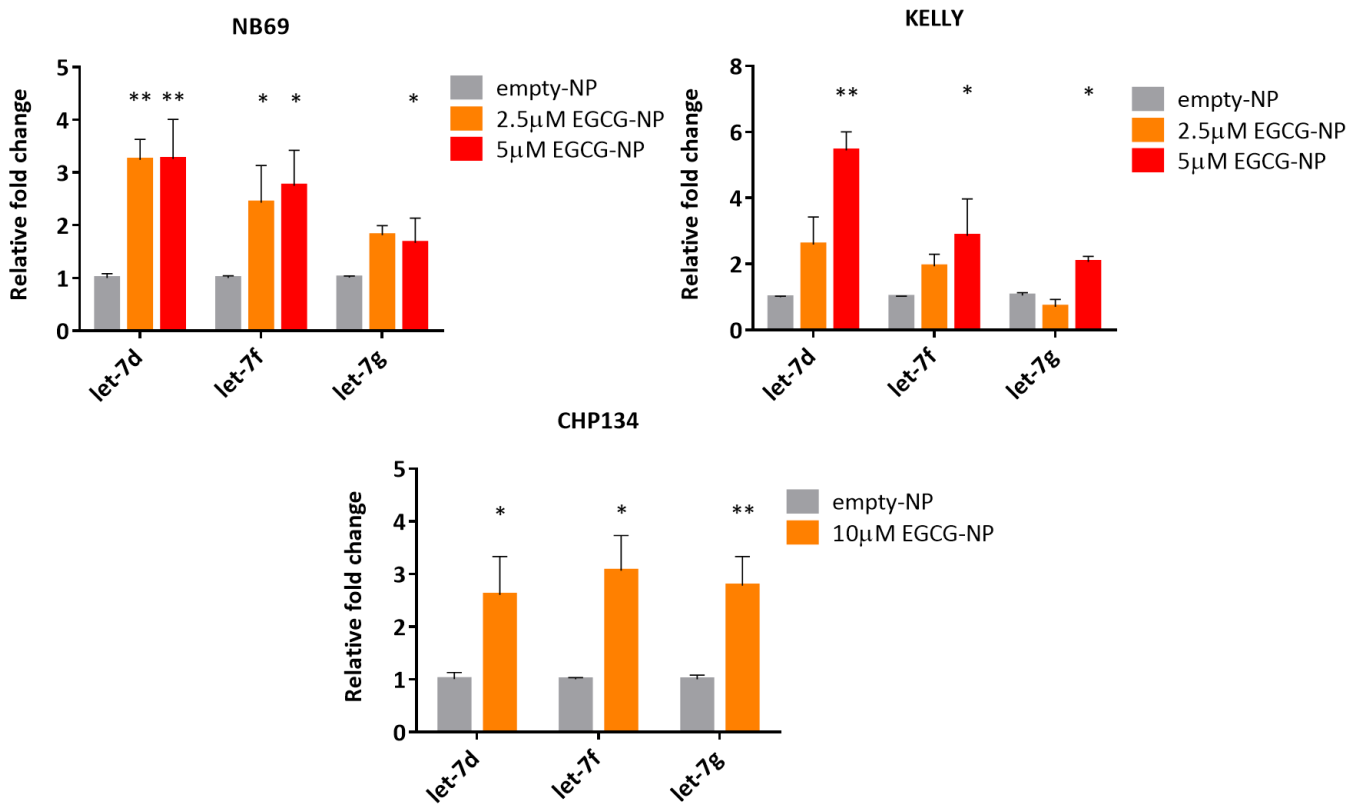

Figure 3.16. Evaluation of le-7miRNA levels upon treatment with EGCG-NP and empty-NP. RT-qPCR analysis of three *let-7* miRNA family members in NB69, KELLY and CHP134 cell lines treated with EGCG-NP. RT-qPCR shows the fold change relative to empty-NP, and the data are normalised on U6. The analysis was performed using GraphPad Prism 6 software, 2 way-Anova (*P< 0.05; ** P< 0.01). n = 3 biological replicates, n= 3 technical replicates each. Mean ± SD. Data distribution has been controlled for normality.

Subsequently, we evaluated if the treatment with EGCG-NP could affect the proliferation of NB69, KELLY and CHP134 cells. We treated the cells with several doses of EGCG-NP around or below the GI_{50} values and assessed the cell growth after 24h, 48h and 72h of treatment. Specifically, we measured the cells viability using the CellTiter-Glo® Luminescent Cell Viability Assay and normalized it on the cell viability on the day of the treatment (day 0). In parallel, we performed the same experiment using empty-NP. We detected a dose-dependent inhibition of cellular proliferation, in all cell lines tested (**Figure 3.17**, *left*). Moreover, the results showed that the nanocarrier alone (empty-NP) did not impact cell growth, even at higher concentration (**Figure 3.17**, *right*), and therefore it is comparable to a condition where cells are not treated (NT).

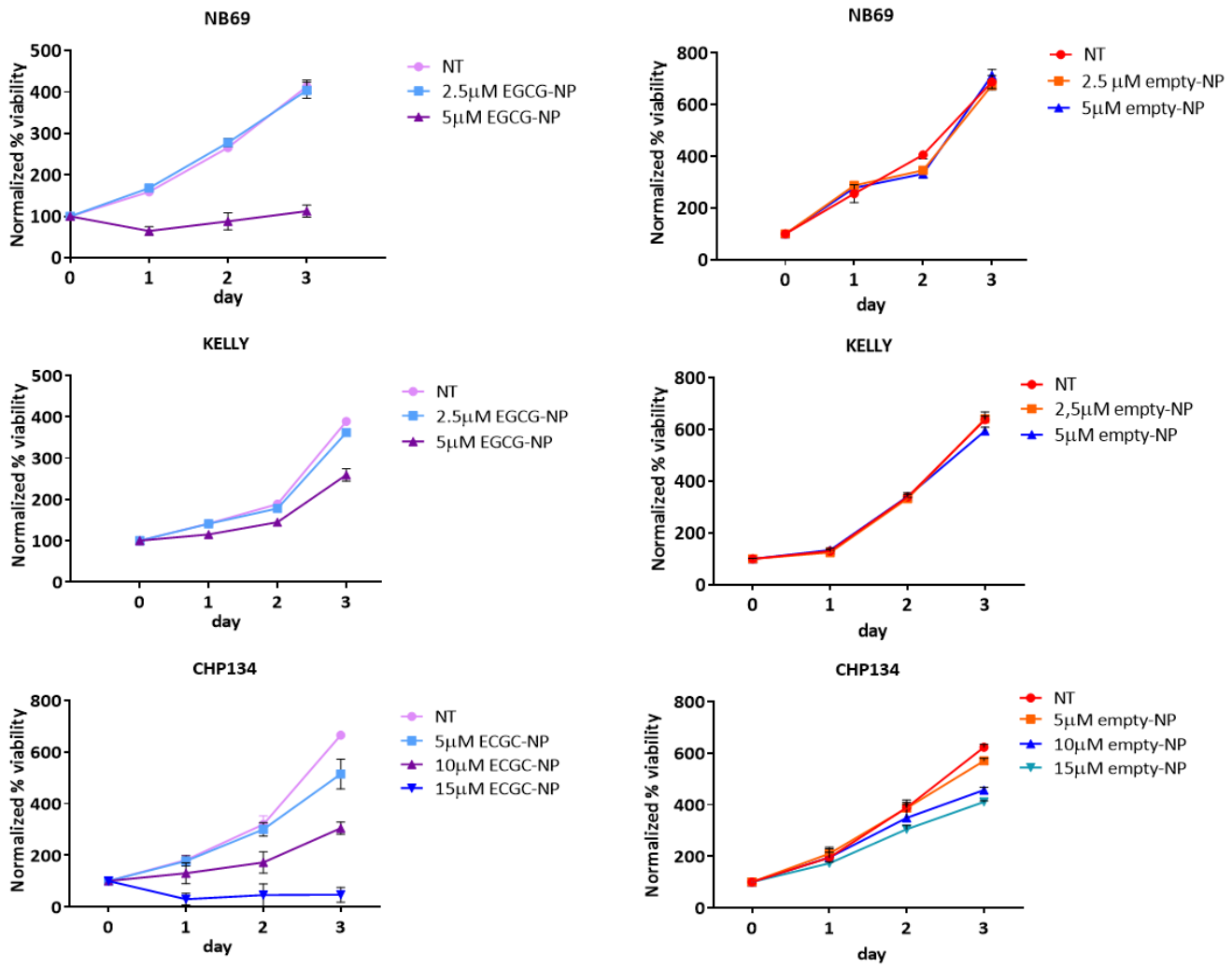

Figure 3.17. Evaluation of EGCG-NP and empty-NP treatment on cellular proliferation. Representative growth curves showing the effects of different EGCG-NP concentrations on NB69, KELLY and CHP134 proliferation. The viability was measured using the CellTiter-Glo® Luminescent Cell Viability Assay and normalized it on the cell viability on the day of the treatment (day 0). In parallel, we performed treatments using empty-NP. NT = not treated cells. The curves were plotted using GraphPad Prism 6 software. A representative result is shown, n=3 biological replicates, n=3 technical replicates each.

The increase of *let-7* miRNAs and the inhibition of cell proliferation observed upon EGCG-NP treatment led us to evaluate if the increase in the *let-7* miRNA amount obtained was enough to induce the differentiation of the cells. For this purpose, we treated CHP134 cells with different concentrations of EGCG-NP and empty-NP for 96h and we evaluated the variation of some differentiation markers. In detail, we considered the variation of β-III-TUBULIN and GAP43, two markers of mature neurons. Moreover, as a reference of a drug able to induce NB cell

differentiation, we used the 13-cis-retinoic acid (RA), the drug used in the maintenance phase of NB treatment, which has been shown to be able to induce differentiation in NB cells (Matthay et al., 1999; Reynolds et al., 2003). In particular, based on the published data regarding the sensitivity of CHP134 to retinoids we chose to use RA at a concentration of 5μM (Ponthan et al., 2001). We evaluated the variation of β-III-TUBULIN and GAP43 markers by immunofluorescence in the two treatment conditions: EGCG-NP (10 μM) or empty-NP (**Figure 3.18A**). We quantified the cells' fluorescence intensity by the Operetta-High Content Imaging System, detecting an increase of the fluorescence intensity of about 24% for β-III-TUBULIN and 22% for GAP43. The 13-cis retinoic acid showed higher differentiative activity, leading to an increase of β-III-TUBULIN and GAP43, respectively of 60% and 53% (**Figure 3.18B**).

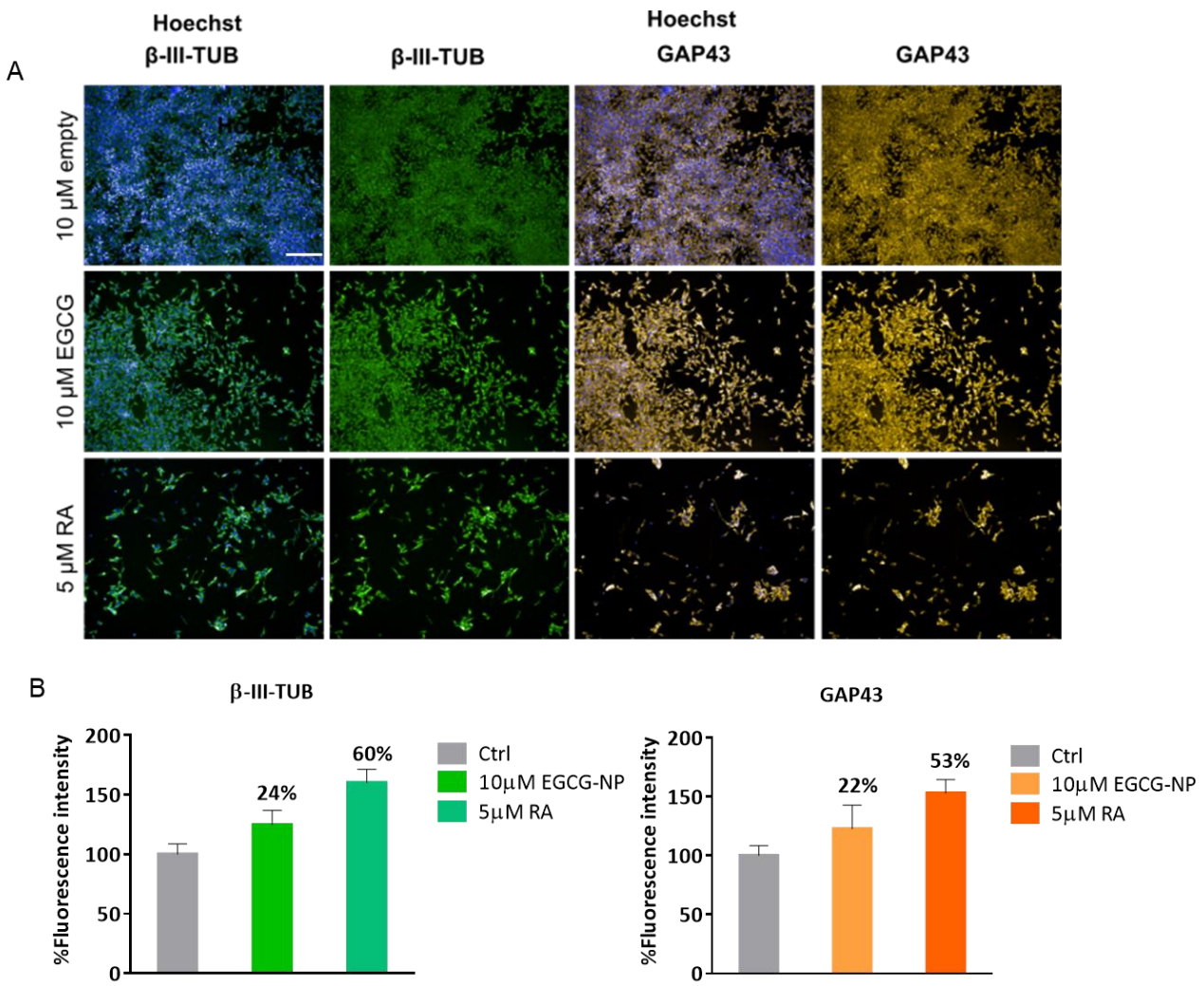

Figure 3.18. EGCG-NP and 13-cis retinoic acid treatments lead to an increase of the differentiation markers.

(A) Immunofluorescence analysis of GAP43 (orange) and β-III-TUBULIN (green) in CHP134 cells after 96h of treatments. Nuclei were stained with Hoechst 33342 (blue). Images were acquired using the Operetta-High Content Imaging System. Scale bar 100 μm **(B)** Fluorescence intensity quantification normalized on empty-NP signal for EGCG-NP or DMSO signal for RA. The analysis was performed with the Harmony software. n = 3 technical replicates, mean ± SD.

To further characterize the differentiation state of the cells, we evaluated the levels of SOX2, SOX9, GAP43 and β-III-TUBULIN by RT-qPCR in CHP134 cells after 96h treatment with EGCG-NP and empty-NP. As expected in a differentiative process and as detected in the LIN28B down-regulated models (**Figure 3.2**), SOX2 and SOX9 mRNA levels were significantly decreased by the treatment. At the same time, the level of GAP43 and β-III-TUBULIN mRNA were significantly increased, confirming the protein variation detected by immunofluorescence (**Figure 3.19A**). The increase in β-III-TUBULIN protein levels was also confirmed by immunoblot analysis (**Figure 3.19B**).

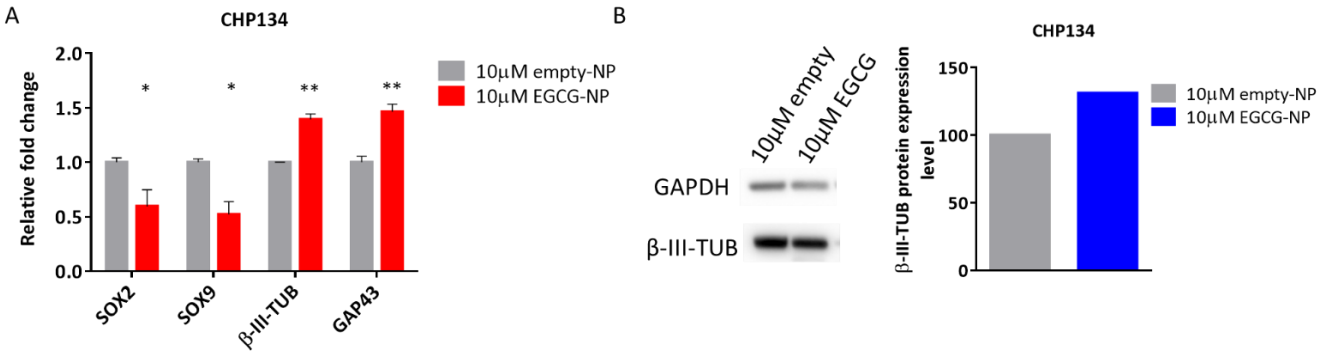

Figure 3.19. EGCG-NP treatment leads to increased levels of different differentiation markers.

(A) RT q-PCR analysis showing the variation of SOX2, SOX9, β-III-TUBULIN and GAP43 mRNA levels after 96h of EGCG-NP treatment. Data were normalized on the empty-NP treatment. SDHA was used as housekeeping. The statistical analysis was performed using GraphPad Prism 6, unpaired *t*-test analysis (*P< 0.05; ** P< 0.01;). n = 3 biological replicates, n = 3 technical replicates each. Data distribution has been controlled for normality. **(B)** Immunoblotting showing the protein levels of β-III-TUBULIN, the 10 μM empty-NP is the control (indicated as value of 100). One biological replicate quantified by densitometry analysis using Image Lab 3 Biorad Software.

Afterwards, we evaluated if the changes detected in the differentiation markers expression were also accompanied by phenotypic changes. In particular, we assessed neurite formation. We

quantified the length of the neurite-like protrusions of CHP134 cells treated with 5 μM and 10 μM of EGCG-NP and with 5 μM of 13-cis retinoic acid. As shown in **Figure 3.20**, a dose-dependent increase of neurite-like protrusion length was observed in cells treated with EGCG-NP.

In conclusion, the described results suggested that the treatment with EGCG-NP is able to increase the *let-7* miRNA levels, and consequently induce differentiation in NB cell lines.

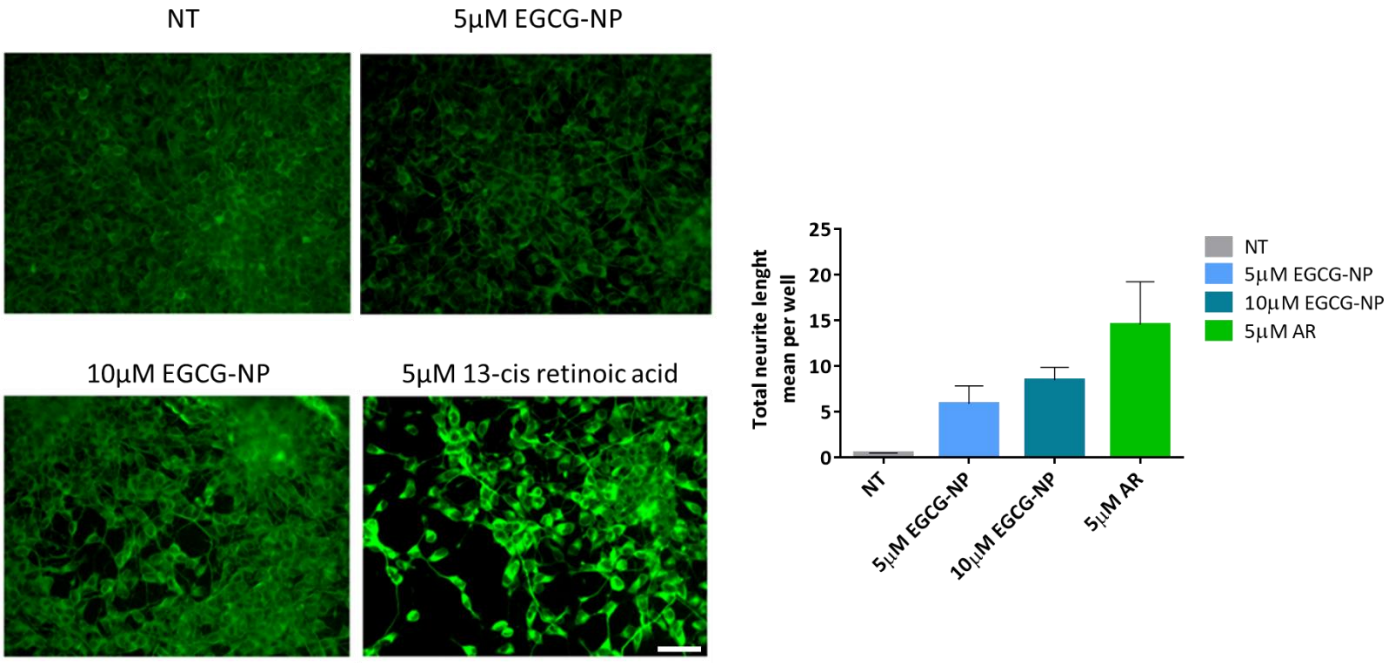

Figure 3.20. Measurement of neurite-like protrusion length upon EGCG-NP and 13-*cis*-retinoic acid treatment.

Representative images of immunofluorescence analysis of β-III-TUBULIN in CHP134 cells after 96h treatments with EGCG-NP (5 μM and 10 μM) and 13-*cis*-retinoic acid (5 μM). Scale bar 50 μm. Images were acquired using the Operetta-High Content Imaging System. The graph shows the total neurite length (μm), mean per well ± SD. n = 3 technical replicates. The quantification was performed using the Harmony software.

4. DISCUSSION

Neuroblastoma (NB) is a neuroendocrine tumour arising from any neural crest element during the sympathetic nervous system development. NB is a highly heterogeneous pathology regarding several aspects: genetics, clinics but also symptoms, the severity of disease and response to treatments.

This complexity has been an obstacle to identifying new therapeutic strategies, especially for the most aggressive form of the tumour. Indeed, despite in the last years, the approach to cure this aggressive form has been based on an increase of chemotherapeutic dose intensity, in the high-risk NB, the mortality rate is still high. Still up 20% of patients are refractory to the therapy, and 60% relapse after a complete treatment (Cole and Maris, 2012).

In this panorama, new therapeutic approaches aimed at dealing with the most aggressive forms of NB could hold promise for further improvements in survival and long-term quality of life. In particular, identifying treatments aimed to "cure" the cancer cells by inducing their differentiation could reduce the elevated general toxicity of therapies focused on the elimination of cancer cells. Indeed, the induction of tumour cells differentiation should lead to the spontaneous reduction of tumour size (Enane et al., 2018; Jögi et al., 2012). Moreover, the association of this approach with targeted therapy could further decrease the drugs' side effects.

In normal condition, LIN28B protein, whose expression is high in the early stage of development and in undifferentiated cells and tissues and decreases as the development proceeds or upon differentiation, is absent in most differentiated cells in adults (Guo et al., 2006). LIN28B is reactivated in NB and is associated with high-risk disease and with poor prognosis (Diskin et al., 2012). In addition, it has been demonstrated that LIN28B acts as an oncogenic driver in NB (Molenaar et al., 2012a). When the overexpression of this protein occurs, the principal molecular consequence is the inhibition of *let-7* miRNAs maturation and expression (Piskounova et al., 2011). *Let-7* miRNAs are essential tumour suppressors, which exert their activity by directly interacting and regulating genes involved in different cellular functions such as cell proliferation, differentiation and migration (Wang et al., 2012). LIN28B reactivation and the consequent decrease of *let-7* miRNAs level promote the undifferentiated state of cells, leading to uncontrolled cell proliferation and to the increase of tumour growth. The essential role of the LIN28B/*let-7* axis in cell differentiation, the dramatic consequences of LIN28B overexpression in NB, and the

fact that LIN28B is almost not present in adult differentiated tissues make this axis an interesting target for the identification of new therapies.

In this scenario, we decided to create an appropriate model to evaluate the biological effects of the LIN28B/*let-7* miRNAs complex inhibition in NB cells. In particular, LIN28B down-regulation in NB cells mimics the effect of a molecule able to interfere with the interaction between the protein and *let-7* miRNAs, representing an opportunity to understand the consequences of an increase in *let-7* miRNA maturation and therefore representing the positive control of cellular treatments. We used the CHP134 and NB69 cell lines, both carrying LIN28B overexpression but harbouring different MYCN status (amplified in the case of CHP134 and non-amplified in the case of NB69), representative of the different NB cell lines used in this work. We focused on LIN28B and MYCN different status because these alterations represent two of the most unfavourable prognostic factors for high-risk NB. We obtained stable LIN28B down-regulation by transfecting the cells with lentiviral particles carrying an shRNA complementary to the LIN28B sequence (shLIN28B), and as expected, we reported an increase of *let-7* miRNAs maturation (**Figure 3.1**). This outcome led us to biologically evaluate the effect of *let-7* miRNAs maturation, with a particular interest in the differentiative potential of LIN28B inhibition. To do so, we investigated the variation of some stemness- and differentiation-associated markers such as SOX2, SOX9 and GAP43 (Wakamatsu et al., 2004; Zhao et al., 2012). In both cell lines, we detected a significant decrease in the mRNA levels of SOX2 and SOX9. It is noted that SOX9 is a direct *let-7* miRNAs target (Barh et al., 2010; Mizuno et al., 2018a), and therefore, its down-regulation can be directly correlated to the miRNAs' activity, as previously observed in lung cancer cells (Johnson et al., 2007). Taken together, these results suggested that increased *let-7* miRNA levels in the down-regulated models could induce neuronal differentiation of NB cell lines (**Figure 3.2**). These results are supported by the previous demonstration of the correlation between LIN28B expression and neuronal differentiation or neurogenesis (Balzer et al., 2010; Eda et al., 2009; Olsson-Carter and Slack, 2010). Our evidence suggests that let-7 miRNAs modulation by LIN28B could be one mechanism that directly influences this differentiation process.

Confident of these results, we set out to identify a small molecule able to disrupt the LIN28B/*let-7* miRNA interaction, exploiting both biochemical and biological approaches.

Interestingly, in the last years, four high throughput screenings aimed at identifying molecules able to interfere with the LIN28/*let-7* miRNA axis have been reported (Lightfoot et al., 2016; Lim et al., 2016; Roos et al., 2016; Wang et al., 2018). All these studies used either fluorescence resonance energy transfer (FRET) or fluorescence polarization-based assays and mainly focused

on the biochemical validation of the selected hits, with minimal further biological validation in cells using *in vitro* experiments.

In order to identify a molecule able to interfere with the LIN28/*let-7* miRNA axis, we performed a drug screening on two commercial libraries of natural products and FDA approved molecules. We decided to use these libraries for two main reasons: first, a library of natural products is a source of large chemical variability, allowing us to perform a broad investigation; secondly, a library of FDA approved drugs allows a repositioning strategy. The screening was conducted exploiting the Alpha technique, which allows the evaluation of molecules activity in a high throughput format, while the validation of the selected hits was performed by REMSA (**Figure 3.3** and **3.4**). The use of two complementary biochemical methods increased the strength of our final results. At the end of the validation phase, we selected three molecules: the epigallocatechin-3'-monogallate (EGCG), the theaflavin monogallate (TFMG) and the aurintricarboxylic acid (ATA). Interestingly, the EGCG and TFMG share a similar sub-scaffold and are characterised by structural similarity, while ATA was selected as a LIN28B inhibitor by another group exploiting a different biochemical approach (Lightfoot et al, 2016).

The biochemical results obtained and the structure-based molecular docking studies (**Figure 3.6**) suggested that the three molecules can successfully inhibit the LIN28B/*let-7* miRNA interaction by binding to LIN28B protein. However, the hits' chemical structure is characterised by high hydrophilicity, a feature that could lead to low permeability through cellular membranes, determining non-optimal pharmacokinetics. In order to ameliorate this issue, we proceeded with the synthesis of catechin (scaffold shared by EGCG and TFMG) and aurintricarboxylic acid analogues by converting the hydroxyl groups into acetyl or ether derivatives and by inserting hydrophobic moieties to decrease the hydrophilicity of the molecules (**Figure 3.7** and **3.8**). We tested the analogues activity with Alpha assay and REMSA and calculated LIN28B/pre-*let-7*g miRNA complex inhibition percentages. However, the EGCG resulted in being the molecule with the best inhibitory activity, suggesting that the molecule's hydrophilicity is essential for the interaction with LIN28B/*let-7* complex (**Table 3.1**). Therefore, we selected EGCG as a drug candidate for further biological characterization.

EGCG is a well-known polyphenol compound already studied for different applications. In fact, EGCG has a strong antioxidant activity and works by several groups demonstrated its important anticancer properties due to the direct inhibition of transduction pathways involved in tumour development, showing an antiproliferative and pro-apoptotic effect on cancer cells (Du et al., 2012; Hou et al., 2004; Khan et al., 2006; Yang et al., 2009).

We started our biological validation of EGCG by treating five NB cell lines characterised by different LIN28B expression levels and MYCN status and evaluating their sensitivity to the molecule (**Figure 3.10**). We hypothesized that cell lines carrying different LIN28B expression levels might show variable sensitivities to EGCG treatment. In particular, we epected two possible scenarios. In a first scenario, a weak expression of the protein could correlate with higher sensitivity to EGCG given that, theoretically, a lower amount of the drug would be sufficient to saturate the LIN28B/*let-7* axis. In a second scenario, opposite to the first proposed, cell lines expressing higher levels of the target could be more sensitive to a drug treatment because even a small reduction of LIN28B might already be effective. The data obtained on the five cell lines tested are not sufficient to support neither the first nor the second scenario. Indeed, further experiments on a larger panel of NB cell lines are required to establish a possible correlation between LIN28B expression levels and sensitivity to EGCG treatment. These further experiments would also be needed to evaluate a possible correlation between the variability of the sensitivity among the cells and their MYCN status. Finally, it has also to be considered that cells present several intrinsic mechanism, such as Multi Drug Resistance (MDR) channels, that account for drug treatment resistance. Indeed, MDR channels are membrane proteins involved in the export of a plethora of xenobiotics, which have been extensively studied in the context of cancer drug resistance (Liu, 2019) Therefore, the differential sensitivity observed upon EGCG treatment could be, at least partially, also related to these intrinsic resistance mechanisms that vary among different cell lines.

The GI_{50} value calculation was essential to select treatments concentrations that avoid an excessive cytotoxic effect on the cells, allowing the evaluation of other biological effects of EGCG, especially the differentiation-inducing potential. The first parameter to be evaluated after the treatment has been the increase of *let-7* miRNAs to assess if the molecule could inhibit the LIN28B/*let-7* miRNA interaction also in cells. Disappointingly, the detected increase of miRNAs levels was much lower than expected (**Figure 3.11**) and than that observed in our LIN28 down-regulation models.

It has been reported that EGCG has low stability in solution and that it quickly deteriorates, losing its original chemical structure and, therefore, its activity and effects (Fangueiro et al., 2014). We confirmed by HPLC analysis that EGCG is not stable in the cell-culture conditions used for our experiments, observing that EGCG is reduced by more than 50% after 15 minutes and is completely degraded after 45 minutes (**Figure 3.12**). We hypothesised that the moderate increase in *let-7* miRNAs observed upon EGCG treatment was due to its degradation. Indeed, the

molecule's low stability suggested that the amount of EGCG within the cells might not be enough to induce and detect an effect on *let-7* miRNAs modulation.

In the last years, the cohesion of disciplines as biology, chemistry, engineering, and medicine allowed the introduction of nanotechnology in therapies. In particular, the application of nanoparticles for the encapsulation of drugs in cancer has assumed an increasing interest due to the possibility of enhancing the delivery of a specific drug while reducing the general toxicity of treatments (Ferrari, 2005; Nie et al., 2007). Indeed, nanoparticles' structure and the variability of components used to synthesise these carriers allow the inclusion of different drugs, independently by their chemical characteristics (Ma et al., 2013). Another essential aspect that makes these devices suitable for improving current and future therapies is the possibility to be functionalized on their surface, allowing targeted therapies (Mout et al., 2012).

To solve the EGCG stability issue, we decided to encapsulate the molecule into nanoparticles. Among the large variety of existing nanosystems, we decided to use the PLGA-PEG nanocarriers due to their exhaustive characterisation *in vitro* and *in vivo*, resulting in one of the most biocompatible systems (Cheng et al., 2007; Elmowafy et al., 2019). Most importantly, PLGA-PEG nanoparticles have been already used for the nano-encapsulation of EGCG, resulting in a significant increment of molecule effect both in cells and in mouse models (Sanna et al., 2017).

We first evaluated the capacity of the nanoparticles to permeate NB cells by treating the cells with PLGA-PEG nanoparticles carrying Coumarin-6 fluorophore and quantifying the amount of fluorescence inside the cells (**Figure 3.14**). The results showed a stable accumulation of the fluorophore inside the cells, suggesting that the PLGA-PEG nanosystem could be suitable for our purpose.

Subsequently, we proceeded by treating the cells with PLGA-PEG nanoparticles carrying EGCG (EGCG-NP). As a control, we used empty nanoparticles (empty-NP) (**Figure 3.15**). This experiment elucidated essential aspects. First, the molecule's encapsulation leads to a significative decrease of the GI_{50} value compared to the free drug in all cell lines analysed, suggesting that the PLGA-PEG nanocarrier protects and stabilises the EGCG, leading to a significant increase in molecule accumulation within the cells. Secondly, the treatment with empty-NP did not affect the viability of the cells, confirming the biocompatibility of the polymers. The evaluation of *let-7* miRNA variation after the treatment using different EGCG-NP concentrations showed a significant increase in all the *let-7* miRNA family members analysed (**Figure 3.16**), demonstrating that the molecule effectively interferes with LIN28B/*let-7* miRNAs interaction not only biochemically but also biologically. Moreover, the increase of *let-7* miRNAs

is not dependent on MYCN status, suggesting that the EGCG-NP treatment could be effective also in cells carrying this NB critical aberration.

We next treated the NB cell lines with different concentrations of EGCG-NP and evaluated the effect on cell growth. We observed a dose-dependent inhibition of proliferation in all cell lines analysed (**Figure 3.17**). We noticed that the lower concentrations of EGCG-NP able to efficiently increase *let-7* miRNAs' expression do not inhibit proliferation (e.g. concentration of 2.5uM in Kelly and NB69 cells). Therefore, we observed that increasing the levels of *let-7* was not always sufficient to affect proliferation. It would be possible to use a genetic approach, i.e. knock out of LIN28B by CRISPR/Cas9 technology, to create a cell model characterized by LIN28B complete knock-out. We could then use this model to evaluate if the absence of LIN28B and the consequent increase of the *let-7* miRNA leves would result in a reduction or even inhibition of cell proliferation in our cell lines. Nevertheless, our data clearly show that it is difficult to establish a direct correlation between the increase of *let-7* miRNA family members' levels due to LIN28B-*let7* axis alteration upon drug treatment, and the inhibition of cell proliferation. In fact, there could be a shift in time between the pharmacological induction of *let-7* miRNA levels, which shoud occur quickly upon LIN28B inhibition, and the effect on cell proliferation. This consideration, could partially explain the observation that the lower concentrations of EGCG-NP, able to efficiently increase *let-7* miRNAs' expression, do not inhibit proliferation.

Higher doses are necessary for cell growth inhibition, which appears stronger in NB69 cells (with lower LIN28B expression) compared to Kelly cells. The different results observed in NB69 and Kelly cells at higher doses of EGCG-NP could be explained by considering the different MYCN status of the two cell lines, indeed Kelly cells could respond differently to the treatments due to the pronounced MYCN-amplification (Sidarovich et al., 2014). The influence of MYCN amplification on the LIN28B/*let-7* axis remains to be clarified. Still, it seems that the presence of this amplification leads to a reduction of *let-7* miRNAs effects also in the presence of LIN28B down-regulation (Powers et al., 2016), limiting the effect of LIN28B inhibition.

In addition, given the reported antiproliferative and pro-apoptotic effect of EGCG on other cancer cells we can not exclude that the effect on cell growth observed upon EGCG treatment could be related also to other pathways independent on the LIN28B/*let-7* signalling axis. Some of these pathways could be anyway related to LIN28B circuit inhibition (Tao et al., 2020; Chikano et al., 2015; Gonzalez Malagon et al., 2018; Hur and Zhou, 2010; Raveh et al., 2009).

Since the LIN28B/*let7* miRNA signalling axis is involved in the maintenance of cellular stemness and its inhibition results in differation promotion, we investigated if the EGCG-NP treatment

could induce differentiation. First, we assessed a variation of differentiation markers, as observed in our LIN28B down-regulated models. As a reference compound, we use the 13-cis-retinoic acid (RA), which has an important role in current NB therapies as a differentiation-inducing drug. In particular, the treatment with RA has been shown to induce the reduction of proliferation and the neuronal differentiation of NB cells, among which CHP134 (Voigt et al., 2000).

The increase of the β-III-TUBULIN and GAP43, two neuronal differentiation markers, was detected by immunofluorescence after CHP134 cells treatment with both EGCG-NP and RA (**Figure 3.18**), although with a greater extent upon RA treatment. The mRNA variation of these markers was confirmed in EGCG-NP treatment by RT-PCR. This evidence was supported by the concomitant decrease of the stemness markers SOX2 and SOX9 (**Figure 3.19**). We also detected cells phenotypic changes, especially at higher EGCG-NP concentration and upon RA treatment such as development of neurite-like protrusions (**Figure 3.20**) (Takada et al., 2001; Voigt et al., 2000).

Taken together these data suggest a partial induction of neuronal differentiation of CHP134 upon EGCG-NP treatment, although less efficient compared to the differentiation induced by RA treatment. Based on the lower effect of EGCG-NP on differentiation promotion, EGCG treatment seems to have no significant advantage compared to a strategy already included in clinical standards (AR alone). However, at present, we have analysed only one early time point (96h) and further experiments after prolonged exposure to EGCG-NP are needed to deeply evaluate the molecule capability to promote differentiation. In addition, experiments aimed at evaluating the effects of EGCG-NP and RA combined treatment have definitely to be conducted to explore an eventual additive or even synergic effect of the two molecules. For example, the EGCG anticancer activity has been evaluated in synergism with breast and ovarian cancers' primary treatments, demonstrating that EGCG improves these drugs' effect, resulting in an adjuvant in treating these tumours (Stuart and Rosengren, 2008; Wang et al., 2015). An additive or synergic effect betweenEGCG-NP and RA could lead to an improvement of RA differentiative effect and lead to a possibility of improvement of the clinical standards.

5. CONCLUSIONS

This thesis aimed at identifying a molecule able to interfere with the LIN28B/*let-7* miRNA interaction in order to increase *let-7* miRNA cellular levels, finally leading to cellular differentiation induction.

First, to simulate the pharmacological inhibition of the LIN28B/*let-7* miRNA axis and evaluate the consequent effects on cellular differentiation, we created a cellular model by down-regulating LIN28B in the NB cell lines. As expected, LIN28B downregulation resulted in increased *let-7* miRNA levels and increased differentiation markers.

Pushed by these promising results, we performed a high-throughput screening using two commercial libraries, carried out the subsequent validation experiments and selected three molecules (EGCG, TFMG and ATA) with a variable inhibitory effect on the LIN28B/*let-7* miRNAs complex interaction. We tried to improve the molecules' pharmacokinetic properties by synthesizing analogues presenting acetyl, methyl ether or hydrophobic moieties. After the experimental evaluation of the synthesized analogues, the EGCG resulted to be the most potent molecule, able to completely inhibit the LIN28B/*let-7* miRNA complex at the highest concentrations tested and was thus selected for further experiments.

We proceeded by evaluating EGCG effects in cells, using drug concentrations below or around the GI_{50} value in order to avoid excessive cytotoxic effects and thus observe the differentiation-inducing potential of EGCG. It has to be noted that EGCG resulted in being very unstable in the cell culture conditions, therefore we decided to encapsulate it into PLGA-PEG nanoparticles, a nanocarrier system that has been shown to prevent the molecule degradation and to enhance its delivery inside the cells. Upon EGCG nanoparticle treatment, we detected the increase of *let-7* miRNAs in all the cell lines analysed, and we observed the consequent inhibition of cellular growth. Furthermore, the evaluation of the variation in differentiation marker levels suggested that the increase of *let-7* miRNAs obtained upon EGCG nanoparticle treatment is able to lead to the induction of neuronal differentiation processes in NB cells.

Although these last results need to be confirmed with further experiments to better characterize the differentiation process and better elucidate the molecular biology behind the inhibition of LIN28B/*let-7* miRNA interaction, the LIN28B/*let-7* miRNA axis represents definitely a good therapeutic target. EGCG and/or other molecules able to interfere with this interaction deserve for sure further preclinical and clinical evaluation.

6. ONGOING WORK AND FUTURE RESEARCH

Our results suggest that inhibiting the LIN28B/*let-7* axis either by LIN28B silencing or by chemically perturbing the axis *via* EGCG treatment results in *let-7* miRNA levels increase and in the consequent induction of NB cell line differentiation. This biological effect could be crucial for NB treatment because the differentiation of cancer cells should lead to tumour growth reduction. Nevertheless, the consequences of *let-7* miRNA increase still need to be investigated in more detail. Indeed, *let-7* miRNAs interact with several targets, each of them involved in specific pathways. Since our focus is the induction of differentiation, we would need to understand which targets of *let-7* miRNAs are involved in this process. Our results suggest that EGCG-NP affects the expression levels of several stemness and differentiation markers, such as SOX2, SOX9, GAP43 and, β-III-TUBULIN and induces phenotypic changes in the cells, such as an increase in neurite-like protrusion length. However, these data need further cellular validations. For example, it would be crucial to perform a broader analysis, to better understand if other differentiation markers are affected or what are the biological consequences of the phenotypic changes observed.

Furthermore, it would be crucial to validate the activity of EGCG-NP using *in vivo* models. As a first step, we decided to test the molecule's activity on zebrafish embryos. Indeed, this animal model presents several advantages, such as the fast embryonic generation rate and the animal's transparency that allows live and non-invasive fluorescent imaging (Gutiérrez-Lovera et al., 2017). In collaboration with Dr. Sanja Aveic and Dr. Diana Corallo (Pediatric Research Institute - Città della Speranza, Neuroblastoma Laboratory; Padua), we evaluated the capability of CHP134 cells pretreated with EGCG to extravasate blood vessels after injection in zebrafish embryos. This feature can be used as a proxy to assess cancer cell aggressiveness. In detail, we used embryos of the transgenic (fli1: EGFP) zebrafish line, in which the promoter of endothelial marker fli1 allows the expression of EGFP in blood vessels (Stoletov et al., 2007), to better visualize blood vessels. CHP134 cells were pretreated with either EGCG-NP (10 μM) or empty-NP for 48h. CHP134 cells not-treated (NT) were used as further control. After 48h of treatment, the cells were detached, labelled with the Vybrant® DiI dye and injected into embryos. The extravasation of labelled-CHP134 was monitored at two-time points: 2h and 24h post-injection (respectively 2hpi, 24hpi) (**Figure 6.1**). The relative fluorescence quantification showed comparable extravasation among

the treated conditions and the NT (**Figure 6.1**, *right*). However, we detected a significantly low engraft in embryos injected with CHP134 cells, suggesting that this cell line does not possess a strong engrafting ability.

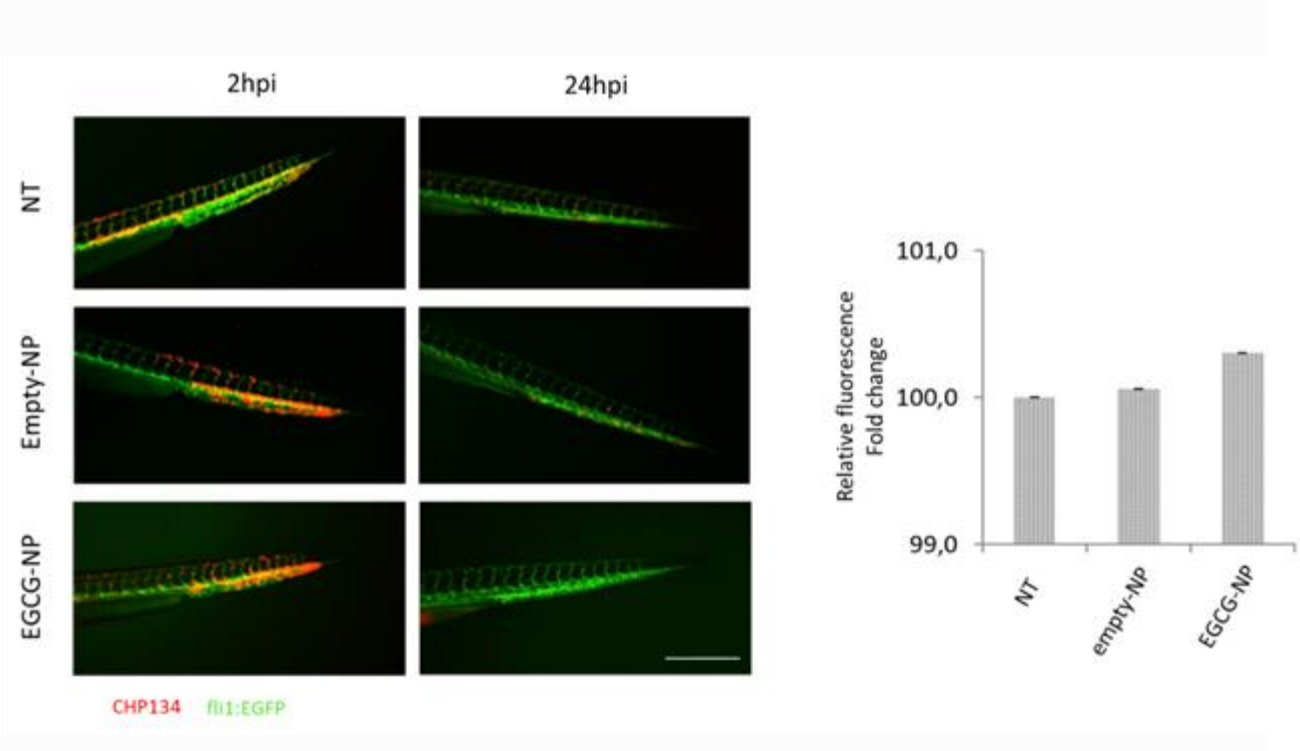

Figure 6.1. Extravasation of CHP134 treated cells in a zebrafish xenotransplantation model.

Representative fluorescent microscopy images of transgenic (fli1: EGFP) zebrafish line embryos injected with pre-treated CHP134 (NT, empty-NP, EGCG-NP) and labelled with the Vybrant® DiI (red). The graph shows the average fluorescence of CHP134 cells (red) in each group, 24h post-injection. The data were normalised on NT (100%). n = 1 biological replicate.

Since we suspected that the non-optimal CHP134 cell engraftment capability might alter the preliminary results obtained, we decided to repeat these experiments using another NB cell line, the SK-N-Be(2) cell line, also characterised by high LIN28B expression. This cell line's engraftment capacity has been already verified by our collaborators, suggesting that this cell model might be better for our purpose. We evaluated the sensitivity of SK-N-Be(2) cells to the EGCG-NP and empty-NP treatment by testing different doses and constructing dose-response curves (**Figure 6.2A**). We then calculated the GI_{50} value deriving from the dose-response curves in order to select and avoid molecule concentrations leading to critical cytotoxicity. We then assess the variation of *let-7* miRNA levels upon treatment with two EGCG-NP concentrations around and below the GI_{50} value (10 μM and 15 μM). Empty-NP were used as control. The results

showed increased *let-7*d and *let-7f*, even if lower at higher concentration (**Figure 6.2B**), but these preliminary results need further confirmation. Currently, we are performing the experiments on zebrafish embryos injected with SK-N-Be(2) cells pretreated with NT, empty-NP or EGCG-NP, therefore evaluating if the original engraftment ability, associated with tumour aggressiveness, is maintained or reduced in treated cells.

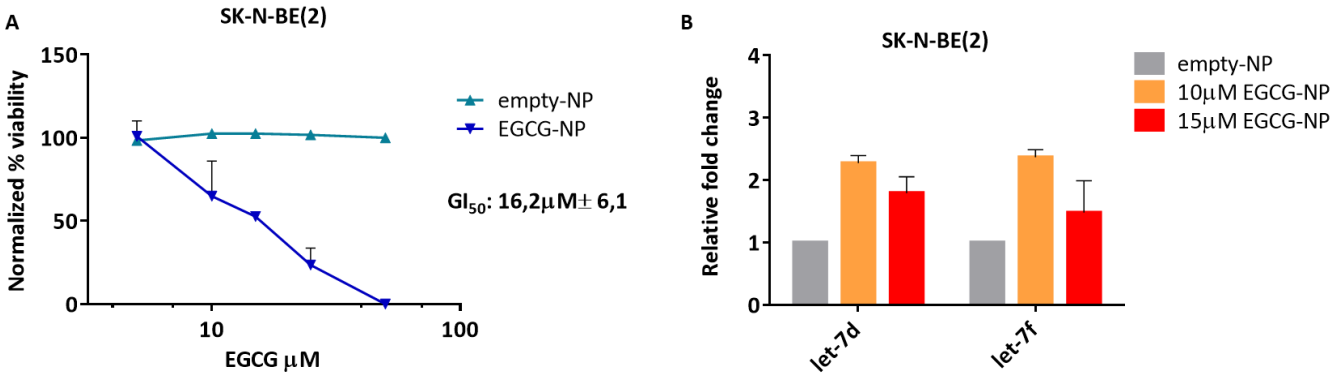

Figure 6.2. Dose-response curve on SK-N-Be(2) cells and evaluation of *let-7 miRNA*s variation.

(A) Dose-response curves on SK-N-Be(2) cells. The cells were treated using different concentrations of EGCG-NP and empty-NP, ranging from 5 µM to 50 µM. The data are expressed as the percentage of viability normalized on NT. After 48h of treatment, the cell viability was measured using the Cell Titer-Glo Assay. n = 2 biological replicates, n = 3 technical replicates each. GI_{50} value was calculated from the dose-response curves. Mean ± SD. **(B)** RT-qPCR analysis of the expression of two *let-7* miRNA family members after EGCG-NP and empty-NP treatment. RT-qPCR shows the fold change relative to empty-NP, and the data are normalised on U6. The graph was plotted using GraphPad Prism 6 software, n= 3 technical replicates, mean ± SD.

7. METHODS

7.1 CELL CULTURES

Human neuroblastoma cell lines **SK-N-AS** (ECACC 94092302) and **SK-N-FI** (ECACC 94092304) were cultured in DMEM supplemented with 2mM Glutamine (Thermo Fisher Scientific), 1% of Non-Essential Amino Acid (NEAA) (Thermo Fisher Scientific), 10% of Foetal Bovine Serum (FBS) (Thermo Fisher Scientific) and 1% of Penicillin-Streptomycin (10,000 U/mL) (Gibco). Human neuroblastoma cell lines **NB69** (ECACC 99072802) and **KELLY** (ECACC 92110411), and **CHP134** (ECACC 06122002) were cultured in RPMI 1640 (Sigma-Aldrich) supplemented with 2mM Glutamine (Thermo Fisher Scientific), 10% of Foetal Bovine Serum (FBS) (Thermo Fisher Scientific) and 1% of Penicillin-Streptomycin (10,000 U/mL) (Gibco). Human neuroblastoma cell line **SK-N-Be(2)** (ECACC 95011815) were cultured in EMEM (EBSS) supplemented with 1% of Non-Essential Amino Acids (NEAA) and Ham's F12 (Thermo Fisher Scientific and Lonza 1:1 ratio), 10% of Foetal Bovine Serum (FBS) (Thermo Fisher Scientific) and 1% of Penicillin-Streptomycin (10,000 U/mL) (Gibco). Human embryonic kidney **HEK293T** (ECACC 12022001) were cultured in DMEM supplemented with 2mM Glutamine (Thermo Fisher Scientific), 1% of Non-Essential Amino Acid (NEAA) (Thermo Fisher Scientific), 10% of Foetal Bovine Serum (FBS) (Thermo Fisher Scientific), and 1% of Penicillin-Streptomycin (10,000 U/mL) (Gibco).
The cells were grown at 37°C and 5% CO_2. Cultures were passed by using Trypsin-EDTA (0.05%), phenol red (Gibco).

7.2 GENERATION OF LIN28B DOWN-REGULATED CELL LINES

To produce the lentiviral particles, HEK293T were seeded at a density of 4 x 10^6 cells in 10 cm^2 dishes. The cells were co-transfected in OPTI-MEM (Gibco) with 10 µg of LIN28B shRNA (MISSION shRNA plasmid DNA, Sigma Aldrich) or scramble shRNA (PLKO.1-puro, Sigma-Aldrich), 5 µg of psPAX2 (Addgene #12260), and 2.5 µg of pMD2.G (Addgene #12259) for each dish. The transfection was performed using Lipofectamine 2000 (Thermo Fisher Scientific) in a 1:1 ratio with LIN28B shRNA or scramble shRNA. To obtain LIN28B down-regulation, NB69 and CHP134 cells were transduced with the viral particles containing LIN28B shRNA or scramble

shRNA. The NB69 were selected with 5 μg/mL puromycin, while the CHP134 were selected with 3 μg/mL puromycin (InvivoGen).

7.3 rLIN28B PROTEIN PURIFICATION PROTOCOL

To produce the recombinant LIN28B (rLIN28B) protein HEK293T cells were seeded at a density of 7.5 x 10^6 cells in a 150 cm^2 dish. After 24h, cells were transiently transfected with pCMV6-LIN28B-MYC-HIS (Origene) using polyethylenimine (PEI 408727, Sigma-Aldrich) as transfection reagent in a ratio vector: PEI = 1:3. After 24h, rLIN28B was purified according to the following protocol. The composition of the buffers used during purification is reported in **Table 4.1**.
Briefly, 24h after transfection, the media of the cells was removed, and 2ml of EQ buffer were added. Using a cell scraper, the cells were detached from the dish and collected in a 2ml tube. The solution was sonicated on ice at 4°C (45 of amplitude, 7 cycles of 10 seconds, and 10 seconds of pause between each cycle, power at about 250 W). The lysate was then centrifuged at Vmax (about 13200 rpm) for 20 minutes at 4°C, and the supernatant was collected in a 15 ml tube.
In parallel Ni^{2+} agarose beads (Qiagen), stored in 20% ethanol, were equilibrated in EQ buffer, which was discarded after a centrifugation step of 2000 rpm for 30 seconds. The beads were then added to the lysate and incubated for 4 hours at 4°C on rotor shaking. After the incubation, the solution was centrifuged at 2000 rpm for 2 minutes, and the supernatant was discarded. The beads were resuspended in 1ml of W1 buffer and incubated in rotor shaking for 15 minutes, and the solution was centrifuged again. The same procedure was repeated, resuspending the beads in W2. At the end of the washing phase, the beads were incubated with EL1 for 30 minutes at 4°C on rotor shaking. Then the solution was centrifuged, and the supernatant containing the protein was collected. This step was repeated two times. The same procedure was repeated, resuspending the beads in El2.
The protein contained in EL1 and EL2 was dialyzed using D-Tube™ Dialyzers midi (Merk Millipore) for 2 hours in a cold room. The protein was divided into aliquots and stored at -80°C.

Table 4.1. The composition of the buffers used during rLIN28B purification.

Buffer	Composition
Equilibration buffer (EQ)	25 mM Tris-Cl pH 8; 100 mM NaCl; 0.05% NP-40; 1 mM DTT; 3 mM $MgCl_2$; 10 mM Imidazole; Protease inhibitors (diluted 1:100)
Wash1 (W1)	25 mM Tris-Cl pH 8; 200 mM NaCl; 0.05% NP-40; 1 mM DTT; 3 mM $MgCl_2$; 50 mM Imidazole.
Wash2 (W2)	25 mM Tris-Cl pH 8; 300 mM NaCl; 0.05% NP-40; 1 mM DTT; 3 mM $MgCl_2$; 50 mM Imidazole
Wash3 (W3)	25 mM Tris-Cl pH 8; 300 mM NaCl; 0.05% NP-40; mM DTT; 3 mM $MgCl_2$; 70 mM Imidazole
Wash4 (W4)	25 mM Tris-Cl pH 7; 500 mM NaCl; 0.05% NP-40; 1 mM DTT; 3 mM $MgCl_2$; 70 mM Imidazole
Elution buffer (EL)	25 mM Tris-Cl pH 8; 250 mM NaCl; 3 mM $MgCl_2$; 400 mM Imidazole
Dialysis buffer	25mM HEPES pH 7.4; 110mM KCl; 10Mm NaCl; 1Mm $MgCl_2$ 15uM $ZnCl_2$; 0.02% Tween; 0.1 % p/v ultrapure BSA

Stock solutions: 1 M Tris-HCl, pH 8.0; 1 M Tris-HCl, pH 7.0; 100 mM MgCl2; 1 M NaCl; 1 M Imidazole; 10% NP-40. The purification buffers were prepared in DEPC-water (MilliQ).

7.4 ALPHASCREEN ASSAY

The AlphaScreen assay was performed following the manufacturer's instructions (PerkinElmer guide).

Briefly, to avoid false-negative results due to a disequilibrium among the beads and the number of ligands, we calculated the hook point, which is the exact point at which the beads are saturated with the protein. Additional protein will not bind the beads, therefore this phase is essential to identify the protein concentration to be used Using the Alpha screen Kit (AlphaScreen c-Myc Detection kit, PerkinElmer) and 384-well white opaque plates (PerkinElmer), we determined the

hook point by testing several rLIN28B dilutions and adding for each well 100nM of BI-pre-let-7g miRNA and 20 µg/ml of anti-His acceptor beads (PerkinElmer). The reaction was evaluated using a specific buffer containing: 25 mM HEPES pH 7.4, 110 mM KCl, 10 mM NaCl, 1 mM $MgCl_2$, 15 µM $ZnCl_2$, 0.02% Tween-20, 0.1% p/v ultrapure BSA. The reaction was incubated at room temperature in the dark, for 30 min. Then, 20 µg/ml of Streptavidin-coated donor beads (PerkinElmer) were added, and the reaction was incubated at room temperature for 1 h. At the end of the incubation, the Fluorescence was detected using the Enspire Multimode Plate reader (Perkin Elemer).
For the screening, the optimal concentration for rLIN28B was 10nM. The molecules were tested at the fixed concentration of 75nM.

7.5 RNA-Electrophoresis Mobility Shift Assay (REMSA)

To perform the REMSA assay, 10 µM of molecule was incubated with rLIN28B and 6 nM of Cy3-labeled pre-let-7g RNA, in a final volume of 20 µl (20 mM HEPES pH 7.5, 50 mM KCl, 0.5 µg BSA, 0.25% Glycerol) at room temperature, in the dark for 1h. Then, the reaction was loaded into a 6% polyacrylamide gel with 0,5% Glycerol. The run was performed using a TBE (5,5x) buffer, at 80 V at 4°C for 45 min. The signal was detected with Typhoon Instrument (GE Healthcare; 00-4277-85 AC). The images were quantified using ImageJ Fiji software.

7.6 Evaluation of EGCG, EGCG-NP and empty-NP cytotoxicity

For the evaluation of the cytotoxic effect of EGCG, EGCG-NP or empty-NP on NB cell lines, cells were seeded into 96-well laminin-coated microtiter plates in 100 µL of media. The plates were incubated for 24h prior to drug treatment. Serial drug dilutions were prepared in PBS. 5 µL of these dilutions were added to each well, and the plates were incubated for additional 48h. Each treatment was performed in technical triplicate.
The cell viability was evaluated using the CellTiter-Glo® Luminescent Cell Viability Assay (Promega, cat. G7570), following the manufacturer's instructions. The viability was expressed as percentage of the non-treated control. Dose-response curves were plotted and the deriving GI_{50} values were calculated using the GraphPad Prism software.

7.7 IMMUNOBLOTTING

Total cell lysates were prepared from cells. Cells were washed with PBS and resuspended in RIPA lysis buffer supplemented with protease inhibitors (Thermo Scientific). Proteins were quantified with Pierce™ BCA Protein Assay Kit (Thermo Fisher Scientific, cat. 23227). The same amounts of protein were separated on SDS-PAGE and transferred to a nitrocellulose membrane. The proteins signal was detected with anti-LIN28B (Cell Signaling, #4196); anti-β-tubulin (Santa Cruz, cat. sc-53140) and secondary antibody HRP-conjugate (Santa Cruz Biotechnology). The signal was detected using Amersham ECL Prime or Select Western Blotting Detection Reagent (GE Healthcare Life Sciences) and ChemiDoc Imaging System (Bio-Rad). Protein expression was quantified using ImageLab software (Bio-Rad).

7.8 IMMUNOFLUORESCENCE

Cells were fixed with paraformaldehyde (4% v/v; Sigma-Aldrich) for 15 min at room temperature. The permeabilization was performed with 0.3% Triton X-100 in PBS for 15 min and then incubated in blocking solution (PBS, 5% FBS, 0.2% Triton X-100) for 1h at room temperature. Primary antibodies were diluted in 0,2% Triton X-100 +2% FBS in PBS and incubated at 4°C overnight. The incubation with the proper Alexa Fluor secondary antibodies (Thermo Fisher Scientific) was conducted at room temperature for 1h. Nuclei were stained with Hoechst 33342 (1 µg/mL, Thermo Fisher Scientific, cat. H1399) and incubated 5 min at room temperature. Cells were stained with HCS CellMask™ Deep Red Stain (Thermo Fisher Scientific, cat. H32721, 1:2000, 20 min, room temperature) to determine their morphology. The fluorescence was read using the Operetta-High Content Imaging System (Perkin Elmer) and quantified by Harmony Software.

7.9 DETECTION OF COUMARIN-6-NANOPARTICLES

NB69 cells were seeded on a six-well plate (100.000 cell/well) and treated with different dilutions (NT, 0.0003µg/µl, 0.003µg/µl and 0.03µg/µl) of Coumarin-6-containing nanoparticles (Cou-6-NP) for 48h. Cell cultures were washed with PBS and fixed with diluted paraformaldehyde (4% v/v; Sigma-Aldrich) incubated for 15 min at room temperature. Hoechst

33342 (1µg/mL, Thermo Fisher Scientific) and HCS CellMask™ Deep Red Stain (Thermo Fisher Scientific) were used to identify cell nuclei and cell surface, respectively. The fluorescence was read using the Operetta-High Content Imaging System (Perkin Elmer) and quantified by Harmony Software.

CHP134 cells were seeded on glass slides previously leaned in a 6 well plate (150.000 cells/well) and treated with Cou-6-NP at a concentration of 0.003 µg/µl for 48h and then fixed with paraformaldehyde (4% v/v; Sigma-Aldrich). The cells were imaged with a Leica TCS SP8 confocal microscope equipped with a 63x/1.4 oil objective. Images were acquired at 400 Hz unidirectional scan speed with 2x zoom and 130 nm z-step. Cou-6 signal was excited at 458 nm using Argon as a laser source and collected using a HyD at 490-560 nm. Hoechst 33342 (1µg/mL, Thermo Fisher Scientific) and HCS CellMask™ Deep Red Stain (Thermo Fisher Scientific, cat. H32721) were used to identify cell nuclei and cell surface, respectively.

7.10 RNA EXTRACTION AND REAL-TIME QPCR

Total RNA was extracted using Trizol Reagent (Thermo Fisher Scientific) according to the manufacturer's instructions. Reverse transcription was performed on 1 µg of RNA with RevertAid RT Reverse Transcription Kit (Thermo Fisher Scientific). The cDNA was diluted 1:10, and qRT-PCR was performed using KAPA SYBR FAST qPCR Master Mix (2X) kit (Kapa Biosystems) according to the manufacturer's indications and ran using CFX96 Real-Time System (BioRad). The data were analysed with CFX Manager software (BioRad) and normalised on SDHA or GAPDH. The following primers were used:

Gene	**Primers**
LIN28B	Fw 5' GAGTCAATACGGGTAACAGGAC 3' Rev 5'CACCACAGTTGTAGCATCTATCT 3'
SOX2	Fw 5' GTATCAGGAGTTGTCAAGGCAGAG 3' Rev 5' CTAGTCTTAAAGAGGCAGCAAAC 3'
SOX9	Fw 5' GTACCCGCACTTGCACAC 3' Rev 5' TCTCGCTCGTTCAGAAGTC 3'

GAP43	Fw 5' GGC CGC AAC CAA AAT TCA GG 3' Rev 5'CGGCAGTAGTGGTGCCTTC 3'
β-III-tubulin	Fw 5' TCAGCGTCTACTACAACGAGGC 3' Rev 5' GCCTGAAGAGATGTCCAAAGGC 3'
HPRT1	Fw 5' TGACACTGGCAAAACAATGCA 3' Rev 5' GGTCCTTTTCACCAGCAAGCT 3'
SDHA	Fw 5' TGGGAACAAGAGGGCATCTG 3' Rev 5' CCACCACTGCATCAAATTCATG 3'

7.11 miRNAs QUANTIFICATION

The RNA was extracted using Trizol Reagent (Thermo Fisher Scientific) according to the manufacturer's instructions. The reverse transcription was performed using the miRCURY LNA RT Kit (Qiagen cat. 339340). Briefly, the RNA was diluted at 30 ng/µl and added to the kit components (5X miRCURY RT Reaction Buffer; 10x miRCURY RT Enzyme Mix; RNase-free water) and retro transcribed following the manufacturer's instructions. qRT-PCR was performed using the miRCURY LNA SYBR Green PCR Kit (Qiagen 339345). In particular, the cDNA was diluted 1:10, added to the kit components (2x miRCURY SYBR Green Master Mix; PCR primer mix; RNase-free Water). The qRT-PCR was performed using the CFX96 Real-Time System (BioRad). The data were analysed with CFX Manager software (BioRad) and normalised on U6. The following primers were used: U6 snRNA (hsa, mmu) (cat n. 339306, YP00203907); hsa-let-7d-5p (cat n. 339306, YP00204124); hsa-let-7f-5p (cat n. 339306, YP00204359); hsa-let-7g-5p (cat n. 339306, YP00204565); hsa-let-7i-5p (cat n. 339306, YP00204394).

7.12 EGCG STABILITY EVALUATION BY HPLC ANALYSIS

EGCG stock solution was prepared by dissolving 1.51 mg in 32.94 µL of DMSO (100 mM). 1 mM aqueous solution (1% DMSO v/v) were prepared by dilution of DMSO stock solution with RPMI. The solutions were further diluted to get six different concentrations (10 µM, 25 µM, 50 µM, 100 µM, 250 µM, 500 µM, 1% DMSO each).

The calibration curve was constructed by injecting EGCG dilutions in an Agilent 1200 High-Performance Liquid Chromatography (HPLC) system equipped with an autosampler, a binary pump, a diode array detector. Phenomenex Gemini 5 µm C18 110 Å column was used, and the elution was performed in isocratic conditions with 80:20 water: acetonitrile and 0.01% TFA (pH 4-4.5). The flow rate and the detection were set at 1 mL·min−1 and at 280 nm, respectively. The injection volume was 5 µL, and the total run was set at 15 min. The temperature was set at 25.0 °C. Due to compound instability, every tested solution was injected within 1 minute from its preparation by dilution of DMSO stock solution. The calibration curve obtained by plotting the area of the peaks as a function of the concentration presented a R^2 of 0.9978.
The stability evaluation was performed using a solution with a concentration of 50 µM, by incubating EGCG in the same cell culture media used in the *in vitro* experiments (RPMI), and by evaluating the stability of the molecule by HPLC at different time points (0, 15, 30, 45, 60, 75 min).
The HPLC experiments were performed three times.

7.13 STATISTICAL ANALYSIS

The statistical analyses were performed using GraphPad Prism 6 software (GraphPad Software Inc.). Tested used were: One-way ANOVA, Two-way ANOVA and t-test. Data were presented as mean ± standard deviation (SD), as indicated for the figure legend's specific experiment.
$P < 0.05$ was considered statistically significant.

8. AUTHOR CONTRIBUTIONS

In this thesis, some results discussed by the Ph.D. candidate were performed in collaborations with other researchers. In detail:

Principal author of the experiments: Simona Cocchi;

Primary screening and identification of EGCG: Dr. Vito D'agostino, Dr. Valentina Greco, Dr. Valentina Adami;

Structure-based molecular modelling studies: Dr. Mattia Sturlese;

Synthesis of analogues: Prof. Ines Mancini and Dr. Andrea Defant;

HPLC analysis: Dr. Denise Sighel and Jacopo Vigna;

Synthesis of PGLA-PEG nanoparticles: Vanna Sanna and prof. Mario Sechi

In vivo experiments: Dr. Sanja Aveic and Dr. Diana Corallo.

9. REFERENCES

Acheson, A., Conover, J. C., Fandl, J. P., DeChiara, T. M., Russell, M., Thadani, A., Squinto, S. P., Yancopoulos, G. D., & Lindsay, R. M. (1995). A BDNF autocrine loop in adult sensory neurons prevents cell death. *Nature*, *374*(6521), 450–453.

Akao, Y., Nakagawa, Y., & Naoe, T. (2006). *let-7* microRNA functions as a potential growth suppressor in human colon cancer cells. *Biological & Pharmaceutical Bulletin*, *29*(5), 903–906.

Albihn, A., Johnsen, J. I., & Henriksson, M. A. (2010). MYC in oncogenesis and as a target for cancer therapies. *Advances in Cancer Research*, *107*, 163–224.

Ambros, P. F., Ambros, I. M., Brodeur, G. M., Haber, M., Khan, J., Nakagawara, A., Schleiermacher, G., Speleman, F., Spitz, R., London, W. B., Cohn, S. L., Pearson, A. D. J., & Maris, J. M. (2009). International consensus for neuroblastoma molecular diagnostics: report from the International Neuroblastoma Risk Group (INRG) Biology Committee. *British Journal of Cancer*, *100*(9), 1471–1482.

Ambros, V., & Horvitz, H. R. (1984). Heterochronic mutants of the nematode Caenorhabditis elegans. *Science (New York, N.Y.)*, *226*(4673), 409–416.

Amiel, J., Laudier, B., Attié-Bitach, T., Trang, H., de Pontual, L., Gener, B., Trochet, D., Etchevers, H., Ray, P., Simonneau, M., Vekemans, M., Munnich, A., Gaultier, C., & Lyonnet, S. (2003). Polyalanine expansion and frameshift mutations of the paired-like homeobox gene PHOX2B in congenital central hypoventilation syndrome. *Nature Genetics*, *33*(4), 459–461.

Anastas, J. N., & Moon, R. T. (2013). WNT signalling pathways as therapeutic targets in cancer. *Nature Reviews. Cancer*, *13*(1), 11–26.

Auton, A., Brooks, L. D., Durbin, R. M., Garrison, E. P., Kang, H. M., Korbel, J. O., Marchini, J. L., McCarthy, S., McVean, G. A., & Abecasis, G. R. (2015). A global reference for human genetic variation. *Nature*, *526*(7571), 68–74.

Bachetti, T., Di Zanni, E., Ravazzolo, R., & Ceccherini, I. (2015). miR-204 mediates post-transcriptional down-regulation of PHOX2B gene expression in neuroblastoma cells. *Biochimica et Biophysica Acta*, *1849*(8), 1057–1065

Bagca, B. G., & Avci, C. B. (2017). Molecular Approach to Neuroblastoma. *Intech*. https://doi.org/http://dx.doi.org/10.5772/intechopen.69374

Balzeau, J., Menezes, M. R., Cao, S., & Hagan, J. P. (2017). The LIN28/*let-7* pathway in cancer. *Frontiers in Genetics*, *8*(MAR), 1–16. https://doi.org/10.3389/fgene.2017.00031

Barh, D., Malhotra, R., Ravi, B., & Sindhurani, P. (2010). MicroRNA *let-7*: An emerging next-generation cancer therapeutic. *Current Oncology*, *17*(1), 70–80.

Barr, E. K., & Applebaum, M. A. (2018). Genetic Predisposition to Neuroblastoma. *Children (Basel, Switzerland)*, *5*(9).

Bird, A. (2007). Perceptions of epigenetics. *Nature*, *447*(7143), 396–398.

Black, J., & Williams, D. I. (1973). Natural history of adrenal haemorrhage in the newborn. *Archives of Disease in Childhood*, *48*(3), 183–190.

Blockus, H., & Chédotal, A. (2016). Slit-Robo signaling. *Development (Cambridge, England)*, *143*(17), 3037–3044. https://doi.org/10.1242/dev.132829

Bourdeaut, F., Trochet, D., Janoueix-Lerosey, I., Ribeiro, A., Deville, A., Coz, C., Michiels, J.-F., Lyonnet, S., Amiel, J., & Delattre, O. (2005). Germline mutations of the paired-like homeobox 2B (PHOX2B) gene in neuroblastoma. *Cancer Letters*, *228*(1–2), 51–58.

Bower, K., Napier, C. E., Cole, S. L., Dagg, R. A., Lau, L. M. S., Duncan, E. L., Moy, E. L., & Reddel, R. R. (2012). Loss of wild-type ATRX expression in somatic cell hybrids segregates with activation of Alternative Lengthening of Telomeres. *PloS One*, *7*(11), e50062.

Boyerinas, B., Park, S.-M., Hau, A., Murmann, A. E., & Peter, M. E. (2010). The role of *let-7* in cell differentiation and cancer. *Endocrine-Related Cancer*, *17*(1), F19-36.

Boyerinas, B., Park, S.-M., Shomron, N., Hedegaard, M. M., Vinther, J., Andersen, J. S., Feig, C., Xu, J., Burge, C. B., & Peter, M. E. (2008). Identification of *let-7*-regulated oncofetal genes. *Cancer Research*, *68*(8), 2587–2591.

Brennecke, J., Stark, A., Russell, R. B., & Cohen, S. M. (2005). Principles of microRNA-target recognition. *PLoS Biology*, *3*(3), e85.

Bresler, S. C., Weiser, D. A., Huwe, P. J., Park, J. H., Krytska, K., Ryles, H., Laudenslager, M., Rappaport, E. F., Wood, A. C., McGrady, P. W., Hogarty, M. D., London, W. B., Radhakrishnan, R., Lemmon, M. A., & Mossé, Y. P. (2014). ALK mutations confer differential oncogenic activation and sensitivity to ALK inhibition therapy in neuroblastoma. *Cancer Cell*, *26*(5), 682–694.

Brodeur, G. M., Seeger, R. C., Barrett, A., Berthold, F., Castleberry, R. P., D'Angio, G., De Bernardi, B., Evans, A. E., Favrot, M., Freeman, A. I., Haase, G., Hartmann, O., Hayes, F. A., Helson, L., Kemshead, J., Lampert, F., Ninane, J., Ohkawa, H., Philip, T., … Voute, P. A. (1988). International criteria for diagnosis, staging, and response to treatment in patients with neuroblastoma. *Journal of Clinical Oncology*, *6*(12), 1874–1881.

Brodeur, G M, Pritchard, J., Berthold, F., Carlsen, N. L., Castel, V., Castelberry, R. P., De Bernardi, B., Evans, A. E., Favrot, M., & Hedborg, F. (1993). Revisions of the international criteria for neuroblastoma diagnosis, staging, and response to treatment. *Journal of Clinical Oncology : Official Journal of the American Society of Clinical Oncology*, *11*(8), 1466–1477.

Brodeur, Garrett M. (2003). Neuroblastoma: Biological insights into a clinical enigma. *Nature Reviews Cancer*, *3*(3), 203–216.

Carén, H., Kryh, H., Nethander, M., Sjöberg, R.-M., Träger, C., Nilsson, S., Abrahamsson, J., Kogner, P., & Martinsson, T. (2010). High-risk neuroblastoma tumors with 11q-deletion display a poor prognostic, chromosome instability phenotype with later onset. *Proceedings of the National Academy of Sciences of the United States of America*, *107*(9), 4323–4328.

Caussinus, E., & Gonzalez, C. (2005). Induction of tumor growth by altered stem-cell asymmetric division in Drosophila melanogaster. *Nature Genetics*, *37*(10), 1125–1129.

Cazes, A., Lopez-Delisle, L., Tsarovina, K., Pierre-Eugène, C., De Preter, K., Peuchmaur, M., Nicolas, A., Provost, C., Louis-Brennetot, C., Daveau, R., Kumps, C., Cascone, I., Schleiermacher, G., Prignon, A., Speleman, F., Rohrer, H., Delattre, O., & Janoueix-Lerosey, I. (2014). Activated Alk triggers prolonged neurogenesis and Ret upregulation providing a therapeutic target in ALK-mutated

neuroblastoma. *Oncotarget*, *5*(9), 2688–2702.

Chen, Y., Takita, J., Choi, Y. L., Kato, M., Ohira, M., Sanada, M., Wang, L., Soda, M., Kikuchi, A., Igarashi, T., Nakagawara, A., Hayashi, Y., Mano, H., & Ogawa, S. (2008). Oncogenic mutations of ALK kinase in neuroblastoma. *Nature*, *455*(7215), 971–974.

Cheung, N. K. V., & Dyer, M. A. (2013). Neuroblastoma: Developmental biology, cancer genomics and immunotherapy. *Nature Reviews Cancer*, *13*(6), 397–411.

Cheung, N.-K. V, Zhang, J., Lu, C., Parker, M., Bahrami, A., Tickoo, S. K., Heguy, A., Pappo, A. S., Federico, S., Dalton, J., Cheung, I. Y., Ding, L., Fulton, R., Wang, J., Chen, X., Becksfort, J., Wu, J., Billups, C. A., Ellison, D., … Dyer, M. A. (2012). Association of age at diagnosis and genetic mutations in patients with neuroblastoma. *JAMA*, *307*(10), 1062–1071.

Childs, G., Fazzari, M., Kung, G., Kawachi, N., Brandwein-Gensler, M., McLemore, M., Chen, Q., Burk, R. D., Smith, R. V, Prystowsky, M. B., Belbin, T. J., & Schlecht, N. F. (2009). Low-level expression of microRNAs *let-7*d and miR-205 are prognostic markers of head and neck squamous cell carcinoma. *The American Journal of Pathology*, *174*(3), 736–745.

Clynes, D., Jelinska, C., Xella, B., Ayyub, H., Scott, C., Mitson, M., Taylor, S., Higgs, D. R., & Gibbons, R. J. (2015). Suppression of the alternative lengthening of telomere pathway by the chromatin remodelling factor ATRX. *Nature Communications*, *6*, 7538.

Corallo, D., Donadon, M., Pantile, M., Sidarovich, V., Cocchi, S., Ori, M., De Sarlo, M., Candiani, S., Frasson, C., Distel, M., Quattrone, A., Zanon, C., Basso, G., Tonini, G., Aveic, S. (2020). LIN28B increases neural crest cell migration and leads to transformation of trunk sympathoadrenal precursors. *Cell Death and Differentiation 27*(4) 1225-1242

Cullen, B. R. (2004). Transcription and processing of human microRNA precursors. *Molecular Cell*, *16*(6), 861–865.

Darr, H., & Benvenisty, N. (2009). Genetic analysis of the role of the reprogramming gene LIN-28 in human embryonic stem cells. *Stem Cells (Dayton, Ohio)*, *27*(2), 352–362.

Decock, A., Ongenaert, M., Hoebeeck, J., De Preter, K., Van Peer, G., Van Criekinge, W., Ladenstein, R., Schulte, J. H., Noguera, R., Stallings, R. L., Van Damme, A., Laureys, G., Vermeulen, J., Van Maerken, T., Speleman, F., & Vandesompele, J. (2012). Genome-wide promoter methylation analysis in neuroblastoma identifies prognostic methylation biomarkers. *Genome Biology*, *13*(10), R95.

Diskin, S. J., Capasso, M., Schnepp, R. W., Cole, K. A., Attiyeh, E. F., Hou, C., Diamond, M., Carpenter, E. L., Winter, C., Lee, H., Jagannathan, J., Latorre, V., Iolascon, A., Hakonarson, H., Devoto, M., & Maris, J. M. (2012). Common variation at 6q16 within HACE1 and LIN28B influences susceptibility to neuroblastoma. *Nature Genetics*, *44*(10), 1126–1130.

Dubreuil, V., Hirsch, M. R., Pattyn, A., Brunet, J. F., & Goridis, C. (2000). The Phox2b transcription factor coordinately regulates neuronal cell cycle exit and identity. *Development*, *127*(23), 5191–5201.

Dyberg, C., Fransson, S., Andonova, T., Sveinbjörnsson, B., Lännerholm-Palm, J., Olsen, T. K., Forsberg, D., Herlenius, E., Martinsson, T., Brodin, B., Kogner, P., Johnsen, J. I., & Wickström, M. (2017). Rho-associated kinase is a therapeutic target in neuroblastoma. *Proceedings of the National Academy of Sciences of the United States of America*, *114*(32), E6603–E6612.

Esquela-Kerscher, A., & Slack, F. J. (2006). Oncomirs - microRNAs with a role in cancer. *Nature Reviews. Cancer*, *6*(4), 259–269.

Fabian, J., Opitz, D., Althoff, K., Lodrini, M., Hero, B., Volland, R., Beckers, A., de Preter, K., Decock, A., Patil, N., Abba, M., Kopp-Schneider, A., Astrahantseff, K., Wünschel, J., Pfeil, S., Ercu, M., Künkele, A., Hu, J., Thole, T., … Deubzer, H. E. (2016). MYCN and HDAC5 transcriptionally repress CD9 to trigger invasion and metastasis in neuroblastoma. *Oncotarget*, *7*(41), 66344–66359.

George, R. E., Sanda, T., Hanna, M., Fröhling, S., Luther, W. 2nd, Zhang, J., Ahn, Y., Zhou, W., London, W. B., McGrady, P., Xue, L., Zozulya, S., Gregor, V. E., Webb, T. R., Gray, N. S., Gilliland, D. G., Diller, L., Greulich, H., Morris, S. W., … Look, A. T. (2008). Activating mutations in ALK provide a therapeutic target in neuroblastoma. *Nature*, *455*(7215), 975–978.

Goldstein, A. M., Brewer, K. C., Doyle, A. M., Nagy, N., & Roberts, D. J. (2005). BMP signaling is

necessary for neural crest cell migration and ganglion formation in the enteric nervous system. *Mechanisms of Development*, *122*(6), 821–833.

Graham-Pole, J., Salmi, T., Anton, A. H., Abramowsky, C., & Gross, S. (1983). Tumor and urine catecholamines (CATs) in neurogenic tumors. Correlations with other prognostic factors and survival. *Cancer*, *51*(5), 834–839.

Grinshtein, N., Datti, A., Fujitani, M., Uehling, D., Prakesch, M., Isaac, M., Irwin, M. S., Wrana, J. L., Al-Awar, R., & Kaplan, D. R. (2011). Small molecule kinase inhibitor screen identifies polo-like kinase 1 as a target for neuroblastoma tumor-initiating cells. *Cancer Research*, *71*(4), 1385–1395.

Grosshans, H., Johnson, T., Reinert, K. L., Gerstein, M., & Slack, F. J. (2005). The temporal patterning microRNA *let-7* regulates several transcription factors at the larval to adult transition in C. elegans. *Developmental Cell*, *8*(3), 321–330.

Guo, Y., Chen, Y., Ito, H., Watanabe, A., Ge, X., Kodama, T., & Aburatani, H. (2006). Identification and characterization of lin-28 homolog B (LIN28B) in human hepatocellular carcinoma. *Gene*, *384*(1–2), 51–61.

Haddad, Y., Adam, V., & Heger, Z. (2017). Trk Receptors and Neurotrophin Cross-Interactions: New Perspectives Toward Manipulating Therapeutic Side-Effects. *Frontiers in Molecular Neuroscience*, *10*, 130.

Hagan, J. P., Piskounova, E., & Gregory, R. I. (2009). Lin28 recruits the TUTase Zcchc11 to inhibit *let-7* maturation in mouse embryonic stem cells. *Nature Structural & Molecular Biology*, *16*(10), 1021–1025.

Helland, Å., Anglesio, M. S., George, J., Cowin, P. A., Johnstone, C. N., House, C. M., Sheppard, K. E., Etemadmoghadam, D., Melnyk, N., Rustgi, A. K., Phillips, W. A., Johnsen, H., Holm, R., Kristensen, G. B., Birrer, M. J., Pearson, R. B., Børresen-Dale, A.-L., Huntsman, D. G., deFazio, A., … Bowtell, D. D. L. (2011). Deregulation of MYCN, LIN28B and LET7 in a molecular subtype of aggressive high-grade serous ovarian cancers. *PloS One*, *6*(4), e18064.

Hennchen, M., Stubbusch, J., Makhfi, I. A. El, Kramer, M., Deller, T., Pierre-Eugene, C., Janoueix-

Lerosey, I., Delattre, O., Ernsberger, U., Schulte, J. B., & Rohrer, H. (2015). Lin28b and *let-7* in the control of sympathetic neurogenesis and neuroblastoma development. *Journal of Neuroscience*, *35*(50), 16531–16544.

Heo, I., Joo, C., Cho, J., Ha, M., Han, J., & Kim, V. N. (2008). Lin28 mediates the terminal uridylation of *let-7* precursor MicroRNA. *Molecular Cell*, *32*(2), 276–284.

Hovestadt, V., Jones, D. T. W., Picelli, S., Wang, W., Kool, M., Northcott, P. A., Sultan, M., Stachurski, K., Ryzhova, M., Warnatz, H.-J., Ralser, M., Brun, S., Bunt, J., Jäger, N., Kleinheinz, K., Erkek, S., Weber, U. D., Bartholomae, C. C., von Kalle, C., … Lichter, P. (2014). Decoding the regulatory landscape of medulloblastoma using DNA methylation sequencing. *Nature*, *510*(7506), 537–541.

Howard, M. J., Stanke, M., Schneider, C., Wu, X., & Rohrer, H. (2000). The transcription factor dHAND is a downstream effector of BMPs in sympathetic neuron specification. *Development (Cambridge, England)*, *127*(18), 4073–4081.

Huang, M., & Weiss, W. A. (2013). Neuroblastoma and MYCN. *Cold Spring Harbor Perspectives in Medicine*, *3*(10), a014415.

Huang, P., Kishida, S., Cao, D., Murakami-Tonami, Y., Mu, P., Nakaguro, M., Koide, N., Takeuchi, I., Onishi, A., & Kadomatsu, K. (2011). The neuronal differentiation factor NeuroD1 downregulates the neuronal repellent factor Slit2 expression and promotes cell motility and tumor formation of neuroblastoma. *Cancer Research*, *71*(8), 2938–2948.

Hungate, E. A., Applebaum, M. A., Skol, A. D., Vaksman, Z., Diamond, M., McDaniel, L., Volchenboum, S. L., Stranger, B. E., Maris, J. M., Diskin, S. J., Onel, K., & Cohn, S. L. (2017). Evaluation of Genetic Predisposition for MYCN-Amplified Neuroblastoma. *Journal of the National Cancer Institute*, *109*(10).

Hutvágner, G., McLachlan, J., Pasquinelli, A. E., Bálint, E., Tuschl, T., & Zamore, P. D. (2001). A cellular function for the RNA-interference enzyme Dicer in the maturation of the *let-7* small temporal RNA. *Science (New York, N.Y.)*, *293*(5531), 834–838.

Irminger-Finger, I., & Jefford, C. E. (2006). Is there more to BARD1 than BRCA1? *Nature Reviews.*

Cancer, *6*(5), 382–391.

Irwin, M. S., & Park, J. R. (2015). Neuroblastoma: paradigm for precision medicine. *Pediatric Clinics of North America*, *62*(1), 225–256.

Janoueix-Lerosey, I., Lequin, D., Brugières, L., Ribeiro, A., de Pontual, L., Combaret, V., Raynal, V., Puisieux, A., Schleiermacher, G., Pierron, G., Valteau-Couanet, D., Frebourg, T., Michon, J., Lyonnet, S., Amiel, J., & Delattre, O. (2008). Somatic and germline activating mutations of the ALK kinase receptor in neuroblastoma. *Nature*, *455*(7215), 967–970.

Javanmardi, N., Fransson, S., Djos, A., Sjöberg, R.-M., Nilsson, S., Truvé, K., Kogner, P., & Martinsson, T. (2019). Low Frequency ALK Hotspots Mutations In Neuroblastoma Tumours Detected By Ultra-deep Sequencing: Implications For ALK Inhibitor Treatment. *Scientific Reports*, *9*(1), 2199.

Jin, Y., Xu, X. L., Yang, M. C., Wei, F., Ayi, T. C., Bowcock, A. M., & Baer, R. (1997). Cell cycle-dependent colocalization of BARD1 and BRCA1 proteins in discrete nuclear domains. *Proceedings of the National Academy of Sciences of the United States of America*, *94*(22), 12075–12080.

Johnsen, J. I., Dyberg, C., & Wickström, M. (2019). Neuroblastoma-A Neural Crest Derived Embryonal Malignancy. *Frontiers in Molecular Neuroscience*, *12*, 9.

Johnson, C. D., Esquela-Kerscher, A., Stefani, G., Byrom, M., Kelnar, K., Ovcharenko, D., Wilson, M., Wang, X., Shelton, J., Shingara, J., Chin, L., Brown, D., & Slack, F. J. (2007). The *let-7* microRNA represses cell proliferation pathways in human cells. *Cancer Research*, *67*(16), 7713–7722.

Johnson, S. M., Grosshans, H., Shingara, J., Byrom, M., Jarvis, R., Cheng, A., Labourier, E., Reinert, K. L., Brown, D., & Slack, F. J. (2005). RAS is regulated by the *let-7* microRNA family. *Cell*, *120*(5), 635–647.

Jubierre, L., Soriano, A., Planells-Ferrer, L., París-Coderch, L., Tenbaum, S. P., Romero, O. A., Moubarak, R. S., Almazán-Moga, A., Molist, C., Roma, J., Navarro, S., Noguera, R., Sánchez-Céspedes, M., Comella, J. X., Palmer, H. G., Sánchez de Toledo, J., Gallego, S., & Segura, M. F. (2016). BRG1/SMARCA4 is essential for neuroblastoma cell viability through modulation of cell death and survival pathways. *Oncogene*, *35*(39), 5179–5190.

Kemshead, J. T., Goldman, A., Fritschy, J., Malpas, J. S., & Pritchard, J. (1983). Use of panels of monoclonal antibodies in the differential diagnosis of neuroblastoma and lymphoblastic disorders. *Lancet (London, England)*, *1*(8314–5), 12–15.

Kim, C., Attiyeh, E. F., Mosse, Y. P., Cole, K., Iolascon, A., Hakonarson, H., Li, H. K., & Maris, J. M. (2011). *Phenotype Restricted Genome-Wide Association Study Using a Gene-Centric Approach Identifies Three Low-Risk Neuroblastoma Susceptibility Loci*. *7*(3), 1–9.

Knudson, A. G., & Strong, L. C. (1972). Mutation and cancer: neuroblastoma and pheochromocytoma. *American Journal of Human Genetics*, *24*(5), 514–532.

Kogner, P., Barbany, G., Dominici, C., Castello, M. A., Raschellá, G., & Persson, H. (1993). Coexpression of messenger RNA for TRK protooncogene and low affinity nerve growth factor receptor in neuroblastoma with favorable prognosis. *Cancer Research*, *53*(9), 2044–2050.

Kugimiya, N., Nishimoto, A., Hosoyama, T., Ueno, K., Enoki, T., Li, T.-S., & Hamano, K. (2015). The c-MYC-ABCB5 axis plays a pivotal role in 5-fluorouracil resistance in human colon cancer cells. *Journal of Cellular and Molecular Medicine*, *19*(7), 1569–1581.

Kumar, M. S., Erkeland, S. J., Pester, R. E., Chen, C. Y., Ebert, M. S., Sharp, P. A., & Jacks, T. (2008). Suppression of non-small cell lung tumor development by the *let-7* microRNA family. *Proceedings of the National Academy of Sciences of the United States of America*, *105*(10), 3903–3908.

LaBrosse, E. H., Com-Nougué, C., Zucker, J. M., Comoy, E., Bohuon, C., Lemerle, J., & Schweisguth, O. (1980). Urinary excretion of 3-methoxy-4-hydroxymandelic acid and 3-methoxy-4-hydroxyphenylacetic acid by 288 patients with neuroblastoma and related neural crest tumors. *Cancer Research*, *40*(6), 1995–2001.

Ladenstein, R., Weixler, S., Baykan, B., Bleeke, M., Kunert, R., Katinger, D., Pribill, I., Glander, P., Bauer, S., Pistoia, V., Michon, J., Garaventa, A., & Lode, H. N. (2013). Ch14.18 antibody produced in CHO cells in relapsed or refractory Stage 4 neuroblastoma patients: a SIOPEN Phase 1 study. *MAbs*, *5*(5), 801–809.

Lai, E. C. (2002). Micro RNAs are complementary to 3′ UTR sequence motifs that mediate negative

post-transcriptional regulation. *Nature Genetics*, *30*(4), 363–364.

Lammie, G., Cheung, N., Gerald, W., Rosenblum, M., & Cordoncardo, C. (1993). Ganglioside gd(2) expression in the human nervous-system and in neuroblastomas - an immunohistochemical study. *International Journal of Oncology*, *3*(5), 909–915.

Lawrie, C. H., Chi, J., Taylor, S., Tramonti, D., Ballabio, E., Palazzo, S., Saunders, N. J., Pezzella, F., Boultwood, J., Wainscoat, J. S., & Hatton, C. S. R. (2009). Expression of microRNAs in diffuse large B cell lymphoma is associated with immunophenotype, survival and transformation from follicular lymphoma. *Journal of Cellular and Molecular Medicine*, *13*(7), 1248–1260.

Lee, C. C., Jia, Y., Li, N., Sun, X., Ng, K., Ambing, E., Gao, M.-Y., Hua, S., Chen, C., Kim, S., Michellys, P.-Y., Lesley, S. A., Harris, J. L., & Spraggon, G. (2010). Crystal structure of the ALK (anaplastic lymphoma kinase) catalytic domain. *The Biochemical Journal*, *430*(3), 425–437.

Lee, H., Han, S., Kwon, C. S., & Lee, D. (2016). Biogenesis and regulation of the *let-7 miRNA*s and their functional implications. *Protein & Cell*, *7*(2), 100–113.

Lee, Y., Ahn, C., Han, J., Choi, H., Kim, J., Yim, J., Lee, J., Provost, P., Rådmark, O., Kim, S., & Kim, V. N. (2003). The nuclear RNase III Drosha initiates microRNA processing. *Nature*, *425*(6956), 415–419.

Lee, Y. S., & Dutta, A. (2007). The tumor suppressor microRNA *let-7* represses the HMGA2 oncogene. *Genes & Development*, *21*(9), 1025–1030.

Lightfoot, H., Miska, E., Balasubramanian, S. (2016). Identification of small molecule inhibitors of the Lin28-mediated blockage of pre-let-7g processing. *Organic and Biomolecular Chemistry 14*(43) 10208-10216.

Lodrini, M., Oehme, I., Schroeder, C., Milde, T., Schier, M. C., Kopp-Schneider, A., Schulte, J. H., Fischer, M., De Preter, K., Pattyn, F., Castoldi, M., Muckenthaler, M. U., Kulozik, A. E., Westermann, F., Witt, O., & Deubzer, H. E. (2013). MYCN and HDAC2 cooperate to repress miR-183 signaling in neuroblastoma. *Nucleic Acids Research*, *41*(12), 6018–6033.

Lubanska, D., & Porter, L. A. (2014). The atypical cell cycle regulator Spy1 suppresses differentiation of the neuroblastoma stem cell population. *Oncoscience*, *1*(5), 336–348.

Manier, S., Powers, J. T., Sacco, A., Glavey, S. V, Huynh, D., Reagan, M. R., Salem, K. Z., Moschetta, M., Shi, J., Mishima, Y., Roche-Lestienne, C., Leleu, X., Roccaro, A. M., Daley, G. Q., & Ghobrial, I. M. (2017). The LIN28B/*let-7* axis is a novel therapeutic pathway in multiple myeloma. *Leukemia*, *31*(4), 853–860.

Maris, J. M. (2010). Recent advances in neuroblastoma. *The New England Journal of Medicine*, *362*(23), 2202–2211.

Maris, J. M., Hogarty, M. D., Bagatell, R., & Cohn, S. L. (2007). Neuroblastoma. *Lancet*, *369*(9579), 2106–2120.

Maris, J. M., Morton, C. L., Gorlick, R., Kolb, E. A., Lock, R., Carol, H., Keir, S. T., Reynolds, C. P., Kang, M. H., Wu, J., Smith, M. A., & Houghton, P. J. (2010). Initial testing of the aurora kinase A inhibitor MLN8237 by the Pediatric Preclinical Testing Program (PPTP). *Pediatric Blood & Cancer*, *55*(1), 26–34.

Maris, J. M., Mosse, Y. P., Bradfield, J. P., Hou, C., Monni, S., Scott, R. H., Asgharzadeh, S., Attiyeh, E. F., Diskin, S. J., Laudenslager, M., Winter, C., Cole, K. A., Glessner, J. T., Kim, C., Frackelton, E. C., Casalunovo, T., Eckert, A. W., Capasso, M., Rappaport, E. F., … Hakonarson, H. (2008). Chromosome 6p22 locus associated with clinically aggressive neuroblastoma. *The New England Journal of Medicine*, *358*(24), 2585–2593.

Marshall, G. M., Carter, D. R., Cheung, B. B., Liu, T., Mateos, M. K., Meyerowitz, J. G., & Weiss, W. A. (2014). The prenatal origins of cancer. In *Nature reviews. Cancer* (Vol. 14, Issue 4, pp. 277–289).

Matsumoto, K., Wada, R. K., Yamashiro, J. M., Kaplan, D. R., & Thiele, C. J. (1995). Expression of brain-derived neurotrophic factor and p145TrkB affects survival, differentiation, and invasiveness of human neuroblastoma cells. *Cancer Research*, *55*(8), 1798–1806.

Matthay, K. K. (1995). Neuroblastoma: a clinical challenge and biologic puzzle. *CA: A Cancer Journal for Clinicians*, *45*(3), 179–192.

Matthay, K. K., Maris, J. M., Schleiermacher, G., Nakagawara, A., Mackall, C. L., Diller, L., & Weiss, W. A. (2016). Neuroblastoma. *Nature Reviews. Disease Primers*, *2*, 16078.

Mayol, G., Martín-Subero, J. I., Ríos, J., Queiros, A., Kulis, M., Suñol, M., Esteller, M., Gómez, S., Garcia, I., de Torres, C., Rodríguez, E., Galván, P., Mora, J., & Lavarino, C. (2012). DNA hypomethylation affects cancer-related biological functions and genes relevant in neuroblastoma pathogenesis. *PloS One*, *7*(11), e48401.

Mayr, C., Hemann, M. T., & Bartel, D. P. (2007). Disrupting the pairing between *let-7* and Hmga2 enhances oncogenic transformation. *Science (New York, N.Y.)*, *315*(5818), 1576–1579.

McDaniel, L. D., Conkrite, K. L., Chang, X., Capasso, M., Vaksman, Z., Oldridge, D. A., Zachariou, A., Horn, M., Diamond, M., Hou, C., Iolascon, A., Hakonarson, H., Rahman, N., Devoto, M., & Diskin, S. J. (2017). Common variants upstream of MLF1 at 3q25 and within CPZ at 4p16 associated with neuroblastoma. *PLoS Genetics*, *13*(5), e1006787.

Mi, S., Lu, J., Sun, M., Li, Z., Zhang, H., Neilly, M. B., Wang, Y., Qian, Z., Jin, J., Zhang, Y., Bohlander, S. K., Le Beau, M. M., Larson, R. A., Golub, T. R., Rowley, J. D., & Chen, J. (2007). MicroRNA expression signatures accurately discriminate acute lymphoblastic leukemia from acute myeloid leukemia. *Proceedings of the National Academy of Sciences of the United States of America*, *104*(50), 19971–19976.

Mizuno, R., Chatterji, P., Andres, S., Hamilton, K., Simon, L., Foley, S. W., Jeganathan, A., Gregory, B. D., Madison, B., & Rustgi, A. K. (2018). Differential regulation of *LET-7* by LIN28B isoform-specific functions. *Molecular Cancer Research*, *16*(3), 403–416.

Mody, R., Naranjo, A., Van Ryn, C., Yu, A. L., London, W. B., Shulkin, B. L., Parisi, M. T., Servaes, S.-E.-N., Diccianni, M. B., Sondel, P. M., Bender, J. G., Maris, J. M., Park, J. R., & Bagatell, R. (2017). Irinotecan-temozolomide with temsirolimus or dinutuximab in children with refractory or relapsed neuroblastoma (COG ANBL1221): an open-label, randomised, phase 2 trial. *The Lancet. Oncology*, *18*(7), 946–957.

Molenaar, J. J., Domingo-Fernández, R., Ebus, M. E., Lindner, S., Koster, J., Drabek, K., Mestdagh, P., van Sluis, P., Valentijn, L. J., van Nes, J., Broekmans, M., Haneveld, F., Volckmann, R., Bray, I.,

Heukamp, L., Sprüssel, A., Thor, T., Kieckbusch, K., Klein-Hitpass, L., … Schulte, J. H. (2012). LIN28B induces neuroblastoma and enhances MYCN levels via *let-7* suppression. *Nature Genetics*, *44*(11), 1199–1206.

Molenaar, J. J., Koster, J., Zwijnenburg, D. A., van Sluis, P., Valentijn, L. J., van der Ploeg, I., Hamdi, M., van Nes, J., Westerman, B. A., van Arkel, J., Ebus, M. E., Haneveld, F., Lakeman, A., Schild, L., Molenaar, P., Stroeken, P., van Noesel, M. M., Ora, I., Santo, E. E., … Versteeg, R. (2012). Sequencing of neuroblastoma identifies chromothripsis and defects in neuritogenesis genes. *Nature*, *483*(7391), 589–593.

Morgenstern, D. A., London, W. B., Stephens, D., Volchenboum, S. L., Hero, B., Di Cataldo, A., Nakagawara, A., Shimada, H., Ambros, P. F., Matthay, K. K., Cohn, S. L., Pearson, A. D. J., & Irwin, M. S. (2014). Metastatic neuroblastoma confined to distant lymph nodes (stage 4N) predicts outcome in patients with stage 4 disease: A study from the International Neuroblastoma Risk Group Database. *Journal of Clinical Oncology : Official Journal of the American Society of Clinical Oncology*, *32*(12), 1228–1235.

Moss, E. G., & Tang, L. (2003). Conservation of the heterochronic regulator Lin-28, its developmental expression and microRNA complementary sites. *Developmental Biology*, *258*(2), 432–442.

Moss, E., Lee, R., & Ambros, V. (1997). Control of developmental timing by the cold shock domain protein Lin-28 and its regulation by the lin-4 RNA. *Cell*, *88*(637–646), 637–646.

Mossé, Y. P., Laudenslager, M., Longo, L., Cole, K. A., Wood, A., Attiyeh, E. F., Laquaglia, M. J., Sennett, R., Lynch, J. E., Perri, P., Laureys, G., Speleman, F., Kim, C., Hou, C., Hakonarson, H., Torkamani, A., Schork, N. J., Brodeur, G. M., Tonini, G. P., … Maris, J. M. (2008). Identification of ALK as a major familial neuroblastoma predisposition gene. *Nature*, *455*(7215), 930–935.

Nagashimada, M., Ohta, H., Li, C., Nakao, K., Uesaka, T., Brunet, J.-F., Amiel, J., Trochet, D., Wakayama, T., & Enomoto, H. (2012). Autonomic neurocristopathy-associated mutations in PHOX2B dysregulate Sox10 expression. *The Journal of Clinical Investigation*, *122*(9), 3145–3158.

Nakagawara, A., Azar, C. G., Scavarda, N. J., & Brodeur, G. M. (1994). Expression and function of

TRK-B and BDNF in human neuroblastomas. *Molecular and Cellular Biology*, *14*(1), 759–767.

Nam, S., Kim, B., Shin, S., & Lee, S. (2008). miRGator: an integrated system for functional annotation of microRNAs. *Nucleic Acids Research*, *36*(Database issue), D159–D164.

Nam, Y., Chen, C., Gregory, R. I., Chou, J. J., & Sliz, P. (2011). Molecular basis for interaction of *let-7* MicroRNAs with Lin28. *Cell*, *147*(5), 1080–1091.

Newman, M. A., Thomson, J. M., & Hammond, S. M. (2008a). Lin-28 interaction with the *Let-7* precursor loop mediates regulated microRNA processing. *Rna*, *14*(8), 1539–1549.

Newman, M. A., Thomson, J. M., & Hammond, S. M. (2008b). Lin-28 interaction with the *Let-7* precursor loop mediates regulated microRNA processing. *RNA (New York, N.Y.)*, *14*(8), 1539–1549.

Nilsen, T. W. (2007). Mechanisms of microRNA-mediated gene regulation in animal cells. *Trends in Genetics : TIG*, *23*(5), 243–249.

Nishino, J., Kim, I., Chada, K., & Morrison, S. J. (2008). Hmga2 promotes neural stem cell self-renewal in young but not old mice by reducing p16Ink4a and p19Arf Expression. *Cell*, *135*(2), 227–239.

Northcott, P. A., Fernandez-L, A., Hagan, J. P., Ellison, D. W., Grajkowska, W., Gillespie, Y., Grundy, R., Van Meter, T., Rutka, J. T., Croce, C. M., Kenney, A. M., & Taylor, M. D. (2009). The miR-17/92 polycistron is up-regulated in sonic hedgehog-driven medulloblastomas and induced by N-myc in sonic hedgehog-treated cerebellar neural precursors. *Cancer Research*, *69*(8), 3249–3255.

Ogawa, S., Takita, J., Sanada, M., & Hayashi, Y. (2011). Oncogenic mutations of ALK in neuroblastoma. *Cancer Science*, *102*(2), 302–308.

Ohmi, Y., Ohkawa, Y., Yamauchi, Y., Tajima, O., Furukawa, K., & Furukawa, K. (2012). Essential roles of gangliosides in the formation and maintenance of membrane microdomains in brain tissues. *Neurochemical Research*, *37*(6), 1185–1191.

Otto, T., Horn, S., Brockmann, M., Eilers, U., Schüttrumpf, L., Popov, N., Kenney, A. M., Schulte, J. H., Beijersbergen, R., Christiansen, H., Berwanger, B., & Eilers, M. (2009). Stabilization of N-Myc is a critical function of Aurora A in human neuroblastoma. *Cancer Cell*, *15*(1), 67–78.

Ozen, M., Creighton, C. J., Ozdemir, M., & Ittmann, M. (2008). Widespread deregulation of microRNA expression in human prostate cancer. *Oncogene*, *27*(12), 1788–1793.

Pandey, G. K., Mitra, S., Subhash, S., Hertwig, F., Kanduri, M., Mishra, K., Fransson, S., Ganeshram, A., Mondal, T., Bandaru, S., Ostensson, M., Akyürek, L. M., Abrahamsson, J., Pfeifer, S., Larsson, E., Shi, L., Peng, Z., Fischer, M., Martinsson, T., … Kanduri, C. (2014). The risk-associated long noncoding RNA NBAT-1 controls neuroblastoma progression by regulating cell proliferation and neuronal differentiation. *Cancer Cell*, *26*(5), 722–737.

Pang, M., Wu, G., Hou, X., Hou, N., Liang, L., Jia, G., Shuai, P., Luo, B., Wang, K., & Li, G. (2014). LIN28B promotes colon cancer migration and recurrence. *PloS One*, *9*(10), e109169.

Pasquinelli, A. E., McCoy, A., Jiménez, E., Saló, E., Ruvkun, G., Martindale, M. Q., & Baguñà, J. (2003). Expression of the 22 nucleotide *let-7* heterochronic RNA throughout the Metazoa: a role in life history evolution? *Evolution & Development*, *5*(4), 372–378.

Pasquinelli, A. E., Reinhart, B. J., Slack, F., Martindale, M. Q., Kuroda, M. I., Maller, B., Hayward, D. C., Ball, E. E., Degnan, B., Müller, P., Spring, J., Srinivasan, A., Fishman, M., Finnerty, J., Corbo, J., Levine, M., Leahy, P., Davidson, E., & Ruvkun, G. (2000). Conservation of the sequence and temporal expression of *let-7* heterochronic regulatory RNA. *Nature*, *408*(6808), 86–89.

Pattyn, A., Morin, X., Cremer, H., Goridis, C., & Brunet, J.-F. (1999a). The homeobox gene Phox2b is essential for the development of autonomic neural crest derivatives. *Nature*, *399*(6734), 366–370.

Peifer, M., Hertwig, F., Roels, F., Dreidax, D., Gartlgruber, M., Menon, R., Krämer, A., Roncaioli, J. L., Sand, F., Heuckmann, J. M., Ikram, F., Schmidt, R., Ackermann, S., Engesser, A., Kahlert, Y., Vogel, W., Altmüller, J., Nürnberg, P., Thierry-Mieg, J., Fischer, M. (2015). Telomerase activation by genomic rearrangements in high-risk neuroblastoma. *Nature*, *526*(7575), 700–704.

Peng, Y., Laser, J., Shi, G., Mittal, K., Melamed, J., Lee, P., & Wei, J.-J. (2008). Antiproliferative effects by *Let-7* repression of high-mobility group A2 in uterine leiomyoma. *Molecular Cancer Research : MCR*, *6*(4), 663–673.

Pinto, N. R., Applebaum, M. A., Volchenboum, S. L., Matthay, K. K., London, W. B., Ambros, P. F., Nakagawara, A., Berthold, F., Schleiermacher, G., Park, J. R., Valteau-Couanet, D., Pearson, A. D. J., & Cohn, S. L. (2015). Advances in risk classification and treatment strategies for neuroblastoma. *Journal of Clinical Oncology*, *33*(27), 3008–3017.

Piskounova, E., Polytarchou, C., Thornton, J. E., Lapierre, R. J., Pothoulakis, C., Hagan, J. P., Iliopoulos, D., & Gregory, R. I. (2011). Lin28A and Lin28B inhibit *let-7* MicroRNA biogenesis by distinct mechanisms. *Cell*, *147*(5), 1066–1079.

Qian, Z. R., Asa, S. L., Siomi, H., Siomi, M. C., Yoshimoto, K., Yamada, S., Wang, E. L., Rahman, M. M., Inoue, H., Itakura, M., Kudo, E., & Sano, T. (2009). Overexpression of HMGA2 relates to reduction of the *let-7* and its relationship to clinicopathological features in pituitary adenomas. *Modern Pathology : An Official Journal of the United States and Canadian Academy of Pathology, Inc*, *22*(3), 431—441.

Raabe, E. H., Laudenslager, M., Winter, C., Wasserman, N., Cole, K., LaQuaglia, M., Maris, D. J., Mosse, Y. P., & Maris, J. M. (2008). Prevalence and functional consequence of PHOX2B mutations in neuroblastoma. *Oncogene*, *27*(4), 469–476.

Reiff, T., Huber, L., Kramer, M., Delattre, O., Janoueix-Lerosey, I., & Rohrer, H. (2011). Midkine and Alk signaling in sympathetic neuron proliferation and neuroblastoma predisposition. *Development (Cambridge, England)*, *138*(21), 4699–4708.

Reinhart, B. J., Slack, F. J., Basson, M., Pasquinelli, A. E., Bettinger, J. C., Rougvie, A. E., Horvitz, H. R., & Ruvkun, G. (2000). The 21-nucleotide *let-7* RNA regulates developmental timing in Caenorhabditis elegans. *Nature*, *403*(6772), 901–906.

Rickman, D. S., Schulte, J. H., & Eilers, M. (2018). The Expanding World of N-MYC-Driven Tumors. *Cancer Discovery*, *8*(2), 150–163.

Riento, K., & Ridley, A. J. (2003). Rocks: multifunctional kinases in cell behaviour. *Nature Reviews. Molecular Cell Biology*, *4*(6), 446–456.

Ritenour, L. E., Randall, M. P., Bosse, K. R., & Diskin, S. J. (2018). Genetic susceptibility to neuroblastoma: current knowledge and future directions. *Cell and Tissue Research*, *372*(2), 287–307.

Rohrer, H. (2011). Transcriptional control of differentiation and neurogenesis in autonomic ganglia. *The European Journal of Neuroscience*, *34*(10), 1563–1573.

Romano, G., Veneziano, D., Nigita, G., & Nana-Sinkam, S. P. (2018). RNA Methylation in ncRNA: Classes, Detection, and Molecular Associations. *Frontiers in Genetics*, *9*, 243.

Ross, R. A., Biedler, J. L., & Spengler, B. A. (2003). A role for distinct cell types in determining malignancy in human neuroblastoma cell lines and tumors. *Cancer Letters*, *197*(1), 35–39.

Roush, S., & Slack, F. J. (2008). The *let-7* family of microRNAs. *Trends in Cell Biology*, *18*(10), 505–516.

Ruby, J. G., Jan, C., Player, C., Axtell, M. J., Lee, W., Nusbaum, C., Ge, H., & Bartel, D. P. (2006). Large-scale sequencing reveals 21U-RNAs and additional microRNAs and endogenous siRNAs in C. elegans. *Cell*, *127*(6), 1193–1207.

Ruggero, D. (2009). The role of Myc-induced protein synthesis in cancer. *Cancer Research*, *69*(23), 8839–8843.

Russell, M. R., Penikis, A., Oldridge, D. A., Alvarez-Dominguez, J. R., McDaniel, L., Diamond, M., Padovan, O., Raman, P., Li, Y., Wei, J. S., Zhang, S., Gnanchandran, J., Seeger, R., Asgharzadeh, S., Khan, J., Diskin, S. J., Maris, J. M., & Cole, K. A. (2015). CASC15-S Is a Tumor Suppressor lncRNA at the 6p22 Neuroblastoma Susceptibility Locus. *Cancer Research*, *75*(15), 3155–3166.

Rybak, A., Fuchs, H., Smirnova, L., Brandt, C., Pohl, E. E., Nitsch, R., & Wulczyn, F. G. (2008). A

feedback loop comprising lin-28 and *let-7* controls pre-*let-7* maturation during neural stem-cell commitment. *Nature Cell Biology*, *10*(8), 987–993.

Sampson, V. B., Rong, N. H., Han, J., Yang, Q., Aris, V., Soteropoulos, P., Petrelli, N. J., Dunn, S. P., & Krueger, L. J. (2007). MicroRNA *let-7*a down-regulates MYC and reverts MYC-induced growth in Burkitt lymphoma cells. *Cancer Research*, *67*(20), 9762–9770.

Schulman, B. R. M., Esquela-Kerscher, A., & Slack, F. J. (2005). Reciprocal expression of lin-41 and the microRNAs *let-7* and mir-125 during mouse embryogenesis. *Developmental Dynamics : An Official Publication of the American Association of Anatomists*, *234*(4), 1046–1054.

Schulte, J. H., Lindner, S., Bohrer, A., Maurer, J., De Preter, K., Lefever, S., Heukamp, L., Schulte, S., Molenaar, J., Versteeg, R., Thor, T., Künkele, A., Vandesompele, J., Speleman, F., Schorle, H., Eggert, A., & Schramm, A. (2013). MYCN and ALKF1174L are sufficient to drive neuroblastoma development from neural crest progenitor cells. *Oncogene*, *32*(8), 1059–1065.

Sebbagh, M., & Borg, J.-P. (2014). Insight into planar cell polarity. *Experimental Cell Research*, *328*(2), 284–295.

Seggerson, K., Tang, L., & Moss, E. G. (2002). Two genetic circuits repress the Caenorhabditis elegans heterochronic gene lin-28 after translation initiation. *Developmental Biology*, *243*(2), 215–225.

Sempere, L. F., Freemantle, S., Pitha-Rowe, I., Moss, E., Dmitrovsky, E., & Ambros, V. (2004). Expression profiling of mammalian microRNAs uncovers a subset of brain-expressed microRNAs with possible roles in murine and human neuronal differentiation. *Genome Biology*, *5*(3), R13.

Shell, S., Park, S.-M., Radjabi, A. R., Schickel, R., Kistner, E. O., Jewell, D. A., Feig, C., Lengyel, E., & Peter, M. E. (2007). *Let-7* expression defines two differentiation stages of cancer. *Proceedings of the National Academy of Sciences*, *104*(27), 11400 LP – 11405.

Smith, M. A., Seibel, N. L., Altekruse, S. F., Ries, L. A. G., Melbert, D. L., O'Leary, M., Smith, F. O., &

Reaman, G. H. (2010). Outcomes for children and adolescents with cancer: challenges for the twenty-first century. *Journal of Clinical Oncology : Official Journal of the American Society of Clinical Oncology*, *28*(15), 2625–2634.

St Pierre, R., & Kadoch, C. (2017). Mammalian SWI/SNF complexes in cancer: emerging therapeutic opportunities. *Current Opinion in Genetics & Development*, *42*, 56–67.

Stallings, R. L. (2009). MicroRNA involvement in the pathogenesis of neuroblastoma: potential for microRNA mediated therapeutics. *Current Pharmaceutical Design*, *15*(4), 456–462.

Sugimoto, T., Sawada, T., Arakawa, S., Matsumura, T., Sakamoto, I., Takeuchi, Y., Reynolds, C. P., Kemshead, J. T., & Helson, L. (1985). Possible differential diagnosis of neuroblastoma from rhabdomyosarcoma and Ewing's sarcoma by using a panel of monoclonal antibodies. *Japanese Journal of Cancer Research : Gann*, *76*(4), 301–307.

Suzuki, H. I., Katsura, A., & Miyazono, K. (2015). A role of uridylation pathway for blockade of *let-7* microRNA biogenesis by Lin28B. *Cancer Science*, *106*(9), 1174–1181.

Takamizawa, J., Konishi, H., Yanagisawa, K., Tomida, S., Osada, H., Endoh, H., Harano, T., Yatabe, Y., Nagino, M., & Nimura, Y. (2004). Reduced expression of the *let-7* microRNAs in human lung cancers in association with shortened postoperative survival. *Cancer Research*, *64*, 3753–3756.

Tang, L., Nogales, E., & Ciferri, C. (2010). Structure and function of SWI/SNF chromatin remodeling complexes and mechanistic implications for transcription. *Progress in Biophysics and Molecular Biology*, *102*(2–3), 122–128.

Tang, X. X., Zhao, H., Robinson, M. E., Cnaan, A., London, W., Cohn, S. L., Cheung, N. K., Brodeur, G. M., Evans, A. E., & Ikegaki, N. (2000). Prognostic significance of EPHB6, EFNB2, and EFNB3 expressions in neuroblastoma. *Medical and Pediatric Oncology*, *35*(6), 656–658.

Thomson, J. M., Parker, J., Perou, C. M., & Hammond, S. M. (2004). A custom microarray platform for analysis of microRNA gene expression. *Nature Methods*, *1*(1), 47–53.

Thornton, J. E., Chang, H.-M., Piskounova, E., & Gregory, R. I. (2012). Lin28-mediated control of

let-7 microRNA expression by alternative TUTases Zcchc11 (TUT4) and Zcchc6 (TUT7). *RNA (New York, N.Y.)*, *18*(10), 1875–1885.

Trochet, D., Bourdeaut, F., Janoueix-Lerosey, I., Deville, A., De Pontual, L., Schleiermacher, G., Coze, C., Philip, N., Frébourg, T., Munnich, A., Lyonnet, S., Delattre, O., & Amiel, J. (2004). Germline Mutations of the Paired-Like Homeobox 2B (PHOX2B) Gene in Neuroblastoma. *American Journal of Human Genetics*, *74*(4), 761–764.

Tsarovina, K., Pattyn, A., Stubbusch, J., Müller, F., van der Wees, J., Schneider, C., Brunet, J.-F., & Rohrer, H. (2004). Essential role of Gata transcription factors in sympathetic neuron development. *Development (Cambridge, England)*, *131*(19), 4775–4786.

Tummala, R., Nadiminty, N., Lou, W., Zhu, Y., Gandour-Edwards, R., Chen, H.-W., Evans, C. P., & Gao, A. C. (2013). Lin28 promotes growth of prostate cancer cells and activates the androgen receptor. *The American Journal of Pathology*, *183*(1), 288–295

Urbach, A., Yermalovich, A., Zhang, J., Spina, C. S., Zhu, H., Perez-Atayde, A. R., Shukrun, R., Charlton, J., Sebire, N., Mifsud, W., Dekel, B., Pritchard-Jones, K., & Daley, G. Q. (2014). Lin28 sustains early renal progenitors and induces Wilms tumor. *Genes & Development*, *28*(9), 971–982.

Valentijn, L. J., Koster, J., Zwijnenburg, D. A., Hasselt, N. E., van Sluis, P., Volckmann, R., van Noesel, M. M., George, R. E., Tytgat, G. A. M., Molenaar, J. J., & Versteeg, R. (2015). TERT rearrangements are frequent in neuroblastoma and identify aggressive tumors. *Nature Genetics*, *47*(12), 1411–1414.

Van Limpt, V., Schramm, A., Lakeman, A., Van Sluis, P., Chan, A., Van Noesel, M., Baas, F., Caron, H., Eggert, A., & Versteeg, R. (2004). The Phox2B homeobox gene is mutated in sporadic neuroblastomas. *Oncogene*, *23*(57), 9280–9288.

Veschi, V., Liu, Z., Voss, T. C., Ozbun, L., Gryder, B., Yan, C., Hu, Y., Ma, A., Jin, J., Mazur, S. J., Lam, N., Souza, B. K., Giannini, G., Hager, G. L., Arrowsmith, C. H., Khan, J., Appella, E., & Thiele, C. J. (2017). Epigenetic siRNA and Chemical Screens Identify SETD8 Inhibition as a Therapeutic Strategy for

p53 Activation in High-Risk Neuroblastoma. *Cancer Cell*, *31*(1), 50–63

Veschi, V., Verona, F., & Thiele, C. J. (2019a). Cancer Stem Cells and Neuroblastoma: Characteristics and Therapeutic Targeting Options. *Frontiers in Endocrinology*, *10*, 782.

Veschi, V., Verona, F., & Thiele, C. J. (2019b). Cancer Stem Cells and Neuroblastoma: Characteristics and Therapeutic Targeting Options. *Frontiers in Endocrinology*, *10*, 782.

Viswanathan, S. R., Daley, G. Q., & Gregory, R. I. (2008). Selective blockade of microRNA processing by Lin28. *Science (New York, N.Y.)*, *320*(5872), 97–100.

Viswanathan, S. R., Powers, J. T., Einhorn, W., Hoshida, Y., Ng, T. L., Toffanin, S., O'Sullivan, M., Lu, J., Phillips, L. A., Lockhart, V. L., Shah, S. P., Tanwar, P. S., Mermel, C. H., Beroukhim, R., Azam, M., Teixeira, J., Meyerson, M., Hughes, T. P., Llovet, J. M., … Daley, G. Q. (2009). Lin28 promotes transformation and is associated with advanced human malignancies. *Nature Genetics*, *41*(7), 843–848.

von Eyss, B., Jaenicke, L. A., Kortlever, R. M., Royla, N., Wiese, K. E., Letschert, S., McDuffus, L.-A., Sauer, M., Rosenwald, A., Evan, G. I., Kempa, S., & Eilers, M. (2015). A MYC-Driven Change in Mitochondrial Dynamics Limits YAP/TAZ Function in Mammary Epithelial Cells and Breast Cancer. *Cancer Cell*, *28*(6), 743–757.

Wang, D. G., Fan, J. B., Siao, C. J., Berno, A., Young, P., Sapolsky, R., Ghandour, G., Perkins, N., Winchester, E., Spencer, J., Kruglyak, L., Stein, L., Hsie, L., Topaloglou, T., Hubbell, E., Robinson, E., Mittmann, M., Morris, M. S., Shen, N., Lander, E. S. (1998). Large-scale identification, mapping, and genotyping of single-nucleotide polymorphisms in the human genome. *Science (New York, N.Y.)*, *280*(5366), 1077–1082.

Wellstein, A. (2012). ALK receptor activation, ligands and therapeutic targeting in glioblastoma and in other cancers. *Frontiers in Oncology*, *2*, 192.

Wislet, S., Vandervelden, G., & Rogister, B. (2018). From Neural Crest Development to Cancer and Vice Versa: How p75(NTR) and (Pro)neurotrophins Could Act on Cell Migration and Invasion? *Frontiers in Molecular Neuroscience*, *11*, 244.

Wong, K., Ren, X. R., Huang, Y. Z., Xie, Y., Liu, G., Saito, H., Tang, H., Wen, L., Brady-Kalnay, S. M., Mei, L., Wu, J. Y., Xiong, W. C., & Rao, Y. (2001). Signal transduction in neuronal migration: roles of GTPase activating proteins and the small GTPase Cdc42 in the Slit-Robo pathway. *Cell*, *107*(2), 209–221.

Wong, M., Tee, A. E. L., Milazzo, G., Bell, J. L., Poulos, R. C., Atmadibrata, B., Sun, Y., Jing, D., Ho, N., Ling, D., Liu, P. Y., Zhang, X. D., Hüttelmaier, S., Wong, J. W. H., Wang, J., Polly, P., Perini, G., Scarlett, C. J., & Liu, T. (2017). The Histone Methyltransferase DOT1L Promotes Neuroblastoma by Regulating Gene Transcription. *Cancer Research*, *77*(9), 2522–2533.

Xu, B., Zhang, K., & Huang, Y. (2009). Lin28 modulates cell growth and associates with a subset of cell cycle regulator mRNAs in mouse embryonic stem cells. In *RNA (New York, N.Y.)* (Vol. 15, Issue 3, pp. 357–361).

Xu, Q., & Wilkinson, D. G. (2013). Boundary formation in the development of the vertebrate hindbrain. *Wiley Interdisciplinary Reviews. Developmental Biology*, *2*(5), 735–745.

Yan, L.-X., Huang, X.-F., Shao, Q., Huang, M.-Y., Deng, L., Wu, Q.-L., Zeng, Y.-X., & Shao, J.-Y. (2008). MicroRNA miR-21 overexpression in human breast cancer is associated with advanced clinical stage, lymph node metastasis and patient poor prognosis. *RNA (New York, N.Y.)*, *14*(11), 2348–2360.

Yanagisawa, M., Yoshimura, S., & Yu, R. K. (2011). Expression of GD2 and GD3 gangliosides in human embryonic neural stem cells. *ASN Neuro*, *3*(2).

Yang, J., AlTahan, A. M., Hu, D., Wang, Y., Cheng, P.-H., Morton, C. L., Qu, C., Nathwani, A. C., Shohet, J. M., Fotsis, T., Koster, J., Versteeg, R., Okada, H., Harris, A. L., & Davidoff, A. M. (2015). The role of histone demethylase KDM4B in Myc signaling in neuroblastoma. *Journal of the National Cancer Institute*, *107*(6), djv080.

Yuan, J., & Yankner, B. A. (2000). Apoptosis in the nervous system. *Nature*, *407*(6805), 802–809.

Zhang, L., Anglesio, M. S., O'Sullivan, M., Zhang, F., Yang, G., Sarao, R., Mai, P. N., Cronin, S., Hara, H., Melnyk, N., Li, L., Wada, T., Liu, P. P., Farrar, J., Arceci, R. J., Sorensen, P. H., & Penninger, J. M.

(2007). The E3 ligase HACE1 is a critical chromosome 6q21 tumor suppressor involved in multiple cancers. *Nature Medicine*, *13*(9), 1060–1069.

Zhu, D., Jiang, X.-H., Jiang, Y.-H., Ding, W.-C., Zhang, C.-L., Shen, H., Wang, X.-L., Ma, D., Hu, Z., & Wang, H. (2014). Amplification and overexpression of TP63 and MYC as biomarkers for transition of cervical intraepithelial neoplasia to cervical cancer. *International Journal of Gynecological Cancer : Official Journal of the International Gynecological Cancer Society*, *24*(4), 643–648.

Zhu, S., Lee, J.-S., Guo, F., Shin, J., Perez-Atayde, A. R., Kutok, J. L., Rodig, S. J., Neuberg, D. S., Helman, D., Feng, H., Stewart, R. A., Wang, W., George, R. E., Kanki, J. P., & Look, A. T. (2012). Activated ALK collaborates with MYCN in neuroblastoma pathogenesis. *Cancer Cell*, *21*(3), 362–373.

Zimmerman, K. A., Yancopoulos, G. D., Collum, R. G., Smith, R. K., Kohl, N. E., Denis, K. A., Nau, M. M., Witte, O. N., Toran-Allerand, D., & Gee, C. E. (1986). Differential expression of myc family genes during murine development. *Nature*, *319*(6056), 780–783.